UNIVERSITY BIELEFELD

DOCTORAL THESIS

DESIGNING SMART SURFACES

Author:
Johannes BOOKHOLD

Supervisor:
Prof. Dr. Thomas HELLWEG
Examiner:
Prof. Dr. Dario ANSELMETTI

A thesis submitted in fulfillment of the requirements for the degree of Doctor rerum naturalium

in the

Physical and Biophysical Chemistry Group
Department of Chemistry

19th September 2017

Eidesstattliche Erklärung

Hiermit versichere ich, Johannes BOOKHOLD, dass die vorliegende Arbeit mit dem Titel, "DESIGNING SMART SURFACES", im Zeitraum von 2013 bis 2017 an der Universität Bielfeld am Lehrstuhl für Physikalische und Biophysikalische Chemie unter Anleitung von Prof. Dr. Thomas Hellweg erstellt wurde. Ich versichere weiter, dass:

- Ich die vorliegende Arbeit selbständig verfasst habe und keine anderen Hilfsmittel, als die angegeben benutzt habe.
- Alle Stellen, die wörtlich oder sinngemäß aus veröffentlichten oder nicht veröffentlichen Schriften entnommen sind, in jedem Einzelfall durch Quellenangeben kenntlich gemacht habe.
- Die vorliegende Arbeit in gleicher oder ähnlicher Form bei keiner anderen Prüfungsbehörde vorgelegt habe oder veröffentlicht habe.

Signed:

Date:

"Science is like sex: sometimes something useful comes out, but that is not the reason we are doing it."

Richard Phillips Feynman

Abstract

The aim of this thesis was the development of smart, thermoresponsive surface coatings based on poly(*N*-isopropylacrylamide) (pNIPAM) microgels for applications in biological and medical research. In order to understand microgel behavior when deposited on a surface the physical properties and the morphology of adsorbed microgels had to be studied and understood.

Initial experiments using atomic force microscopy (AFM) aimed at the characterization of various microgels adsorbed and dried on a surface in order to gain knowledge about the influence of the microgel architecture on their behavior. Further experiments were conducted to examine the deposition behavior of microgels when deposited with standard coating procedures such as spin-coating, dip-coating and spray-coating. Results from these experiments were used to optimize these processes for the manufacturing of microgel monolayers. In the course of a BMBF funded project the obtained results were utilized to develop wound healing essays for medical applications in cooperation with the institutes Fraunhofer IZI, Fraunhofer IAT, the University Bayreuth and the companies Ibidi GmbH and PolyAn GmbH.

Results and insights gained from this cooperation led to the idea to develop transfereable thermoresponsive coatings. The principle idea was to cross-link the microgels in a monolayer in order to obtain a free-standing, thermoresponsive film which than can be deposited on various substrates and surfaces. In order to be able to cross-link the microgel the thermoresponsive monomer NIPAM was copolymerized with the monomer *N*-Benzhydrylacrylamide (NBHAM). The aromatic moieties of the monomer NBHAM enabled the possibility to cross-link the microgels in a monolayer using an electron beam. The cross-linked layer could than be detached from the initial substrate and transferred to any arbitrary substrate. Furthermore it is possible to use the free-standing microgel film as a temperature controllable membrane. In conductivity measurements it has been shown that the resistivity of the membrane can be tuned by changing the external temperature.

Zusammenfassung

Die Zielsetzung dieser Arbeit war die Entwicklung von intelligenten, thermoresponsiven Oberflächenbeschichtungen auf Basis von Poly(*N*-Isopropylacrylamid) (pNIPAM) Mikrogelen für die Anwendung in biologischen und medizinischen Forschungsbereichen. Um ein erweiteretes Verständnis vom Verhalten von Mikrogelen bei deren Abscheidung auf Oberflächen zu erhalten, wurden die physikalischen Eigenschaften und die Morphologie adsorbierter Mikrogele untersucht.

Es wurden zunächst Untersuchungen von verschiedenen Mikrogelen mit Rasterkraftmikroskopie (AFM) durchgeführt um die Morphologie unterschiedlicher Mikrogelarchitekturen im getrockneten Zustand auf Oberflächen zu untersuchen. Es wurden weiterführende Experimente zum Abscheidungsverhalten von Mikrogelen bei verschiedenen Beschichtungsprozessen wie Spin-Coating, Dip-Coating und Spray-Coating durchgeführt, um diese Prozesse für die Deposition von Mikrogelen in Monolagen zu optimieren. Anhand dieser Ergebnisse ist es möglich gewesen im Laufe eines vom BMBF geförderten Projekts in Kooperation mit dem Fraunhofer IZI, dem Fraunhofer IAT, der Universität Bayreuth und den Firmen Ibidi GmbH und PolyAn GmbH ein Produkt, auf Basis von thermoresponsiven Mikrogel-Monolagen, für Wound-Healing-Essays zu entwickeln.

Die gewonnen Ergebnisse dienten als Grundlage für die Idee transferierbare thermoresponsive Schichten zu entwickeln. Dabei war die grundlegende Idee, die Mikrogele in einer Monolage miteinander zu vernetzen um einen freistehenden, thermoresponsiven Film zu erhalten der auf eine Vielzahl an Substraten übertragbar ist. Realisiert wurde die Vernetzbarkeit durch die Copolymerisation von NIPAM mit dem Monomer *N*-Benzhydrylacrylamid (NBHAM). Durch die Benzyl-Gruppen des Monomers NBHAM ist es gelungen die Mikrogele in einer Monolage mittels eines Elekrtonenstrahls miteinander zu vernetzen. Die vernetze Schicht kann vom Trägersubstrat abgelöst und auf jedes beliebige Substrat übertragen werden. Weiter ist es in temperaturabhängigen Widerstandsmessungen gelungen die Möglichkeit nachzuweisen, diese Filme als thermoresponsive Membran zu verwenden. Durch die externe Temperaturkontrolle konnte der Widerstand der Membran gesteuert werden.

Acknowledgements

At this point I would like to thank all the people who have supported and helped me along the course of this thesis.

First and foremost I would like to express my thankfulness towards Prof. Dr. Thomas Hellweg for his patience, his support, the constructive criticism and discussions, but most of all for the possibility to pursue the scientific research I was interested in. Also I would like to thank Thomas for the insights into scientific research and the possibility of a research stay in Donostia-San Sebastian with the research group of Prof. Dr. Luis Liz-Marzan.

To Prof. Dr. Dario Anselmetti I would like to express my gratitude for the acquisition of the second examination of this thesis.

I am grateful beyond measure for the support and love I get from my wife, Jonna. Thank you for everything especially for our beautiful daughter. Thank you for your endless support and giving me everything I need and thank you for standing by my side in good times and in thesis writing times.

My parents, my grandparents and my whole family I want to thank for their support at all times, for their encouragement and for always having an open door.

I would like to thank my whole department, the research group PCIII at the Bielefeld University. Especially I want to thank Bastian Wedel, Michael Zeiser, Elena Hermann, Oliver Wrede and Timo Brändel for interesting discussions, their support of my research, a lot of precious memories of fun days at the office, on conferences, measurement times at neutron scattering facilities and for even funnier nights in the seminar room and some not so precious memories of glass doors and the ICU. To you I will always be grateful for the friendship we share and the time we had. For their support with my neutron scattering experiments I want to express my gratitude to Oliver Wrede and Annegret Günther. I am also thankful for the work and experiments done to support my research by Ina Ehring, Meike Adolph, Uwe Güth, Katja Uhlig, Lars Wiehemeier, Maxim Dirksen, Sebastian Knust, Florian Paneff, Xinaghui Zhang and Tilman Kottke. A special thanks for her extensive support with a lot of matters in and around the lab belongs to Yvonne Hertle and to Sandra Gericke I would like to express my gratitude for her great help with everything organizational.

Prof. Dr. Luis Liz-Marzan and the entire BioNanoPlasmonics group I thank for the possibility of the research stay at the CIC biomaGUNE in Donostia-San-Sebastian. In this course I want to thank especially Juan Jose Giner-Casares, Judith Langer, Eric Hill and Marta Quintanilla for all the support in the new environment and with the new research topic and also a lot of nice and fun days and nights at the beach, in the city and the sidrerias.

For financial support I would like to acknowledge the BMBF project “ThermoCell”.

Contents

Dedicated to my wife and my daughter

Chapter 1

General Introduction

Colloids, natural and artificial in origin, are ubiquitous in our daily life, from soot [1] and fog [2] to our blood-plasma [3] and from food [4], cosmetics [5] and pharmaceutical products [6] to adhesives [7]. Therefore it is not difficult to understand the enormous scientific interest in this topic. The underlying basis of this work are the properties of microgels, which themselves are colloidal polymer particles. Microgel particles are in the size range of a couple of nm to a few hundred nm and their internal structure, the polymer network, is fully permeated by the solvent. [8] The chemical composition of this polymer network not only determines microgel properties in solution [9] but also when adsorbed to a solid surface. The most interesting category of these lyogels are the so-called smart microgels, the prominent feature of which is the ability to react reversibly to an external stimulus like temperature [10], pH [11], pressure [12], ionic strength [13] and solvent composition [14]. Due to these interesting features it is understandable that these immensely versatile and potent colloids have been of interest to the scientific community for the past three decades. [8, 9, 10, 11, 12, 13, 15, 16]

Smart microgels which are stimulated by temperature are referred to as thermoresponsive microgels [8, 13]. One of the most studied polymers within this category is *N*-isopropylacrylamide (NIPAM) [8, 9, 11, 13, 15, 16]. Polymerized NIPAM exhibits a lower critical solution temperature (LCST) at about 31 °C [17, 18]. This means that, when the temperature of the polymer solution exceeds this specific temperature, the solubility of the polymer changes which results in a coil to globule transition of the polymer chain. [17] This effect is caused by the breaking of hydrogen bonds between the amide moieties and the solvent causing the polymer chains to precipitate. This endothermic phase separation process is entropy driven due to the entropic gain caused by the solvent molecules that are released from the polymer chain. [17] Simultaneously, hydrogen bonds are formed between the amide moieties of the polymer leading to polymer-polymer interactions that are stronger than the polymer-solvent interactions. A similar behavior can be observed in pNIPAM microgels. In these gels the polymer network is formed by numerous physically and chemically cross-linked polymer chains. Chemical cross-linking is achieved by introducing molecules that covalently links to polymer chains. For NIPAM-based microgels the most common chemical cross-linker is *N*-*N*'-methylenbisacrylamide (BIS). Physical connections between polymer chains are formed by chain entanglements, dipol-dipol interactions, hydrogen bonds ans ionic interactions. Typically acrylamide microgels are colloidally stabilized by charges as result of the incorporation of the initiator from the radical polymerization reaction. [9, 19] The colloidal stabilization due to the charges inhibits a precipitation, instead the microgels exhibit a change in volume at the LCST of the linear polymer chains. In regard to microgels this temperature is called the volume phase transition temperature (VPTT) and is at about 32 °C. [20, 21, 22, 23]

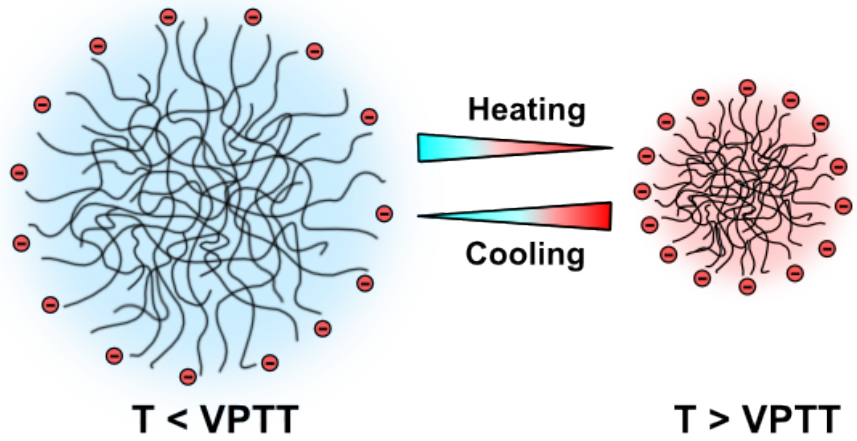

FIGURE 1.1: Schematic illustration of the reversible change in volume of a thermoresponsive microgel. The lines represent the polymer chains and the charges from the initiator are represented by the red circles. Below the VPTT (left) the microgel is in the swollen state. When the temperature exceeds the VPTT the microgel transitions into the collapsed state (right).

However, at this point the field of smart microgels is a very well researched part of the colloidal sciences and most of this research is focused on microgels in solution, their native environment. Most research aims at altering the properties of microgels [8, 24, 25], understanding certain mechanisms in solution [26, 27, 28] and during the synthesis [29, 30, 31] or at finding applications for these microgels as colloidal dispersions such as catalyst- [32, 33, 34] and drug-carriers [35, 36, 37]. Only a minor part of the research today is aimed at the development of applications outside the native environment of these potent particles. This research has led to a number of new applications including anti-fouling coatings [38], photonic materials [39, 40], etalons [41, 42, 40], optical materials [43, 44, 45], sensor devices [46] and cell culture substrates [47]. Such research efforts reveal the possibility of using smart microgels to modify the properties of surfaces in order to create smart surfaces. A lot of this research effort is aimed at bio-mimicking smart surfaces, which are found in nature on almost every level from plants to insects to reptiles, amphibians, and even birds and mammals in which over millions of years their exterior or interior organs have evolved magnificent functionalities utilizing smart surfaces. The most prominent of these surfaces are the leaves of the lotus plant which are structured on a nanoscopic scale in such a way that they repel water almost totally. This observation led to the term lotus effect which can be seen on many other plants for instance on certain types of watercress and cacti. Moreover, some insects like crane flies [48] or some butterflies [49] reveal this effect. Some insects like the head-stander beetle have even developed more complex surfaces where hydrophilic and hydrophobic parts are ordered in such a manner on the exoskeleton that water condenses on hydrophilic spots. Once the drop reaches a critical size it is directed towards the beetles mouth by the hydrophobic parts [50]. The usefulness of such surfaces has long been known and is imitated in various fields from wall paint and glass cleaning agents emulating the lotus effect to marine anti-biofouling coatings [51] based on structured polymer layers [52].

Smart microgels can bring a whole new versatile property into the field of smart surface coatings that most of the researched subjects do not have, stimuli responsive

behavior [47, 53, 54]. This means that the functionalities of a surface coated with a stimulus responsive material can be tuned or even fully switched on and off by exposing the surface to the external stimulus. In addition microgels can provide a naturally structured surface due to their initial spherical shape which is mostly preserved [47, 54, 55]. In order to effectively produce microgel surface coatings that exhibit the desired properties it is crucial to understand the morphology and phase transition behavior of microgels that are adsorbed to a surface. The morphology of adsorbed microgels depends to a large degree on the amount of chemical cross-linker inside of the microgel. The height/width ratio of the adsorbed microgels increases with increasing cross-linker content. This effect is especially pronounced in the collapsed or dried state of the microgels. Microgels with a low cross-linker content (0-2 mol%) tend to spread out on the substrate and form flat structures, whereas microgels with higher cross-linker content (5-10 mol%) form more developed convex structures. [53, 55] This effect is due to the increased rigidity as a result of a higher cross-linker content. These microgels have a more hard sphere like behavior. [55] In addition these particles are less effected by the surface they are adsorbed to. Low cross-linked microgels exhibit a more pronounced hysteresis of the VPTT when adsorbed to a surface than higher cross-linked microgels. [53, 55] Furthermore, the lower cross-linked microgel particles tend to be unstable in their form and therefore change size and shape upon repeated heating and cooling. [11, 55, 56]

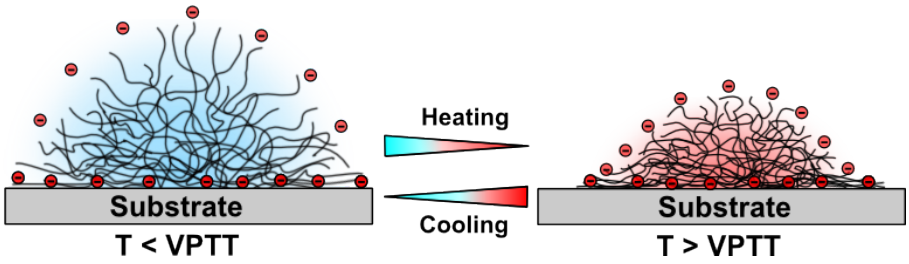

FIGURE 1.2: Schematic illustration of the reversible change in volume of a thermoresponsive microgel adsorbed to a surface. The lines represent the polymer chains and the charges from the initiator are represented by the red circles. Below the VPTT (left) the microgel is in the swollen state. When the temperature exceeds the VPTT the microgel transitions into the collapsed state (right). The morphology of a microgel adsorbed on a surface depends strongly on its architecture.

Resent studies have shown that copolymer microgels show a different behavior than homopolymer microgels when deposited on a surface. These studies focused on pNIPAM-based microgels copolymerized with acrylic acid (AA). [11, 53, 55, 57, 58] In chapter 2 we studied thermoresponsive homopolymer microgels made from the monomers *N*-isopropylacrylamide (NIPAM), *N*-*n*-propylacrylamide (NNPAM) and *N*-isopropylmethacrylamide (NIPMAM). Part of the analysis was the study of the adsorbed microgels on a surface in order to investigate morphological differences between the microgel particles. The major difference between polymers made from these monomers is their LCST. For pNIPAM the LCST is at about 32 °C, whereas the LCST of pNNPAM is at the substantially lower temperature of 22 °C [24] and that of pNIPMAM is significantly above the LCST of pNIPAM at 43 °C [24]. In the following chapter 3 the influence of sodium dodecyl sulfate (SDS) on the growth of microgels during the synthesis was studied. The addition of a surfactant like SDS not only has an impact on the size of the microgels but also on their morphology. Of particular interest was the effect SDS had on the microgel's morphology when

added at different points of time during the synthesis. These studies formed the basis for further research on the deposition behavior of microgels using various deposition techniques like spin-coating, dip-coating and spray-coating (Appendix E). In previous studies these techniques have been used to deposit microgels on a surface. [11, 59, 60] Whereas each of those studies focused on one single technique to coat a surface with microgels, this research focuses on a comparison between the different techniques and an evaluation based on the ability to produce monolayers using microgels with different cross-linker content.

The behavior of microgels in a densely packed layer on a surface is slightly different from that of single microgels adsorbed on a surface. Microgels arranged in a monolayer are more restricted in their swelling than single microgels. Not only are these microgels limited in their expansion by the substrate they are deposited on but also by their neighbors. [11, 59] This can be concluded from ellipsometric measurements that have shown that the hysteresis of the VPTT is increased in comparison to single microgels. [11, 59] Taking these studies and the analysis of single microgels on surfaces into account it can be assumed that the degree in which a single microgel in a densely packed monolayer is limited in its swelling behavior is also dependent on the morphology and the architecture of the microgels.

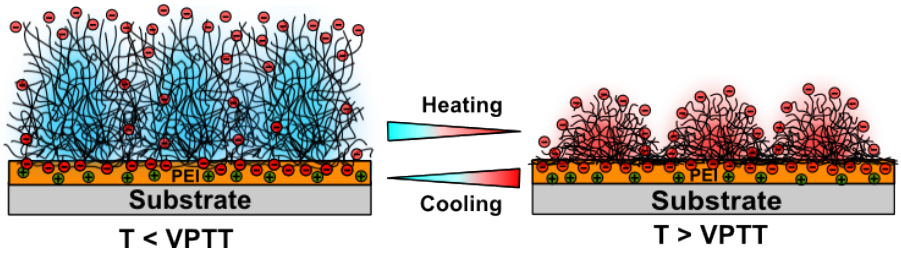

FIGURE 1.3: Schematic illustration of the reversible change in volume of thermoresponsive microgels arranged in a monolayer on a surface. The lines represent the polymer chains and the charges from the initiator are represented by the red circles. Below the VPTT (left) the microgel is in the swollen state. When the temperature exceeds the VPTT the microgel transitions into the collapsed state (right). In the case of negatively charged microgels often the positively charged polymer polyethylenimine (PEI) is used as an adhesive. The positive charges of the PEI layer are represented by the green circles.

The investigation of the behavior of microgels of diverse architecture when deposited on a surfaces has led to the idea of proposing microgel coatings as an ideal surface modification for cell culture substrates could be taken to the next stage. In the course of a cooperation it was possible to develop an advanced cell culture substrate based on smart surface coatings from thermoresponsive microgels. The experience and information gathered on their deposition behavior and the morphology of microgel layers allowed the development of a novel artificial environment for adherently growing cells. This new artificial environment permits non invasive and destruction free cell experiments, which is of high interest for medical and biological research, for example in-vitro drug screening and disease mechanism. Furthermore, we were able to turn the wound healing assay into a possible commercial product for biological and medical applications. The basis of this research is the idea that cells are able to attach themselves to a microgel surface in the collapsed state of the microgels and propagate at physiological temperatures (around 37 °C). By decreasing the temperature the microgels swell and form a less than ideal environment for

the cells to grow on resulting in the cells detaching themselves from the surface. This enables a non invasive way of harvesting cells. The main advantage is, that without the necessary mechanical or chemical stress the cells can be detached from the surface and the cells remain intact and undamaged.

In the final part of this thesis the idea of smart surfaces through microgel-based surface coatings is taken a step further. Until now, microgel coatings could only be directly applied to the desired surface. Due to this only smooth two-dimensional substrates are accessible using the given techniques to deposit microgels on a surface. Three-dimensional substrates of arbitrary shape cannot be coated with microgels. In addition porous substrates and gratings are also in the inaccessible category of substrates for microgel coatings. From the idea to overcome these limitations of microgel surface coatings came the thought to create transferable microgel coatings. This was thought to be realized by producing an entirely transferable layer of microgels. The idea was to produce a microgel coating on a smooth surface like a silicon wafer, cross-link the entire layer, then detach the layer from the initial supporting substrate and transfer it to the desired substrate, thereby creating a free-standing microgel film. The final chapter will depict how this was realized using electron-beam cross-linking of a homogeneous microgel monolayer.This process will be described in detail from the synthesis of novel cross-linkable microgel particles to the process of electron beam cross-linking and the detachment of the layer from the original supporting substrate. The functionality of the obtained free-standing microgel film will be demonstrated through conductivity experiments in which the film was placed as a membrane between two electrodes. This proof of thermoresponsivity also showed the potential use of this free-standing microgel film as a temperature controllable membrane.

References

[1] A. Medalia, D. Rivin, and D. R. Saunders, "A comparison of carbon black with soot," *Sci. Total Environ.*, vol. 31, pp. 1–22, 1983.

[2] W. D. Bancroft, "Some properties of fog," *J. Chem. Soc.*, vol. 29, pp. 309–336, 1876.

[3] A. Odunayo and M. E. Kerl, "Comparison of whole blood and plasma colloid osmotic pressure in health dogs," *J. Vet. Emerg. Crit. Care*, vol. 21, pp. 236–241, 2011.

[4] S. Davidou, M. L. Meste, E. Debever, and D. Bakaert, "A contribution to the study of staling of white bread: effect of water and hydrocolloid," *Food Hydrocolloids*, vol. 10, pp. 375–383, 1996.

[5] S. S. et al., *Colloids in Cosmetics and Personal Care*. Wiley, 2011.

[6] Patent, "Us 5558853 a," *year filed: 1994*, 1996.

[7] I. Benedek, *Pressure-Sensitive AAdhesive and Applications*. CRC Press, 2004.

[8] R. Pelton, "Temperature-sensitive aqueous microgels," *Adv. Colloid Interf. Sci.*, vol. 85, pp. 1–33, 2000. review.

[9] S. Nayak and L. A. Lyon, "Soft nanotechnology with soft nanoparticles," *Angew. Chem. Int. Ed.*, vol. 44, pp. 7686–7708, 2005. Review.

[10] Y. Hertle, M. Zeiser, C. Hasenöhrl, P. Busch, and T. Hellweg, "Responsive p(nipam-*co*-ntbam) microgels: Flory–rehner description of the swelling behaviour," *Colloid and Polymer Science*, vol. 288, pp. 1047–1059, 2010.

[11] S. Schmidt, H. Motschmann, T. Hellweg, and R. von Klitzing, "Thermoresponsive surfaces by spin-coating of pnipam-co-paa microgels. a combined afm and ellipsometry study," *POLYMER*, vol. 49, pp. 749–756, 2008.

[12] E. Kato, "Pressure-induced volume phase transition of polyacrylamide gels in acetone-water mixtures," *J. Chem. Phys.*, vol. 113, no. 3, pp. 1310–1314, 2000.

[13] M. J. Snowden, B. Z. Chowdhry, B. Vincentb, and G. E. Morris, "Colloidal copolymer microgels of *N*-isopropylacrylamide and acrylic acid: ph, ionic strength and temperature effects," *Journal of the Chemical Society, Faraday Transactions*, vol. 92, pp. 5013–5016, 1996.

[14] H. M. Crowther and B. Vincent, "Swelling behavior of poly(n-isopropylacrylamide) microgel particles in alcoholic solutions," *Colloid Polym. Sci.*, vol. 276, pp. 46–51, 1998. Not really very interesting.

[15] M. Antonietti and M. Maskos, "Fine-tuning of phase structures and thermoplasticity of polyelectrolyte-surfactant complexes: Copolymers of ionic monomers with n-alkylacrylamides," *Macromolecules*, vol. 29, pp. 4199–4205, 1996.

[16] Y. Hertle and T. Hellweg, "Thermoresponsive copolymer microgels," *Journal of Materials Chemistry B*, vol. 43, pp. 5874–5885, 2013.

[17] M. Heskins and J. E. Guillet, "Solution properties of poly(n-isopropylacrylamide)," *J. Macromol. Sci. A*, vol. 2, no. 8, pp. 1441–1455, 1968.

[18] M. Meewes, J. Ricka, M. de Silva, R. Nyffenegger, and T. Binkert, "Coil-globule transition of poly(n-isopropylacrylamide). a study of surfactant effects by light scattering," *Macromolecules*, vol. 24, pp. 5811–5816, 1991. The coil-to-globule transition of linear PNIPAM chains seems to be a continuous one.

[19] B. R. Saunders and B. Vincent, "Microgel particles as model colloids: theory, properties, and applications," *Adv. Colloid Interf. Sci.*, vol. 80, pp. 1–25, 1999.

[20] D. Duracher, A. Elaïssari, and C. Pichot, "Preparation of poly(*N*-isopropylmethacrylamide) latexes kinetic studies and characterization," *J. Polym. Sci. Part A: Polymer Chemistry*, vol. 37, no. 12, pp. 1823–1837, 1999.

[21] C. Wu and S. Zhou, "Volume phase transition of swollen gels: Discontinuous or continuous," *Macromolecules*, vol. 30, pp. 574–576, 1997.

[22] M. Shibayama and T. Tanaka, "Small-angle neutron scattering study on weakly charged poly(n-isopropyl acrylamide-co-acrylic acid) copolymer solutions," *J. Chem. Phys.*, vol. 102, no. 23, pp. 9392–9400, 1995.

[23] H. Crowther and B. Vincent, "Swelling behavior of poly-*N*-isopropylacrylamide microgel particles in alcoholic solutions," *Colloid Polymer Science*, vol. 276, pp. 46–51, 1998.

[24] B. Wedel, M. Zeiser, and T. Hellweg, "Non nipam based smart microgels: Systematic variation of the volume phase transition temperature by copolymerization," *Zeitschrift f. Phys. Chem.*, vol. 227, pp. 00–12, 2012.

[25] T. Gilanyi, I. Varga, R. Meszaros, G. Filipcsei, and M. Zrinyi, "Characterisation of monodisperse poly(n-isopropylacrylamide) microgel particles," *Phys. Chem. Chem. Phys.*, vol. 2, pp. 1973–1977, 2000.

[26] N. Dingenouts, S. Seelenmeyer, I. Deike, S. Rosenfeldt, M. Ballauff, P. Lindner, and T. Narayanan, "Analysis of thermosensitive core-shell colloids by small-angle neutron scattering including contrast variation," *Phys. Chem. Chem. Phys.*, vol. 3, pp. 1169–1174, 2001.

[27] E. Daly and B. R. Saunders, "A study of the effect of electrolyte on the swelling and stability of poly(n-isopropylacrylamide," *Langmuir*, vol. 16, pp. 5546–5552, 2000.

[28] J. S. Hyatt, A. M. Douglas, C. Stanley, C. Do, T. H. Barker, and A. Fernandez-Nieves, "Charge segregation in weakly ionized microgels," *Phys. Rev. E*, vol. 95, p. 012608, 2017.

[29] M. Karg, I. Pastoriza-Santos, L. M. Liz-Marzan, and T. Hellweg, "A versatile approach for the preparation of thermosensitive pnipam core-shell microgels with nanoparticle cores," *Journal of Chemical Physics and Physical Chemistry*, vol. 7, pp. 2298–2301, 2006.

[30] J.-T. Zhang, X.-L. Liu, A. Fahr, and K. D. Jandt, "A new strategy to prepare temperature-sensitive poly(n-isopropylacrylamide) microgels," *Colloid Polym. Sci.*, vol. 286, pp. 1209–1213, 2008.

[31] D. Duracher, F. Sauzedde, A. Elaissari, A. Perrin, and C. Pichot, "Cationic amino-containing n-isopropyl-acrylamide-styrene copolymer latex particles: 1-particle size and morphology vs. polymerization process," *Coll. Polym. Sci.*, vol. 276, pp. 219–231, 1998. Interesting.

[32] Y. Lu, M. Yu, M. Drechsler, and M. Ballauff, "Ag nanocomposite particles: Preparation, characterisation and application," *Macromol. Symp.*, vol. 254, pp. 97–102, 2007.

[33] M. I. Martinez-Rubio, T. G. Ireland, G. R. Fern, J. Silver, and M. J. Snowden, "A new application for microgels: Novel method for the synthesis of spherical particles of the y_2o_3:eu phosphor using a copolymer microgel of nipam and acrylic acid," *Langmuir*, vol. 17, pp. 7145–7149, 2001.

[34] N. Singh and L. A. Lyon, "Au nanoparticle templated synthesis of pnipam nanogels," *Chem. Mater.*, vol. 19, pp. 719–726, 2007. .

[35] C. S. O. Silva, R. P. Baptista, A. M. Santos, J. M. G. Martinho, J. M. S. Cabral, and M. A. Taipa, "Adsorption of human igg on to poly(n-isopropylacrylamide)-based polymer particles," *Biotechnol. Lett.*, vol. 28, pp. 2019–2025, 2006.

[36] D. Duracher, A. Elaissari, F. Mallet, and C. Pichot, "Adsorption of modified hiv-1 capsid p24 protien onto thermosensitive and cationic core-shell poly(styrene)-poly(*N*-isopropylacrylamide) particles," *Langmuir*, vol. 16, pp. 9002–9008, 2000.

[37] G. Zhou, L. Veron, A. Elaissari, T. Delair, and C. Pichot, "A new route for the preparation of cyano-containing poly(n-isopropylacrylamide) microgel latex for specific immobilization of antibodies," *Polymer Interntional*, vol. 53, pp. 603–608, 2004.

[38] A. B. South, R. E. Whitmire, A. J. Garcia, and L. A. Lyon, "Centrifugal deposition of microgels for the rapid assembly of nonfouling thin films," *ACS Appl. Mater. Interfaces*, vol. 1, no. 12, pp. 2747–2754, 2009.

[39] M. Zhou, F. Xing, M. Ren, Y. Feng, Y. Zhao, H. Qiu, X. Wang, C. Gao, F. Sun, Y. He, Z. M. an Pu Wen, and J. Gao, "A facile method to assemble pnipam-containing microgel photonic crystals," *Chem. Phys. Chem.*, vol. 10, pp. 523–526, 2009.

[40] L. Hu, A. K. Sarker, M. R. Islam, X. Li, Z. Lu, and M. J. Serpe, "Poly (n-isopropylacrylamide) microgel-based assemblies," *Journal of Polymer Science Part A: Polymer Chemistry*, vol. 51, no. 14, pp. 3004–3020, 2013.

[41] C. D. Sorrell, M. C. D. Carter, and M. J. Serpe, "Color tunable poly(*N*-isopropylacrylamide)-*co*-acrylic acid microgel-au hybrid assemblies," *Adv. Func. Mater.*, vol. 21, pp. 425–433, 2011.

[42] C. D. Sorrell, M. C. Carter, and M. J. Serpe, "A paint-on protocol for the facile assembly of uniform microgel coating for color tunable etalon fabrication," *ACS Appl. Mater. Interfaces*, vol. 3, pp. 1140–1147, 2011.

[43] Y. Gao and M. J. Serpe, "Light-induced color changes of microgel-based etalons," *ACS Applied Materials & Interfaces*, vol. 6, no. 11, pp. 8461–8466, 2014.

[44] J. Kim, M. J. Serpe, and L. A. Lyon, "Hydrogel microparticles as dynamically tunable microlenses," *J. Am. Chem. Soc.*, vol. 126, pp. 9512–9513, 2004.

[45] Q. M. Zhang, X. Li, M. R. Islam, M. Wei, and M. J. Serpe, "Light switchable optical materials from azobenzene crosslinked poly(*N*-isopropylacrylamide)-based microgels," *J. Mater. Chem. C*, vol. 2, pp. 6961–6965, 2014.

[46] M. R.Islam and M. J. Serpe, "Poly(*N*-isopropylacrylamide) microgel-based thin film actuators for humidity sensing," *RSC Adv.*, vol. 4, pp. 31937–31940, 2014.

[47] S. Schmidt, M. Zeiser, T. Hellweg, C. Duschl, A. Fery, and H. Möhwald, "Adhesion and mechanical properties of pnipam microgel films and their potential use as switchable cell culture substrates," *Adv. Func. Mater.*, vol. 20, no. 19, pp. 3235–3243, 2010.

[48] H.-M. S. Hu, G. S. Watson, B. W. Cribb, and J. A. Watson, "Non-wetting wwing and legs of the cranefly aided by fine structures of the cuticle," *J. Exp. Biol.*, vol. 214, pp. 915–920, 2011.

[49] G. D. Bixler and B. Bhushan, "Bioinspired rice leaf and butterfly wing surface structures combining shark skin and lotus effects," *Soft Matter*, vol. 8, pp. 11271–11284, 2012.

[50] L. Zhai, L. C. Berg, F. Cebeci, Y. Kim, J. M. Milwid, M. F. Rubner, and R. E. Cohen, "Patterned suberhydrophobic surfaces: Toward a synthetic mimic of the namib desert beetle," *Nano Lett.*, vol. 6, pp. 1213–1217, 2006.

[51] I. Banerjee, R. C. Pangule, and R. S. Kane, "Antifouling coatings: Recent developments in the design of surfaces that prevent fouling by proteins, bacteria, and marine organisms," *Advanced Materials*, vol. 23, pp. 690–718, 2010.

[52] B. Mizrahi, X. Khoo, and H. H. C. et al., "Long-lasting antifouling coating from multi-armed polymer," *Langmuir*, vol. 29, pp. 10087–10094, 2013.

[53] A. Burmistrova and R. Klitzing, "Control of number density and swelling shrinking behavior of p(nipam–aac) particles at solid surfaces," *Mat. Chem.*, vol. 20, pp. 3502–3507, 2010.

[54] Q. M. Zhang and M. J. Serpe, "Versatilemethode for coating surfaces with functional and responsive polymer-based films," *ACS Appl. Mater. Interfaces*, vol. 7, pp. 27547–27553, 2015.

[55] A. Burmistrova, M. Richter, C. Uzum, and R. von Klitzing, "Effect of cross-linker density of p(nipam-*co*-aac) microgels at solid surfaces on the swelling/shrinking behaviour and the youngs modulus," *Colloid Poly. Sci.*, vol. 289, pp. 613–624, 2011.

[56] W. Wang, K. Troll, G. Kaune, E. Metawalli, M. Ruderer, K. Skrabania, A. Laschewsky, S. V. Roth, C. M. Papadakis, and P. Müller-Buschbaum, "Thin films of poly(*N*-isopropylacrylamide) end-capped with n-butyltrithiocarbonate," *Macromolecules*, vol. 41, pp. 3209–3218, 2008.

[57] A. Burmistrova, M. Richter, M. Eisele, C. Üzüm, and R. von Klitzing, "The effect of co-monomer content on the swelling/shrinking and mechanical behaviour of individually adsorbed pnipam microgel particles," *Polymers*, vol. 3, pp. 1575–1590, 2011.

[58] M. Zeiser, I. Freudensprung, and T. Hellweg, "Linearly thermoresponsive core-shell microgels: Towards a new class of nanoactuators," *Polymer*, vol. 53, pp. 6096–6101, 2012.

[59] A. Burmistrova, R. Steitz, and R. v. Klitzing, "Temperature response of pnipam derivatives at planar surfaces: Comparison between polyelectrolyte multilayers and adsorbed microgels," *ChemPhysChem*, vol. 11, no. 17, pp. 3571–3579, 2010.

[60] S. Schmidt, T. Hellweg, and R. von Klitzing, "Packing density control in p(nipam-*co*-aac) microgel monolayers: Effect of surface charge, ph, and preparation technique," *Langmuir*, vol. 24, pp. 12595–12602, 2008.

Chapter 2

Smart Homopolymer Microgels

Smart Homopolymer Microgels: Influence of the Monomer Structure on the Particle Properties

Bastian Wedel, Yvonne Hertle, Oliver Wrede, Johannes Bookhold and Thomas Hellweg

Published in **Polymers**

Volume:8 Issue:4

Year:2016

DOI:10.3390/polym8040162

http://www.mdpi.com/2073-4360/8/4/162

2.1 Abstract

In this work, we compare the properties of smart homopolymer microgels based on *N*-*n*-propylacrylamide (NNPAM), *N*-isopropylacrylamide (NIPAM) and *N*-isopropylmethacrylamide (NIPMAM) synthesized under identical conditions. The particles are studied with respect to size, morphology and swelling behavior using scanning electron and scanning force microscopy. In addition, light scattering techniques and fluorescent probes are employed to follow the swelling/de-swelling of the particles. Significant differences are found and discussed. Poly(*N*-*n*-propylacrylamide) (PNNPAM) microgels stand out due to their very sharp volume phase transition, whereas Poly(*N*-isopropylmethacrylamide) (PNIPMAM) particles are found to exhibit a more homogeneous network structure compared to the other two systems.

2.2 Introduction

The formation of thermoresponsive microgels is a complex process, and it is of great interest to determine the structural and physical properties of these systems depending on the chemical structure of the used monomer and the synthesis conditions. A microgel basically consists of a cross-linker and a polymer which is responsible for the thermoresponsive properties of the gel network. If only one thermoresponsive polymer is present in the microgel, such systems are called homopolymers in the following.

Smart microgels are the subject of a steadily growing number of publications in recent years [1, 2, 3], which were reviewed by different groups focusing e.g., on core-shell microgels [4, 5], copolymer microgels [6, 7, 8], soft nanotechnology [9, 10], or on nanoparticle carriers [11, 12, 13, 14, 15]. For example, the particle size and the thermal behavior of *N*-isopropylacrylamide (NIPAM) [16, 17] and *N*-isopropylmethacrylamide (NIPMAM) [18], depending on the initiator concentration, the reaction temperature and the cross-linker concentration, have been studied. However, to our knowledge, no systematic comparative study on monosubstituted acrylamides (NIPAM, NIPMAM, ...) exists, and the influence of their chemical structure on the particle formation and the thermoresponsive behavior of the resulting microgels. However, especially, these basic facts are very important to understand the formation of more complex systems like copolymer microgels or core-shell particles, which are suitable for a lot of different applications due to their smart behavior [19, 20]. For this purpose, the crucial point is a precise knowledge about the controllability of the microgel properties. Particularly, the particle size, the volume phase transition temperature (VPTT) as well as the shape of the phase transition curve is very important. The easiest way to understand the interplay between microgel properties, monomer structure and synthesis conditions is to study homopolymers at first.

In this contribution, we want to focus on homopolymer microgels based on NIPAM, NIPMAM and *N*-*n*-propylacrylamide (NNPAM). The influence of the monomer chemical structure on the microgel particle size, the morphology and the swelling behavior is studied and compared in detail. Generally, all synthesis have been performed as precipitation polymerisation without surfactant and under identical conditions to ensure a good comparability of the results. Besides imaging techniques and light scattering, the study of fluorescence probes inside the microgel is used to scrutinize the volume phase transition of the different microgels.

2.3 Materials and Methods

2.3.1 Chemicals

N-isopropylacrylamide (NIPAM; Sigma-Aldrich Chemie GmbH, Munich, Germany; purity 97 %) and *N*-isopropylmethacrylamide (NIPMAM; Sigma-Aldrich Chemie GmbH, Munich, Germany; purity 97 %) were purified by recrystallisation from hexane. The cross-linker *N,N'*-methylenebisacrylamide (BIS; Sigma-Aldrich Chemie GmbH, Munich, Germany; purity 99 %), the initiator ammonium persulfate (APS; Sigma-Aldrich Chemie GmbH, Munich, Germany; purity $\geq$ 98 %) and pyrene (Sigma-Aldrich Chemie GmbH, Munich, Germany; purity $\geq$ 99 %) were used without further purification. For all experiments, purified water from an Arium®pro VF system (Sartorius AG, Göttingen, Germany) was used.

N-n-propylacrylamide (NNPAM) was synthesized via a Schotten–Baumann reaction published by Hirano *et al.* [21]. For this reaction, acryloylchloride (Sigma-Aldrich Chemie GmbH, Munich, Germany; purity 98 %), *n*-propylamine (Fluka, Sigma-Aldrich Chemie GmbH, Munich, Germany; purity 99 %), triethylamine (Grüssing GmbH Analytika, Filsum, Germany; purity 99 %) and methylenchloride (p.a.) were used as received. The obtained monomer NNPAM was washed with $NaHCO_3$ (10 wt%) and dried over $MgSO_4$. After filtration, the solvent was evaporated and the product was distilled in vacuum (115 °C, 10 mbar).

2.3.2 Synthesis of the Homopolymer Microgels

The homopolymer microgels of NNPAM, NIPAM and NIPMAM were synthesized via conventional precipitation polymerization without surfactant. All synthesis were performed in a 250 mL three-neck flask equipped with a reflux condenser, mechanical stirrer and a nitrogen inlet. The monomer (11.05 mmol) and the cross-linker *N,N'*-methylenebisacrylamide (BIS) (5.4 mol% respective to the total monomer amount) were dissolved in 150 mL purified water and were heated up to 70 °C under continuous stirring and purged with nitrogen. After 1 h the polymerization was initiated by the addition of 1 mL of a 2.71 mM solution of APS and left to proceed for 4 h at 70 °C. After the reaction time, the solution was cooled to room temperature and stirred over night. For purification, all samples have been treated by five cycles of centrifugation, decantation and redispersion using purified water.

2.3.3 Scanning Electron Microscopy

SEM investigations were performed on a ESEM-FEG (Philips XL30, Eindhoven, Netherlands) with an acceleration voltage of 3 kV and working distances between 5 and 6 mm. For the sample preparation 50 µl of microgel solution ($c \sim 5 \times 10^{-4}$ wt%) were deposited on cleaned silicon wafers and dried at room temperature in air. The completely dried samples were sputtered (Bio-Rad Laboratories GmbH, Munich, Germany, model E5000) with a thin layer of gold ($\approx$ 3 nm) to increase the conductivity and the contrast in SEM. Before use, the Si wafers have been cleaned with ethanol and afterwards treated with oxygen plasma for 10 min. Then, for high purity, the wafers were additionally cleaned with a solution containing H_2O:NH_3:H_2O_2 in a ratio of 5:1:1 [22]. The particle diameters were analyzed using the program ImageJ (Wayne Rasband, National Institutes of Health, USA) [23].

2.3.4 Atomic Force Microscopy

The Atomic Force Microscopy (AFM) images were recorded using a Nanoscope III (Digital Instruments, now Brucker, Karlsruhe, Germany) working in tapping mode. The samples were prepared on cleaned silicon wafer which have been cleaned before as described in the cleaning procedure in Section 2.3.3. Fifty microlitres of microgel solution with a concentration of $c \sim 5 \times 10^{-4}\,\mathrm{wt\%}$) was deposited on the substrate and dried at room temperature in air. The used cantilevers were from Budget Sensors (Innovative Solutions Bulgaria Ltd., Sofia, Bulgaria) (Tap300Al-G) with a radius of $\leq$10 nm, a resonance frequency of about 300 kHz and a spring constant of 40 N/m.

2.3.5 Light Scattering

Photon Correlation Spectroscopy

For the dynamic light scattering experiments, two different setups were used. The angle dependent measurements were done using an ALV goniometer setup equipped with a multiple-τ digital correlator ALV-5000/E (ALV-Laser Vertriebsgesellschaft mbH, Langen, Germany) and an argon-ion laser (Spectra Physics Stabilite 2017, Newport Spectra-Physics GmbH, Darmstadt, Germany; λ = 514.5 nm) as light source. The temperature dependent measurements were performed at a constant scattering angle of 60 ° with a solid-state laser at λ = 661.4 nm (TOPTICA Photonics AG, Graefelfing, Germany). To detect the time-intensity-autocorrelation function in this second setup, an ALV-6010 multiple-τ correlator (ALV-GmbH, Langen, Germany) was employed. In every case, the sample temperature was adjusted using a temperature controlled decaline matching bath and all measurements were repeated at least three times. The concentration of the microgel solutions was below 0.001 wt% to avoid multiple scattering. The analysis of the measured autocorrelation functions was done by inverse Laplace transformation [24, 25] or with the method of cumulants [26, 27] and provides the mean relaxation rate $\overline{\Gamma}$ of the relaxation rate distribution function. From this, the translational diffusion coefficient D^{T} for diluted particle solution can be calculated via $\overline{\Gamma} = D^{\mathrm{T}} \cdot q^2$ with q as magnitude of the scattering vector ($q = 4\pi n/\lambda \cdot \sin(\theta/2)$, with λ being the wavelength of the used radiation, n the refractive index and θ the scattering angle). Furthermore, using the Stokes–Einstein relation, a calculation of the hydrodynamic radius R_{h} of the microgel particles is possible:

$$D^{\mathrm{T}} = \frac{k_{\mathrm{B}}T}{6\pi\eta R_{\mathrm{h}}}, \tag{2.1}$$

k_{B} is the Boltzmann constant, T the temperature during the measurement and η the corresponding viscosity of the solvent. For a correct evaluation of the obtained data, the values for the refractive index and the viscosity of water were corrected with respect to the measurement temperature [28].

Static Light Scattering

The static light scattering experiments were done applying an ALV/CGS-3 compact goniometer system with a helium-neon laser (JDSU 1145/P, JDS Uniphase Corporation, now Viavi Solutions INC ,Milpitas, USA; λ = 632.8 nm) and toluene as matching bath. The detected intensity of the scattered light for the sample, the solvent, and the

standard at different angles was corrected using the following equation (index i: sol = solvent, s = sample or sta = standard):

$$I_{i,\Theta} = \frac{CR_{i,\Theta} \cdot \sin(\Theta)}{I_{\text{laser}}}. \tag{2.2}$$

Here, $I_{i,\Theta}$ is the detected intensity at a scattering angle Θ , I_{laser} is the incident laser intensity (measured via an additional monitor diode) and $CR_{i,\Theta}$ the measured count rate at the detector. To scale all measured scattering intensities to absolute values $I_{\text{abs},\Theta}$, Equation (2.3) is used, where $I_{\text{s},\Theta}$, $I_{\text{sol},\Theta}$, and $I_{\text{sta},\Theta}$ are the corrected values from Equation (2.2). $R_{\text{sta},\Theta}$ is the Rayleigh ratio of the standard, n_{sol}, and n_{sta} are the refractive indices.

$$I_{\text{abs},\Theta} = \frac{I_{\text{s},\Theta} - I_{\text{sol},\Theta}}{I_{\text{sta},\Theta}} \cdot R_{\text{sta},\Theta} \cdot \left(\frac{n_{\text{sol}}}{n_{\text{sta}}}\right)^2. \tag{2.3}$$

Additionally, the intensity $I_{\text{abs},\Theta}$ was corrected with respect to the back reflection of the laser beam at the glas/solvent interface. Therefore, the intensity $I_{180-\Theta}$ at a scattering angle of 180 ° and the reflection coefficient r of solvent/borosilicate is used:

$$I_{\text{refl.corr},\Theta} = I_{\text{abs},\Theta} \cdot \left(\frac{1 - 2 \cdot r \cdot \frac{I_{180-\Theta}}{I_{\text{abs},\Theta}}}{(1-r)^2}\right). \tag{2.4}$$

2.3.6 Turbidity Measurements

The light attenuation in microgel solutions is generally caused by the scattering of light by the dispersed particles. For large particles (size of the order of the wavelength of light), and when the particle interior is optically very different from the surrounding medium, the Rayleigh–Debye–Gans (RDG) approximation is no longer valid [29]. A criterion to judge the validity of RDG approximation is given by:

$$\frac{4\pi}{\lambda} R|m-1| \ll 1. \tag{2.5}$$

Here, R is the radius of the particle, m is the ratio between the refractive index inside and outside the particle and λ the wavelength of the used radiation. In the case of our homopolymer microgels, the effective refractive index at low temperatures (swollen particles) is sufficiently low, and, therefore, the Rayleigh–Debye–Gans approximation holds in this present case [30]. In contrast to this, at high temperatures (collapsed particles), the refractive index of the microgel is different compared to that of water ($n = 1.46$ [30]) and the experimental data would have to be described by a Mie calculation for a homogeneous sphere. This is relevant in the data treatment of SLS, but not for the turbidity measurements where only the intensity of the transmitted light I_{T} at an angle of 180 ° is analyzed. However, in the present work, we only studied the swollen particles by static light scattering (SLS) and the RDG approximation holds.

Hence, in the turbidity measurement, the scattering from the particles is a combination of differences in the refractive index (between particles and solvent) and of the particle size. Summarizing all processes, the incident light intensity I_0 is reduced by scattering (S) and by absorption (A) and for the measured transmitted intensity I_{T} the following equation holds:

$$I_T = I_0 - I_S - I_A. \tag{2.6}$$

For microgels, the absorption I_A is negligible and the decrease of the transmitted intensity is nearly exclusively caused by scattering processes. For a quantitative description of the intensity of the transmitted light, the Lambert–Beer law at low sample concentrations can be used. D_λ is the light attenuation, c the sample concentration, d the thickness of the measurement cell and δ_λ the attenuation coefficient:

$$D_\lambda = \lg\left(\frac{I_0}{I_T}\right) = \delta_\lambda \cdot c \cdot d. \tag{2.7}$$

During the volume phase transition of microgel particles, the light attenuation D_λ changes due to a reduction in particle size and a simultaneous increase of the refractive index. This characteristic behavior can be followed by UV/Vis spectroscopy [31, 32, 33, 34]. Therefore, light of one wavelength is focused on the sample and the intensity of the transmitted light at an angle of 180 ° at different temperatures is detected. For a better comparison of the phase transition of different microgel solutions the light attenuation D_λ is normalized to the sample concentration (in wt%) and the thickness of the cuvette (1 cm), and the normalized attenuation coefficient δ_λ is given by:

$$\delta_\lambda = \frac{D_\lambda}{c \cdot d}. \tag{2.8}$$

For the turbidity measurements, a UV-Visible spectroscopy system (Agilent 8453, Agilent Technologies Deutschland GmbH, Ratingen, Germany) with a sample changer with 8 positions was used and the attenuation at a wavelength of 700 nm was analyzed. To measure the temperature dependent swelling behavior of the microgels, a constant heating rate of 3 °C/h was chosen and the turbidity was detected every 30 s. For a good signal to noise ratio, the concentration of the samples was set between 0.0015 wt% and 0.25 wt%.

2.3.7 Fluorescence Measurements

The fluorescence experiments were performed with a FP-8300 spectrometer from Jasco (Jasco Labor- u. Datentechnik GmbH, Groß-Umstadt, Germany) equipped with a Peltier temperature controlled sample holder for 4 samples. The temperature equilibration time was 10 min for each sample and the excitation/emission bandwidth was 2.5 nm. The excitation of pyrene was carried out at 336 nm and the fluorescence signal was detected in a range from 350 up to 500 nm with an accuracy of 0.5 nm. For the measurements microgel solutions with concentrations between 0.01 wt% and 0.1 wt% were mixed with a saturated pyrene solution ($c_{\text{Pyrene}} \approx 6\ \mu\text{M}$) and measured in 10 mm quartz Hellma cells.

2.4 Results and Discussion

2.4.1 Imaging Techniques

The three different homopolymer microgels were deposited on Si-wafers, sputtered with a thin layer of gold and imaged by scanning electron microscopy (SEM) as represented in Figure 2.1. The diameters of the particles were graphically analyzed leading to the size distributions displayed below the SEM images. It is clearly observable that the polydispersities of the microgel particles are very low in all cases. Table 2.1 gives the averaged particle diameters $\overline{D}_{\mathrm{SEM}}$ and the respective standard deviation obtained from the half width at half height of the distributions shown in Figure 2.1.

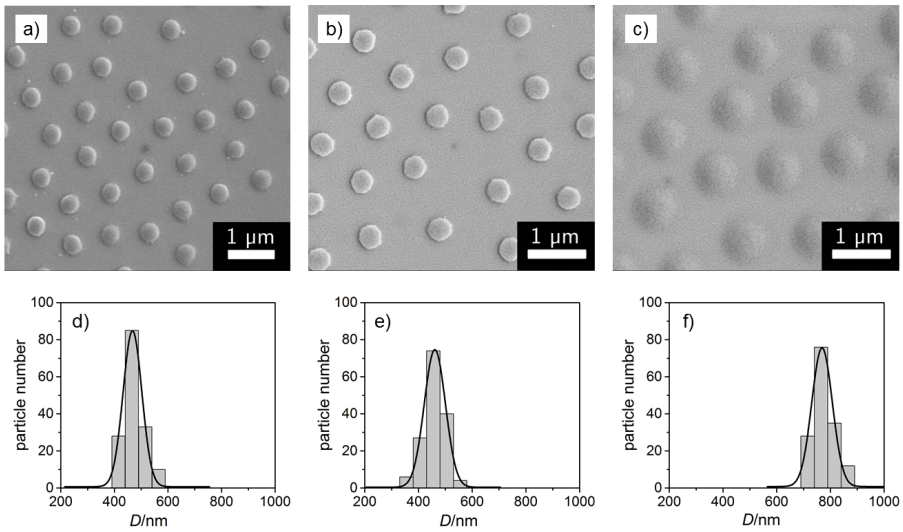

FIGURE 2.1: SEM images of the homopolymer microgels of **a**) NNPAM, **b**) NIPAM and **c**) NIPMAM synthesized without surfactant and the corresponding size distributions (**d**–**f**). The black lines represent a Gaussian distribution function.

The corresponding height images of the three homopolymer particles observed by atomic force microscopy (AFM) using tapping mode are represented in Figure 2.2, and a summary of the obtained diameters $\overline{D}_{\mathrm{AFM}}$ are also given in Table 2.1. From the pictures, it is clear that both methods prove the low polydispersity of the particles. However, a direct comparison of the measured particle radii reveals differences in size for NNPAM and NIPAM depending on the imaging techniques which is used, while, for NIPMAM, the results match within the experimental error (see Table 2.1).

TABLE 2.1: Particle diameters obtained by AFM and SEM. Additionally, the relationship of the diameters to each other was calculated.

Microgel	$\overline{D}_{\mathrm{SEM}}$**/nm**	$\overline{D}_{\mathrm{AFM}}$**/nm**	$\overline{D}_{\mathrm{SEM}}/\overline{D}_{\mathrm{AFM}}$
NNPAM	467 ± 83	790 ± 71	0.59
NIPAM	461 ± 90	776 ± 79	0.59
NIPMAM	769 ± 90	786 ± 89	0.98

The effect of the size differences can be caused by the network structure of the microgel particles in combination with substrate interactions and the way the images

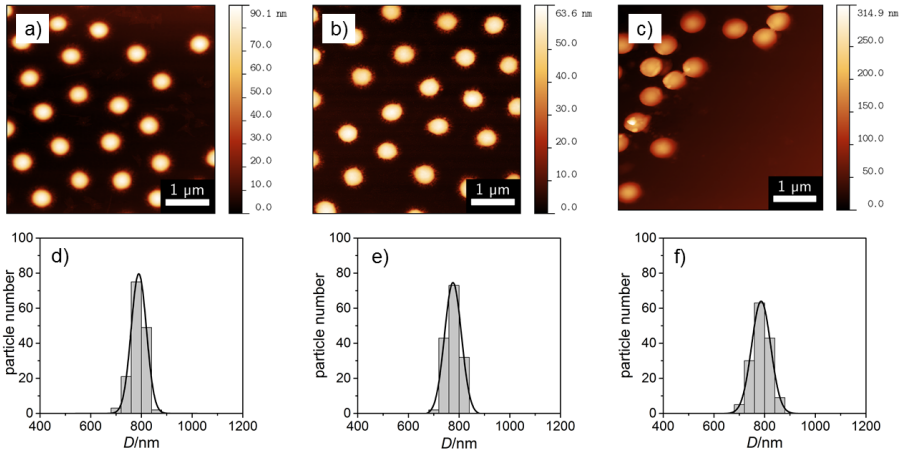

FIGURE 2.2: AFM images of the homopolymers of (**a**) NNPAM, (**b**) NIPAM and (**c**) NIPMAM synthesized without surfactant and the corresponding size distributions (**d**–**f**). The black lines represent a Gaussian distribution function.

are taken. In short, it is known that most acrylamide microgels exhibit an inhomogeneous distribution of the cross-linker due to a different polymerization rate of BIS in contrast to the acrylamide monomers. Therefore, a BIS-gradient from a more dense core to a less cross-linked shell is observed [35, 36, 37, 34]. If these microgels are now deposited on a Si-wafer as substrate, the soft particles change their size due to the drying process required for AFM and SEM. This results in a stiff core area (similar to a hard sphere) and a thin, flat and less cross-linked outer shell. Depending on the characteristics of the cross-linker gradient and on the imaging technique it is not possible to resolve all parts of the microgel particle. With SEM the thin fuzzy shell could not be monitored (but the core) and the particles appear to be smaller than in reality. In contrast to this, with AFM, it is possible to image very thin samples. Hence, it can be assumed that NIPAM and NNPAM consist of a more dense core and a less cross-linked shell while NIPMAM form more homogeneous microgel particles. A more detailed analysis of the AFM height images of all three homopolymer particles shows that, for all microgels, the diameter is nearly the same, while for PNIPMAM, a larger vertical dimension is measurable (see Figure 2.3). This can be caused by different effects like interactions with the substrate, the stiffness of the microgels or even the molecular weight of the particle. However, unfortunately at this point, the method does not clarify if the particles comprise a core-shell structure or not.

From the AFM measurements, it is also possible to obtain the phase images which contain information on the rigidity of the material of observation [38]. Therefore, a core-shell particle with different degrees of rigidity of the core and the shell should be clearly identifiable. These phase images of the three homopolymer microgels are presented in Figure 2.4.

These images reveal the presence of a defined core-shell structure in the case of the PNNPAM and PNIPAM microgels (with a higher rigidity in the inner area of the particles), whereas for PNIPMAM, a more homogeneous structure is observed. A calculation of the inner diameter on the basis of the AFM phase images yields a value of 483 nm for PNNPAM and 461 nm for PNIPAM, which is in good agreement with the results from the SEM measurements (see Table 2.1). Analyzing the phase image of PNIPMAM results in a nearly uniform rigidity for the whole particles, and, as a consequence, these particles seem to consist of a weakly but rather

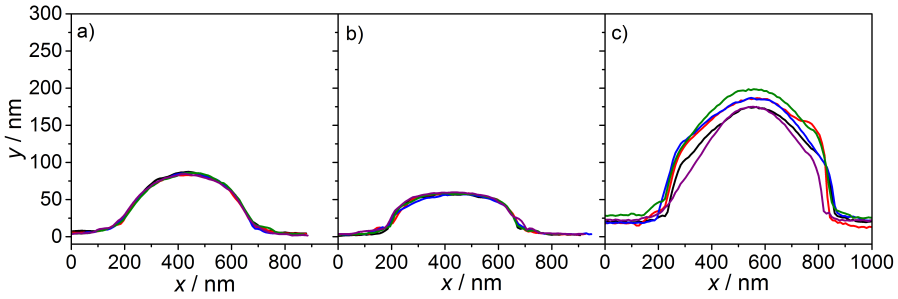

FIGURE 2.3: From left to right: height profiles of (**a**) NNPAM, (**b**) NIPAM and (**c**) NIPMAM homopolymer microgels obtained from AFM measurements in tapping mode. Each line represents one microgel particle of the same sample. The samples are characterized in the dried state.

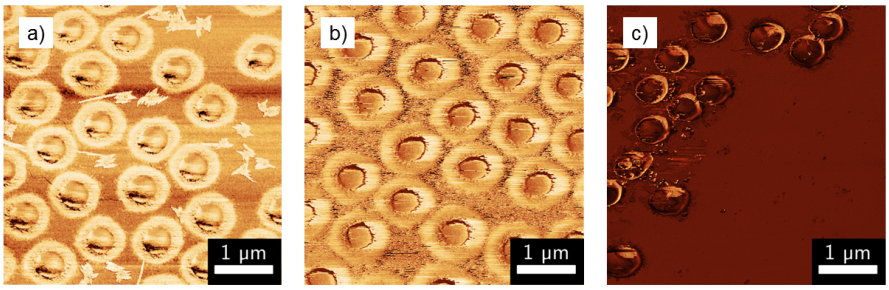

FIGURE 2.4: Phase images of **a**) PNNPAM, **b**) PNIPAM and **c**) PNIPMAM homopolymer microgels obtained from AFM measurements.

homogeneously cross-linked network. However, it has to be mentioned here that the imaging techniques AFM and SEM provide only a rough indication of the structure of the particles and that the microgels are only characterized with these methods in the dried state. Therefore, additional techniques to study the homopolymer particles in bulk solution have to be used.

2.4.2 Static Light Scattering (SLS)

To obtain information about the microgel solution structure, static light scattering experiments at a temperature of 15 °C and in an angular range from 15 ° to 155 ° were performed. The low measurement temperature was chosen to ensure that all polymer particles are in the totally swollen state since the lower critical solution temperature (LCST) of PNNPAM is about 21 °C. In Figure 2.5a, the absolute scattering intensities as a function of the scattering vector q and the corresponding fits are illustrated.

A quantitative analysis of the scattering curves was done by using a homogeneous sphere form factor [39] as well as a fuzzy sphere form factor (Equation (2.9)) [17]. The homogeneous sphere model does not properly describe the intensity of the first resolved form factor maximum, whereas the latter model is in very good agreement with the experimental data (see Figure 2.5a). As an example for the differences in the two form factor models, the scattering curves of PNIPMAM with the fits obtained by the homogeneous and the fuzzy sphere model are shown in Figure 2.5b. To take the size polydispersity of the particles into account, a Gaussian distribution function for the radius R is assumed [17]:

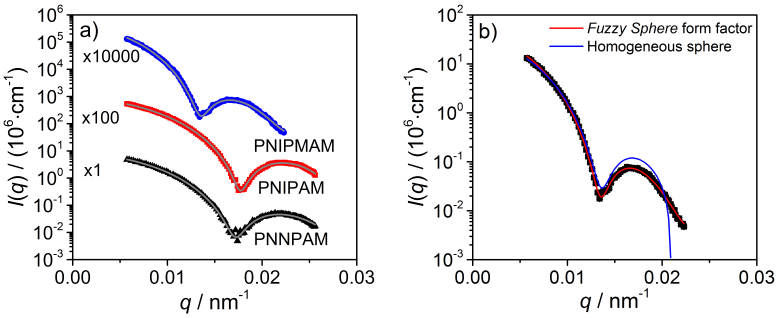

FIGURE 2.5: Plot of the absolute scattering intensities vs. the scattering vector q of PNNPAM, PNIPAM and PNIPMAM at 15 °C and the corresponding fit with the fuzzy sphere model (**left**) [17]. For a better representation of the experimental data, the intensity values were shifted along the y-axis. Comparison of the homogeneous [39] and the fuzzy sphere form factor model on the example of PNIPMAM (**right**).

$$[H]P(q)_{\text{fuzzy sphere}} = \left[\frac{3(\sin(qR) - qR\cos(qR)}{(qR)^3} \cdot \exp\left(-\frac{(\sigma q)^2}{2}\right)\right]^2 \tag{2.9}$$

The fuzzy sphere model describes a microgel particle with two different zones. The polymer density distribution of an inner area (core) can be described by means of a radial boxprofile with the radius $R_{\text{box}} = R - 2\sigma$. The outer zone (shell) is described by an exponential density gradient. At the radius R, the polymer density of the core is reduced to one half and σ takes the cross-linking gradient into account. From the static light scattering experiment in combination with the fuzzy sphere model, the radius of the whole particle with $R_{\text{particle}} = R + 2\sigma = R_{\text{box}} + 4\sigma$ is available, and, accordingly, the σ-value in this equation provides information on the inhomogeneity of cross-linking (low σ: homogeneous sphere; high σ: strong gradient).

From the experimental data and the obtained values from the fits (see Table 2.2), it is clear that all microgel particles exhibit an inhomogeneous density distribution which is in agreement with other results from literature for PNIPAM [17, 40] and PNIPMAM [41]. The form factor minimum at q_{min} for PNNPAM and PNIPAM is nearly at the same position (q = 1.73 $\times 10^{-2}$ nm^{-2}/1.77 $\times 10^{-2}$ nm^{-2}), which indicates that the particles have the same size. The q_{min} value for PNIPMAM is shifted to smaller q-values (1.35 $\times 10^{-2}$ nm^{-2}), and, therefore, the particle size is increased compared to the others. The other obtained parameters from the fuzzy sphere model for the radius of the homopolymer microgels, the polydispersity and the σ-value, are summarized in Table 2.2.

TABLE 2.2: Results from the fit of the experimental static light scattering (SLS) data from the homopolymer microgels with the fuzzy sphere form factor model.

Microgel	$q_{\text{min}}/(10^{-2}nm^{-2})$	R_{particle}/nm	PD_{particle}/%	σ/nm
NNPAM	1.73	300	5.2	20
NIPAM	1.77	284	6.8	16
NIPMAM	1.35	464	5.6	67

Notably, the homopolymer particles differ in size, although they have been prepared under identical conditions. The obtained diameter for PNNPAM and PNIPAM is nearly the same (300 nm/284 nm), while PNIPMAM deviates (464 nm). This can be explained by the differences in the molecular structure of the monomers and hence with their polymerization rate (connected to the amount of precursor particles build in the first step of the emulsion polymerization). NIPMAM has an additional methyl group at the growing polymer radical and due to hyperconjugation a positive inductive effect (+I - effect) causes a stabilization of the radical end. Therefore, the growing polymer radical of NIPMAM is more stable in contrast to the radical of NIPAM and NNPAM. Consequently, a lower amount of precursor particles is formed at the beginning of the polymerization and the resulting particles are larger at the end.

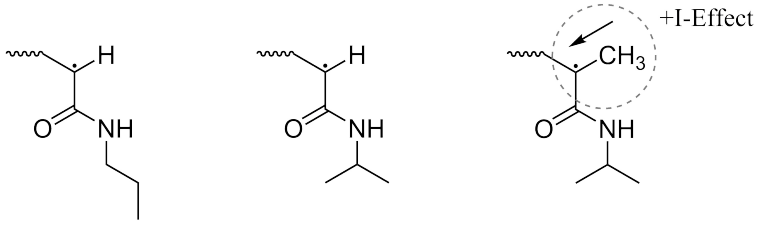

FIGURE 2.6: Structural formulas of the various acrylamide radicals during polymerisation (left to right: NNPAM, NIPAM and NIPMAM). In NIPMAM, the radical is stabilized by the methyl group and its positive inductive effect, whereby the polymerization rate is reduced.

The σ value obtained from the fuzzy sphere analysis of the SLS measurements (see Table 2.2 last column) yields an indication about the density gradient inside the different homopolymer microgels. From this, a comparison of the whole particle radius R_{particle} in contrast to the compact core radius from the boxprofile R_{box} is possible. In the case of PNNPAM and PNIPAM the core engross nearly 75% of the particle while for PNIPMAM it's only about 42%. Therefore, three quarters of the PNNPAM and PNIPAM particles are densely cross-linked in the core region and exhibit a strong cross-linker gradient in a small outer shell. This core-shell structure matches with the results from the AFM measurements under the limitation in AFM the microgels are in the totally collapsed state. For the microgel based on PNIPMAM, there exists a smaller core area and the shell with a continuous, rather flat cross-linker gradient, is more pronounced. This is in line with the AFM phase images which show no rapid change in rigidity for these microgel particles.

But why are these particles so differently cross-linked? The reason for this is the difference in the polymerization rates for the cross-linker BIS in combination with the different acrylamide monomers. In the case of NIPMAM, the cross-linker is mainly consumed at the beginning of the polymerization and builds oligomers without a temperature sensitivity. Afterwards, due to the low polymerization rate of NIPMAM, oligomers (and later particles) of this monomer with a low amount of BIS are formed, leading to lowly cross-linked microgel particles. The pre-build BIS-oligomers might later absorb to the growing PNIPMAM microgel due to hydrophobic interactions and maybe incorporated in the microgel network. The disadvantage of this oligomer/polymer building sequence is that a high amount of

water-soluble polymer, which is not incorporated in the microgel particles, is generated. This assumption was confirmed by analyzing the amount of residual water-soluble polymer after the purification (centrifugation) of the microgel particles. Using NIPMAM/BIS as monomers, nearly 50% of the generated polymer is not part of the obtained microgel particles. For NNPAM and NIPAM, the amount of side-product is between 10% and 19%. Thus, during the formation of the NIPMAM particles compared to NNPAM and NIPAM, a significantly smaller amount of the monomer is used and the cross-linking density deviates strongly between the different homopolymer microgels.

2.4.3 Swelling Behavior

Photon Correlation Spectroscopy (PCS)

In a typical experiment, the particle motion in solution is analyzed and from this the particle size can be calculated [29] if only translational diffusion is observed. To ensure that this is the case, angle dependent PCS measurements of the microgels in the swollen and collapsed state have been performed (PNNPAM: 15 °C and 40 °C; PNIPAM: 20 °C and 50 °C; PNIPMAM: 30 °C and 60 °C) and the obtained mean relaxation rates $\overline{\Gamma}$ were plotted against q^2. The analysis of the autocorrelation function was done by inverse Laplace transformation (CONTIN) and also by the cumulant method. The results obtained from both methods were the same. Hence, only the values from CONTIN are presented in the following. As an example, the relaxation rate distribution of the collapsed homopolymer microgels at a q-value of 1.63 $\times 10^{-2}$ nm^{-1} is illustrated in Figure 2.7a.

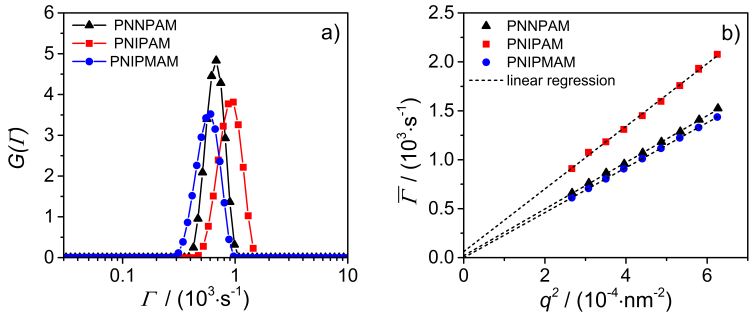

FIGURE 2.7: (**a**) PCS relaxation rate distribution of the collapsed homopolymer microgels; (**b**) Plot of the mean relaxation rate $\overline{\Gamma}$ vs. q^2 and the corresponding linear regression to determine the translational diffusion coefficient D^T.

It is clearly visible that all microgel samples show a monomodal relaxation rate distribution with a narrow full width at half maximum. Both facts confirm the presence of only one particle species with a low polydispersity. Therefore, the results are in good agreement with those from the imaging techniques. An analogous behavior was found for all particles in the swollen and collapsed state at all scattering angles. Plotting the relaxation rate as a function of the magnitude of the scattering vector q^2 results in a linear dependence which can be fitted by a line through the origin (see Figure 2.7b). Hence, the monitored dynamic of the system is only translational diffusion of the particles and from the slope of the linear fit the translational diffusion coefficient can be calculated. Using the Stokes–Einstein equation (see Equation (2.1)), the hydrodynamic radius of the microgels was determined and the results are summarized in Table 2.3. R_h for the swollen and collapsed PNNPAM

and PNIPAM microgels, respectively, are identical within the experimental precision. In contrast, the value for PNIPMAM particles differs clearly. This is in good agreement with the results from the SLS experiments.

From the particle size, the maximum swelling ratio α_{max} according to Equation (2.10) can be calculated. In Equation (2.10), V_{swollen} and $V_{\text{collapsed}}$ represent the particle volume in the swollen and collapsed state, respectively. Based on the assumption that the microgel particles are spherical, the swelling ratio α_{max} is given by:

$$\alpha_{\text{max}} = \frac{V_{\text{swollen}}}{V_{\text{collapsed}}} = \frac{R^3_{\text{h,swollen}}}{R^3_{\text{h,collapsed}}}. \tag{2.10}$$

TABLE 2.3: Summary of the hydrodynamic radii of the homopolymer microgels in the swollen and collapsed state in combination with the maximum swelling ratio α_{max}. The error of the radii corresponds to an estimated deviation of 5 %. This value includes not only the inaccuracy of the measurement but also the very low polydispersity of the sample.

Microgel	$R_{\text{h,swollen}}$ **/nm**	$R_{\text{h,collapsed}}$ **/nm**	α_{max}
NNPAM	291 ± 15	146 ± 7	7.9 ± 1.7
NIPAM	297 ± 15	139 ± 7	9.8 ± 2.1
NIPMAM	431 ± 22	211 ± 11	8.5 ± 1.8

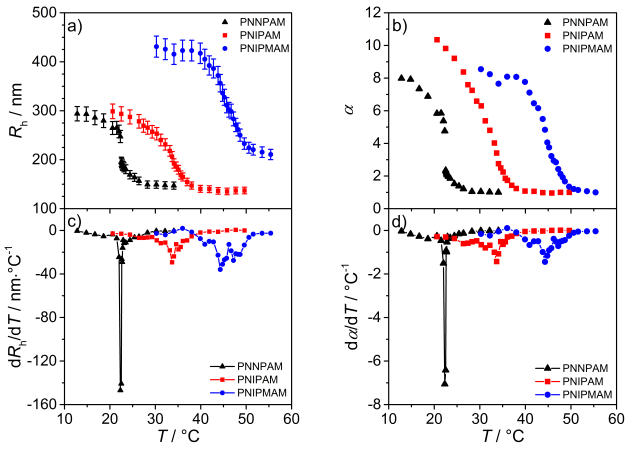

FIGURE 2.8: The swelling curves show the change of the microgel hydrodynamic radius (**a**) and the swelling ratio α (**b**) as a function of temperature for all three homopolymers. The graphs (**c**) and (**d**) represent the numerically calculated first derivative of the swelling curves. The point of inflection is the volume phase transition temperature (VPTT) of the system.

To characterize the thermoresponsive behavior of the homopolymer microgels and to determine the VPTT, temperature dependent measurement of the hydrodynamic radius were additionally performed. The respective swelling curves of the homopolymer particles are illustrated in Figure 2.8a. In general, with increasing temperature the solubility of the acrylamide polymer network decreases and as a consequence the network collapses and the particle size is reduced. To determine the VPTT, an analysis of the point of inflection of the swelling curves was

performed. For this purpose, the curves were first numerically differentiated (Figure 2.8c) and then the maximum of the derivative was determined. The obtained values for the VPTT are 22.3 °C for PNNPAM [42, 43, 44, 45], 33.7 °C for PNIPAM [46, 47, 48, 49, 50, 51, 52], 44.3 °C for PNIPMAM [31, 19, 18, 53, 54, 55, 56] and are in good agreement with literature.

Further comparison of the homopolymer swelling curves or, rather, of the phase transition width shows that PNNPAM particles exhibit a sharper transition than the other two microgels. In a temperature range of 1 °C (for PNNPAM between 22 and 23 °C) the hydrodynamic radius of the particles changes by about 48 % with respect to the maximum volume. In the case of PNIPAM and PNIPMAM, the values are significantly smaller with 16 % and 13 %. Due to the fact that the PNIPMAM particles are generally larger than those made of PNNPAM and PNIPAM, the swelling ratio α was used for a more detailed comparison. Therefore, in Equation (2.10) $R_{\mathrm{h,swollen}}$ was replaced by $R(T)_{\mathrm{h}}^3$ which is the hydrodynamic radius at a given temperature. The calculated values for α as a function of temperature and the corresponding first derivatives are shown in Figure 2.8b,d.

The α *vs.* temperature curves are very similar compared to the swelling curves, and the significant difference in the phase transition width is also clearly visible in the numerical derivatives. Here, the maximum value for PNNPAM is significantly increased compared to PNIPAM and PNIPMAM. Furthermore, the temperature range in which the phase transition occurs is very small. Thus, the transition behavior of homopolymers based on NNPAM can be nearly described by a discontinuous phase transition. It should be mentioned that this sharp phase transition was also observed by Inomata *et al.* for PNNPAM macrogels [43].

The differences in the transition width can be explained by either the cross-linker distribution in the network or by the chemical structure of the used monomers. As discussed earlier (see section AFM and SLS), a pronounced cross-linker gradient in the microgel particle would result in a sharp phase transition due to the simultaneous and fast collapse of a weakly cross-linked shell. However, as confirmed by AFM and SLS, there is no significant difference between the homopolymer microgels of NNPAM and NIPAM regarding the cross-linker distribution but as confirmed by PCS these particles show a different phase transition behavior. Therefore, a strong influence of the monomer chemical structure is likely. Here, the alkyl side chain is similar for NIPAM and NIPMAM (branched isopropyl group) and differs from the linear *n*-propyl group of NNPAM. It is reported in literature that the phase behavior of linear polymers based on NIPAM [54] and NNPAM [57] also differ from each other. In short, the results show that for PNIPAM the second virial coefficient decreases continuously at the Θ-temperature (calculated from SLS measurements) in a range of 8 °C, while, for PNNPAM, the change is more discontinuous. Furthermore, the aggregation behavior of linear polymer chains of NIPAM and NNPAM at the Θ-temperature is different (determined by the hydrodynamic radius (PCS) and the radius of gyration (SLS)). For PNNPAM, the chain aggregation occurs directly at the Θ-temperature. Contrarily, PNIPAM shows a continuous decrease in size until a temperature of nearly 32 °C is reached. According to Ito *et al.* [57] and Kano *et al.* [42] different structural effects cause the sharper phase transition of PNNPAM: the *n*-propyl side chain is more flexible than the isopropyl group and a change in chain conformation at the transition temperature is more likely to occur. This flexibility of the *n*-alkyl chain additionally favors the breakup of hydrogen bonds between the solvent and the amide group of the monomer. All in all the chemical structure of the three monomers used here, play an important role with respect to the phase transition behavior of the synthesized homopolymer microgel particles.

To verify the temperature dependent phase behavior observed from the light scattering experiments, turbidity and later fluorescence measurements have also been performed and subsequently compared with the results above.

Turbidity Measurements

For the following light attenuation measurements, a relatively slow temperature ramp of $3\,^{\circ}\mathrm{C/h}$ in combination with a fast single-measurement time (less than one second) was chosen to ensure that at any time of the measurement the microgel particles are in the equilibrium state. With this special method, it is possible to obtain, at the same time, a higher amount of data points compared to common light scattering experiments. Therefore, a precise analysis and evaluation of the phase transition of the different homopolymer microgels is possible.

First of all, the light attenuation D_{700} as a function of temperature at a wavelength of $700\,\mathrm{nm}$ was measured. Before normalizing D_{700} with respect to the microgel concentration and the thickness of the cuvette (see Equation (2.8)), it has to be confirmed that the light attenuation is independent of the sample concentration. Therefore, UV/Vis measurements of the homopolymer microgels at different concentrations (between 0.0015 wt% and 0.0750 wt%) were performed and a plot of D_{700} as a function of concentration resulted in a line through origin which confirms the validity of the Lambert-Beer law. Hence, the normalized light attenuation δ_{700} can be calculated and is further used for a direct comparison between the different homopolymer microgels in solution. In Figure 2.9, the swelling curves of PNIPAM, PNNPAM and PNIPMAM homopolymers are shown.

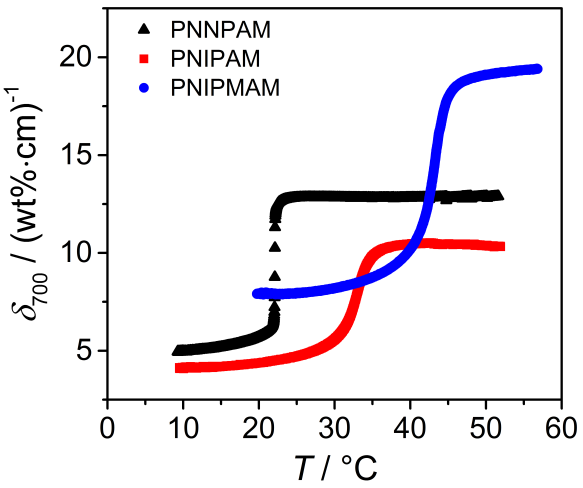

FIGURE 2.9: Normalized light attenuation δ_{700} at $\lambda = 700\,\mathrm{nm}$ for PNNPAM (**black curve**), PNIPAM (**red curve**) and PNIPMAM microgels (**blue curve**) as a function of temperature measured by UV/Vis spectroscopy

At the VPTT, all microgel systems show an increase in the attenuation coefficient δ_{700}, which is mainly caused by the change in refractive index as described in the theory section. Remarkably, the δ_{700} value at all temperatures for PNNPAM is slightly higher than for PNIPAM although the particles nearly have the same size. Therefore, the polymer based NNPAM exhibits a higher refractive index than PNIPAM. The strong deviation of PNIPMAM from the other two homopolymers is also very pronounced in the turbidity measurements, which is in line with the results from

the other characterization methods. Here, the effect is mainly caused by the particle size (R_{particle} from the SLS measurements: swollen state: PNNPAM/PNIPAM $\approx$ 300 nm/284 nm; PNIPMAM $\approx$ 464 nm). Additionally, the PNNPAM microgel shows a sharper phase transition compared to PNIPAM and PNIPMAM, which was also observed in the light scattering experiments. From the high amount of data points observed by this measurement technique, a more detailed analysis of the phase transition and the determination of the VPTT is possible. The temperature dependent light attenuation coefficients are first numerically differentiated, and the numerically obtained derivative is subsequently fitted with an asymmetric Lorentz function [20, 58]:

$$\frac{\mathrm{d}\delta_\lambda}{\mathrm{d}T} = \frac{2a}{\pi w(T)} \cdot \frac{1}{1+4[(T-\mathrm{VPTT})/w(T)]^2} \tag{2.11}$$

$$\text{with} \quad w(T) = \frac{2w_0}{1+\exp[B(T-\mathrm{VPTT})]}.$$

In these equations, a represents the peak area, w_0 the full width at half maximum, and B stands for the asymmetry of the function. At a value of zero for B, a symmetric Lorentz function can be obtained. The results from the analysis of the first derivative of the light attenuation curves and the corresponding asymmetric Lorentz fits are shown in Figure 2.10. To provide a clearer presentation of the PNIPAM and PNNPAM data, the curves are enlarged in the relevant temperature region (see Figure 2.10b). The obtained values of the transition temperature and the full width at half maximum w_0 are listed in Table 2.4.

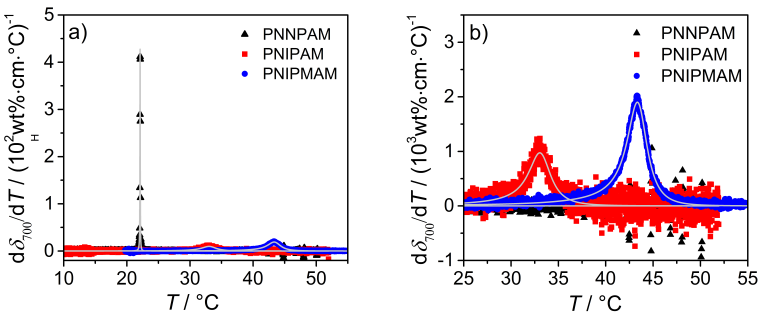

FIGURE 2.10: Analysis of the phase transition of PNNPAM, PNIPAM and PNIPMAM microgels using UV/Vis spectroscopy. (**a**) first derivative of the light attenuation coefficients with respect to temperature as a function of temperature; (**b**) detailed image of the temperature range between 25 °C and 55 °C relevant for PNIPAM and PNIPMAM particles.

The VPTT of the homopolymer microgels are in good agreement with the values from the light scattering experiments. It is notable that the microgel based on NNPAM generally exhibits a steeper phase transition compared to the other two polymers. This fact is clearly visible in the UV/Vis spectra and also in the PCS measurements.

Afterwards, the curves of the phase transition have been numerically differentiated and fitted by the asymmetric Lorentz function from Equation (2.11). The calculated values for the VPTT and w_0 as a function of the microgel concentration are summarized in Figure 2.11c,d. It is clearly visible that both parameters are independent of the concentration. Only for PNIPAM at the lowest concentration of 0.0015 wt%, a slight deviation of w_0, is recognizable. This is due the low signal during the phase

TABLE 2.4: Volume phase transition temperatures of the homopolymer microgels obtained by turbidity measurements. w_0 is the full width at half maximum of the phase transition peak from the Lorentz approximation.

Microgel	**VPTT/°C**	w_0/°C
NNPAM	22.1 ± 0.1	0.06 ± 0.01
NIPAM	33.0 ± 0.1	3.12 ± 0.01
NIPMAM	43.2 ± 0.1	2.70 ± 0.01

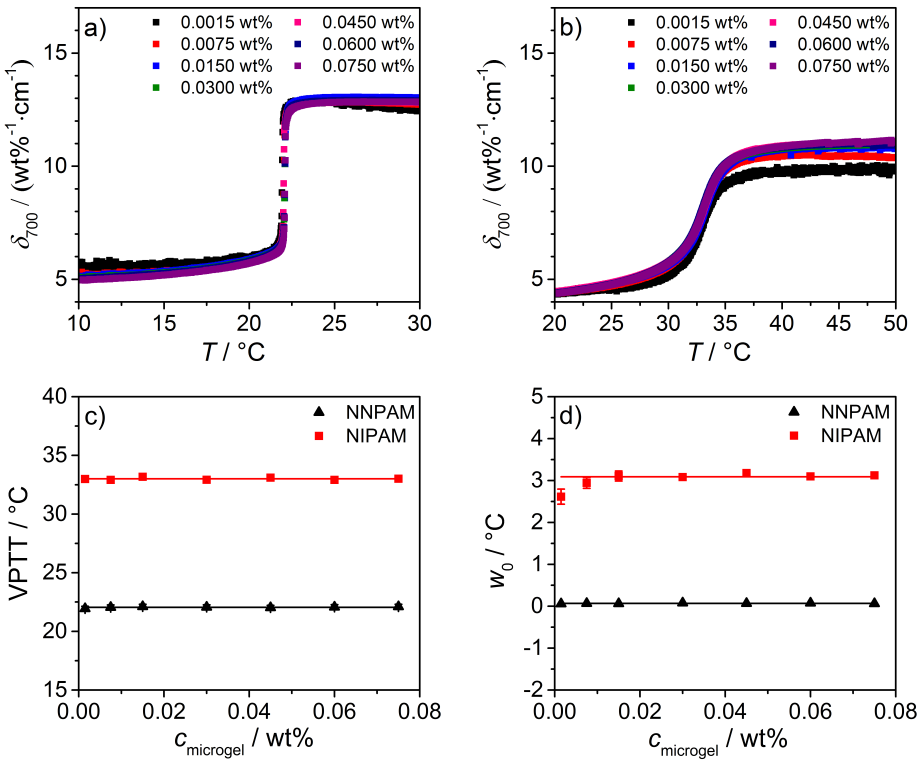

FIGURE 2.11: Normalized light attenuation coefficients for PNNPAM (**a**) and PNIPAM (**b**) microgels solutions with different concentrations as a function of temperature (λ = 700 nm). In graphs (**c**) and (**d**), a summary of the VPTTs and the w_0-values for both microgels as a function of sample concentration is given. The solid lines correspond to the average value. It has to be mentioned that for PNIPAM the first w_0-value (0.0015 wt%) has been neglected.

transition and the corresponding low change in the δ_{700} value. Therefore, the respective data point in the plot of w_0 *vs.* c_{microgel} was neglected for the estimation of the average value.

The presented concentration dependent measurements show that the light attenuation and PCS experiments with respect to the phase transition behavior, the VPTT, and w_0 are in good agreement. Therefore, the attenuation measurement is well suited for the evaluation of the phase behavior of different microgel solutions and is a good alternative to PCS.

Fluorescence Measurements

Until now, the phase transition behavior of the homopolymer microgels has been characterized by PCS experiments (changes in the hydrodynamic properties) and by turbidity measurements (changes in the scattering ability). But these two methods provide no information on the processes occurring on a molecular level inside the microgel particle. One possibility to obtain knowledge about the interior of the colloidal gel particles is to investigate polarity changes during the phase transition. For this purpose, the homopolymers have been dispersed in a saturated solution of pyrene and the phase behavior was followed by fluorescence spectroscopy. To our knowledge, this technique was not yet applied to study the volume phase transition of thermoresponsive microgels. However, the swelling behavior of a NIPAM-dye copolymer system, where the dye molecule is covalently bound to a linear PNIPAM chain, was investigated by Matsumura [59].

After illumination of a pure pyrene solution with light of a wavelength of $355\,\text{nm}$, four characteristic fluorescence bands can be found. Here, the intensity ratio of I_1 at an emission wavelength of $372\,\text{nm}$ to I_3 at $382\,\text{nm}$ depends on the polarity of the environment. According to Kalyanasudaram *et al.* [60], the absolute value I_1/I_3 can therefore serve as a direct measure of the environment polarity. Generally, if the value I_1/I_3 is high, the polarity is high and the environment is more hydrophilic. However, the work of Kalyanasudaram is based on different pure solvents with varying polarities where only the solvent molecules define the environment polarity. In the case of a microgel solution, not only the solvent contributes to the overall polarity of the system but also the polymer. Here, part of the dissolved pyrene molecules can be outside of the microgel particles (surrounded by pure solvent) and another fraction of the pyrene is localized inside the gel network and the hydrophilic/hydrophobic character of the polymer chains also contributes. Therefore, the measured intensity ratio I_1/I_3 will be always an average of both contributions. In responsive microgels based on acrylamides, the hydrophobic properties increase during the phase transition and so pyrene and the intensity ratio I_1/I_3 of the fluorescence bands can be used as a sensor to follow the local polarity inside the particles during the phase transition [33, 61, 62, 63].

For the fluorescence experiments, a microgel concentration of 0.1 wt% in a saturated pyrene solution was used and the I_1/I_3 ratio as a function of temperature was measured. To ensure that the polymer system is in equilibrium at any point, an additional waiting time of 10 min after every temperature step was chosen. The results of the temperature dependent intensity ratios for the homopolymers of PNNPAM, PNIPAM, PNIPMAM and the reference system pyrene are shown in Figure 2.12a. Additionally, on the right hand side of Figure 2.12, the corresponding first derivative of the swelling curves are given.

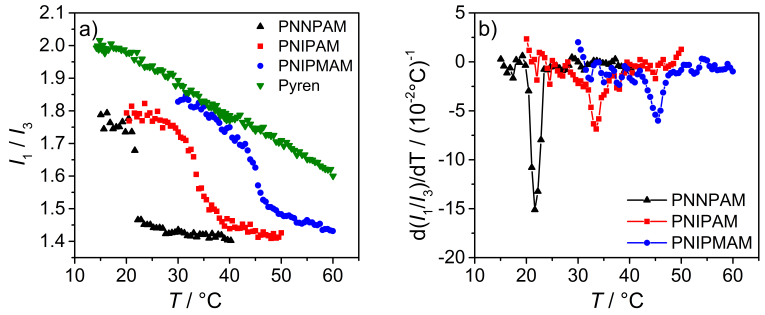

FIGURE 2.12: (**a**) Plot of the intensity ratio I_1/I_3 as a function of temperature for PNNPAM, PNIPAM and NIPMAM solutions mixed with pyrene as well as pure pyrene as reference; (**b**) To quantify the VPTT, the first derivative of I_1/I_3 with respect to temperature as a function of temperature is presented. The concentration of all microgel solutions was 0.1 wt%.

The fluorescence based swelling curves of all three homopolymers clearly show a decrease in polarity with an increase in temperature where the effect is most pronounced at the VPTT. In this temperature region, the polymer network collapses and changes its hydrophobicity. At the same time, one part of the pyrene molecules is caged inside the gel network and the other fraction is of course expelled into the solvent. The measured decrease in I_1/I_3 is not an absolute value for the polarity of the particle interior (as described before), but the trend of the fluorescence swelling curves is in good agreement with the results from the PCS and turbidity measurements. This shows the feasibility of the study of the swelling behavior by the presented fluorescence technique. PNNPAM again shows the steepest phase transition compared to PNIPAM and PNIPMAM, which is related to a dramatic change from a hydrophilic to a more hydrophobic structure connected with a strong decrease in particle size.

A closer look at the phase transition curves in Figure 2.12 shows an additional slight decrease in the intensity ratio before and after the VPTT. This change in I_1/I_3 with increasing temperature is also observable for the pure pyrene solution. The reason for this is a reduction of the dielectric constant of the solvent as a function of temperature and as a consequence, the interactions between pyrene and the water molecules are reduced [64]. Hence, the slight linear decrease in the intensity ratio before and after the VPTT is not caused by the collapse of the microgel particles, but by the interactions of pyrene with the solvent.

The absolute values for I_1/I_3 in the swollen as well as in the collapsed state of the microgels decrease from PNIPMAM over PNIPAM to PNNPAM. This suggests that the hydrophilic character of the polymers is more pronounced for PNIPMAM and the lowest for PNNPAM. This trend is consistent with the location of the VPTTs, and here the transition temperature is higher for more hydrophilic polymers. Winnik *et al.* [65] observed a similar behavior for linear PNIPAM copolymerized with different hydrophobic *N*-*n*-alkyl acrylamides. The absolute value for I_1/I_3 decreased with an increasing content of the hydrophobic comonomer.

To check if there is a saturation concentration of the microgel particles interacting with pyrene, microgel concentration dependent fluorescence measurements were performed to determine the change in I_1/I_3. The results are summarized in Figure 2.13. The left graph shows that, for the microgel particles in the collapsed

state, the intensity ratio decreases continuously with increasing microgel concentration until a certain threshold value is reached. This can be attributed to the effect that at higher microgel concentrations more particles are available to interact with the pyrene molecules. As soon as a concentration of $0.050\,\mathrm{wt\%}$ is reached, the intensity ratio shows the similar behavior. Accordingly, measurements performed at these concentrations, can be easily compared. In contrast to this the microgel/pyrene mixtures show at low temperatures nearly no temperature dependent behavior.

Based on all results shown in this section, it is clear that the hydrophilicity of the microgel particles increases from monomer NNPAM to NIPAM to NIPMAM.

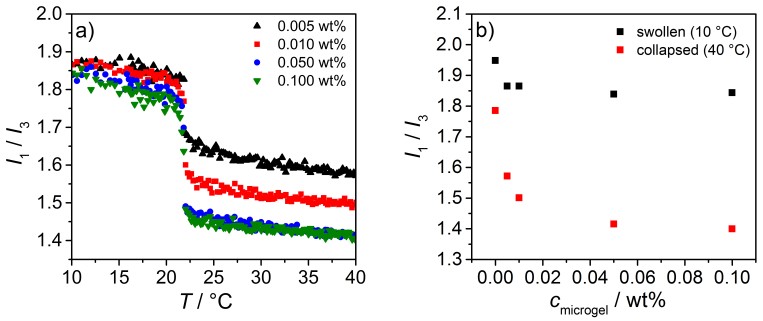

FIGURE 2.13: Plot of the intensity ratio I_1/I_3 as a function of temperature for PNNPAM microgel solutions with different concentrations (**left**). Additionally, the concentration dependent change in I_1/I_3 for the swollen and collapsed microgel is shown (**right**).

2.5 Conclusions

We have studied the influence of the monomer structure on the properties of the respective synthesized microgels employing the monomers NNPAM, NIPAM and NIPMAM. The used experimental conditions were identical for all three microgel types. PNNPAM microgels are found to stand out since they exhibit a very sharp VPT. However, concerning particle size and cross-linker gradient, PNNPAM and PNIPAM microgels are very similar. Both are found to exhibit a core-shell structure with a harder, strongly cross-linked core and a fuzzy shell. PNIPMAM particles are much more homogeneous, which was revealed in the AFM phase images. This points to a different formation mechanism of the PNIPMAM microgels. Moreover, we have shown that fluorescence measurements with pyrene as a probe can be applied to follow the volume phase transition of smart microgels.

References

[1] R. Pelton, "Temperature-sensitive aqueous microgels," *Adv. Colloid Interf. Sci.*, vol. 85, pp. 1–33, 2000. review.

[2] W. Richtering and B. R. Saunders, "Gel architectures and their complexity," *Soft Matter*, vol. 10, pp. 3695–3702, 2014. Review.

[3] A. Pich and W. Richtering, "Polymer nanogels and microgels," *Polymer Science: A Comprehensive Reference*, vol. 6, pp. 309–350, 2012.

[4] T. Hellweg, "Responsive core-shell microgels: Synthesis, characterization, and possible applications," *Journal of Polymer Science Part B: Polymer Physics*, vol. 14, pp. 1073–1083, 2013.

[5] C.Rabe, E. Fleige, K. Vogtt, N. Szekely, P. Lindner, W. Burchard, R. Haag, and M. Ballauff, "The multi-domain nanoparticle structure of a universal core-multi-shell nanocarrier," *Polymer*, vol. 55, no. 26, pp. 6735 – 6742, 2014.

[6] Y. Hertle and T. Hellweg, "Thermoresponsive copolymer microgels," *Journal of Materials Chemistry B*, vol. 43, pp. 5874–5885, 2013.

[7] T. Hoare and R. Pelton, "Highly ph and temperature responsive microgels functionalized with vinylacetic acid," *Macromolecules*, vol. 37, pp. 2544–2550, 2004.

[8] M. Bradley, J. Ramos, and B. Vincent, "Equilibrium and kinetic aspects of the uptake of poly(etylene oxide) by copolymer microgel particles of n-iospropylacrylamide and acrylic acid," *Langmuir*, vol. 21, pp. 1209–1215, 2005.

[9] S. Nayak and L. A. Lyon, "Soft nanotechnology with soft nanoparticles," *Angew. Chem. Int. Ed.*, vol. 44, pp. 7686–7708, 2005. Review.

[10] S. Wellert, Y. Hertle, M. Richter, M. Medebach, D. Magerl, W. Wang, B. Demé, A. Radulescu, P. Müller-Buschbaum, T. Hellweg, and R. von Klitzing, "Inner structure of adsorbed ionic microgel particles," *Langmuir*, vol. 30, pp. 7168–7176, 2014.

[11] Y. Lu, Y. Mei, M. Ballauff, and M. Drechsler, "Thermoresponsive core-shell particles as carrier systems for metallic nanoparticles," *J. Phys. Chem. B*, vol. 110, pp. 3930–3937, 2006.

[12] M. Ballauff and Y. Lu, "Smart nanoparticles: Preparation, characterization and applications," *Polymer*, vol. 48, no. 7, pp. 1815–1823, 2007.

[13] Y. Lu and M. Ballauff, "Thermosensitive core-shell microgels: From colloidal model systems to nanoreactors," *Progr. Polym. Sci.*, vol. 26, pp. 767 –792, 2011. Review.

[14] A. Pich, S. Bhattacharya, Y. Lu, V. Boyko, and H.-J. P. Adler, "Temperature-sensitive hybrid microgels with magnetic properties," *Langmuir*, vol. 20, pp. 10706–10711, 2004.

[15] N. P. B. Tan, C. H. Lee, L. Chen, K. M. Ho, Y. Lu, M. Ballauff, and P. Li, "Facile synthesis of gold/polymer nanocomposite particles using polymeric amine-based particles as dual reductants and templates," *Polymer*, vol. 76, pp. 271 – 279, 2015.

[16] T. Hellweg, K. Kratz, S. Pouget, and W. Eimer, "Internal dynamics in colloidal pnipam microgel particles immobilised in a mesoscopic crystal," *Colloids and Surfaces A*, vol. 202, no. 2-3, pp. 223–232, 2002.

[17] S. Meyer and W. Richtering, "Influence of polymerization conditions on the structure of temperature-sensitive poly(*N*-isopropylacrylamide) microgels," *Macromolecules*, vol. 38, pp. 1517–1519, 2005.

[18] D. Duracher, A. Elaïssari, and C. Pichot, "Preparation of poly(*N*-isopropylmethacrylamide) latexes kinetic studies and characterization," *J. Polym. Sci. Part A: Polymer Chemistry*, vol. 37, no. 12, pp. 1823–1837, 1999.

[19] M. Zeiser, I. Freudensprung, and T. Hellweg, "Linearly thermoresponsive core-shell microgels: Towards a new class of nanoactuators," *Polymer*, vol. 53, pp. 6096–6101, 2012.

[20] B. Wedel, M. Zeiser, and T. Hellweg, "Non nipam based smart microgels: Systematic variation of the volume phase transition temperature by copolymerization," *Zeitschrift f. Phys. Chem.*, vol. 227, pp. 00–12, 2012.

[21] T. Hirano, K. Nakamura, T. Kamikubo, S. Ishii, K. Tani, T. Mori, and T. Sato, "Hydrogen-bond-assisted syndiotactic-specific radical polymerizations of *N*-alkylacrylamides: the effect of the *N*-substituents on the stereospecificities and unusual large hysteresis in the phase-transition behavior of aqueous solution of syndiotactic poly(*N*-*n*-propylacrylamide)," *J. Polym. Sci. Part A: Polymer Chemistry*, vol. 46 (13), pp. 4575–4583, 2008.

[22] W. Kern, "The evolution of silicon wafer cleaning technology," *J. Electrochem. Soc.*, vol. 137, no. 6, pp. 1887–1892, 1990.

[23] W. Rasband, "Imagej 1.50b," *National Institute of Health, USA*, http://imagej.nih.gov/ij/.

[24] S. W. Provencher, "A constrained regularization method for inverting data represented by linear algebraic or integral equations," *Computer Physics Communications*, vol. 27, pp. 213–227, 1982.

[25] S. W. Provencher, "A constrained regularization method for inverting data represented by linear algebraic or integral equations," *Computer Physics Com.*, vol. 27, pp. 213–217, 1982.

[26] D. E. Koppel, "Analysis of macromolecular polydispersity in intensity correlation spectroscopy: the method of cumulants," *The Journal of Chemical Physics*, vol. 57, pp. 4814–4820, 1972.

[27] P. Hassan and S. Kulshreshtha, "Modification to the cumulant analysis of polydispersity in quasielastic light scattering data," *Journal of Polymer and Interface Sciences*, vol. 300, pp. 744–748, 2006.

[28] C. H. Cho, J. Urquidi, S. Singh, and G. W. Robinson, "Thermal offset viscosities of liquid h_2o, d_2o, and t_2o," *Journal of Physical Chemistry B*, vol. 103, pp. 1991–1994, 1999.

[29] B. J. Berne and R. Pecora, *Dynamic Light Scattering*. New York: John Wiley & sons, Inc., 1976.

[30] M. Reufer, P. Diaz-Leyva, L. Lynch, and F. Scheffold, "Temperature-sensitive poly(*N*-isopropyl-acrylamide) microgel particles: A light scattering study," *Eur. Phys. J. E*, vol. 28, pp. 165–171, 2009.

[31] I. Berndt and W. Richtering, "Doubly temperature sensitive core-shell microgels," *Macromolecules*, vol. 36, pp. 8780–8785, 2003.

[32] J. Wu, G. Huang, and Z. Hu, "Interparticle potential and the phase behavior of temperature-sensitive microgel dispersions," *Macromolecules*, vol. 36, pp. 440–448, 2003.

[33] N. C. Woodward, B. Z. Chowdhry, M. J. Snowden, S. A. Leharne, P. C. Griffiths, and A. L. Winnington, "Calorimetric investigation of the influence of cross-linker concentration on the volume phase transition of poly(*N*-isopropylacrylamide) colloidal microgels," *Langmuir*, vol. 19, pp. 3202–3211, 2003.

[34] A. Guillermo, J. P. C. Addad, J. P. Bazile, D. Duracher, A. Elaissari, and C. Pichot, "Nmr investigations into heterogeneous structures of thermosensitive microgel particles," *J. Polym. Sci.: Part B: Polym. Physics*, vol. 38, pp. 889–898, 2000.

[35] H. Senff and W. Richtering, "Influence of cross-link density on rheological properties of temperature-sensitive microgel suspensions," *Colloid Polym. Sci.*, vol. 278, pp. 830–840, 2000.

[36] X. Wu, R. H. Pelton, A. E. Hamielec, D. R. Woods, and W. McPhee, "The kinetics of poly(*N*-isopropylacrylamide) microgel latex formationx," *Colloid Polym. Sci.*, vol. 272, pp. 467–477, 1994.

[37] J. Zhang and R. Pelton, "Poly(*N*-isopropylacrylamide) microgels at the air-water interface," *Langmuir*, vol. 15, pp. 8032–8036, 1999.

[38] S. N. Magonov, V. Elings, and M.-H. Whangbo, "Phase imaging and stiffness in tapping-mode atomic force microscopy," *Surface Science Letters*, vol. 375, pp. L385–L391, 1997.

[39] L. Rayleigh, "The incidence of light upon a transparent sphere of dimensions comparable with the wavelength," *Proceedings of the Royal Society of London, Series A*, vol. 84, no. 567, pp. 25–46, 1910.

[40] R. G. Deen, T. Alsted, W. Richtering, and J. S. Pedersen, "Synthesis and characterization of nanogels of poly(*N*-isopropylacrylamide) by a combination of light and small-angle x-ray scattering," *Phys. Chem. Chem. Phys.*, vol. 13, pp. 3108–3114, 2011.

[41] I. Berndt, *Structure of Multi-Temperature Sensitive Core-Shell Microgels*. PhD thesis, Christian-Albrechts-Universität zu Kiel, 2005.

[42] M. Kano and E. Kokufuta, "On the temperature-responsive polymers and gels based on *N*-propylacrylamides and *N*-propylmethacrylamides," *Langmuir*, vol. 25, no. 15, pp. 8649–8655, 2009.

[43] H. Inomata, S. Goto, and S. Saito, "Phase transition of *N*-substituted acrylamide gels," *Macromolecules*, vol. 23, no. 22, pp. 4887–4888, 1990.

[44] S. Kawaguchi, A. Yekta, and M. A. Winnik, "Surface characterization and dissociation properties of carboxylic acid core-shell latex particle by potentiometric and conductometric titration," *Journal of Colloid and Interface Science*, vol. 176, no. 2, pp. 362–369, 1995.

[45] D. Ito and K. Kubota, "Thermal response of poly(*N*-*n*-propylacrylamide)," *Polymer Journal*, vol. 31, pp. 254–257, 1999.

[46] L. Arleth, X. Xia, R. P. Hjelm, J. Wu, and Z. Hu, "Volume transition and internal structures of small poly(*N*-isopropylacrylamide) microgels," *Journal of Polymer Science Part B: Polymer Physics*, vol. 43 (7), pp. 849–860, 2005.

[47] T. Hellweg, C. D. Dewhurst, E. Brückner, K. Kratz, and W. Eimer, "Colloidal crystals made of pnipa-microgel particles," *Colloid & Polymer Sci.*, vol. 278, no. 10, pp. 972–978, 2000.

[48] Y. Hertle, M. Zeiser, C. Hasenöhrl, P. Busch, and T. Hellweg, "Responsive p(nipam-*co*-ntbam) microgels: Flory–rehner description of the swelling behaviour," *Colloid and Polymer Science*, vol. 288, pp. 1047–1059, 2010.

[49] C. Wu, S. Zhou, S. C. F. Au-yeung, and S. Jiang, "Volume phase transition of spherical microgel particles," *Die Angewandte Makromolekulare Chemie*, vol. 240, no. 1, pp. 123–136, 1996.

[50] P. W. Zhu and D. H. Napper, "Coil-to-globule type transitions and swelling of poly(*N*-isopropylacrylamide) and poly(acrylamide) at latex interfaces in alcohol-water mixtures," *Journal of Colloid and Interface Science*, vol. 177, no. 2, pp. 343 – 352, 1996.

[51] S. Seelenmeyer, I. Deike, S. Rosenfeldt, C. Norhausen, N. Dingenouts, M. Ballauff, T. Narayanan, and P. Lindner, "Small-angle x-ray and neutron scattering studies of the volume phase transition in thermosensitive core-shell colloids," *J. Chem. Phys.*, vol. 114, no. 23, pp. 10471–10478, 2001.

[52] Y. Maeda, M. Tsubota, and I. Ikeda, "Fourier transform ir spectroscopic study on phase transitions of copolymers of *N*-isopropylacrylamide and alkyl acrylates in water," *Colloid and Polymer Science*, vol. 281, no. 1, pp. 79–83, 2003.

[53] K. v. Nessen, M. Karg, and T. Hellweg, "Thermoresponsive poly-(*N*-isopropylmethacrylamide) microgels: Tailoring particle size by interfacial tension control," *Polymer*, vol. 54, no. 21, pp. 5499–5510, 2013.

[54] K. Kubota, S. Fujishige, and I. Ando, "Solution properties of poly(*N*-isopropylacrylamide) in water," *Polymer Journal*, vol. 22, p. 15, 1990.

[55] E. I. Tiktopulo, V. N. Uversky, V. B. Lushchik, S. I. Klenin, V. E. Bychkova, and O. B. Ptitsyn, "Domain coil-globule transition in homopolymers," *Macromolecules*, vol. 28, no. 22, pp. 7519–7524, 1995.

[56] M. Netopilik, M. Bohdanecky, V. Chytry, and K. Ulbrich, "Cloud point of poly(*N*-isopropylmethacrylamide) solutions in water: Is it really a point?," *Macromolecular Rapid Communications*, vol. 18, no. 2, pp. 107–111, 1997.

[57] D. Ito and K. Kubota, "Solution properties and thermal behavior of poly(*N*-*n*-propylacrylamide) in water," *Macromolecules*, vol. 30, pp. 7828–7834, 1997.

[58] A. L. Stancik and E. B. Brauns, "A simple asymmetric lineshape for fitting infrared absorption spectra," *Vibrational Spectroscopy*, vol. 47, no. 1, pp. 66 – 69, 2008.

[59] Y. Matsumura and K. Iwai, "Thermo-responsive behavior and microenvironments of poly(*N*-isopropylacrylamide) microgel particles as studied by fluorescent label method," *Journal of Colloid and Interface Science*, 2006.

[60] K. Kalyanasundaram and J. K. Thomas, "Environmental effects on vibronic band intensities in pyrene monomer fluorescence and their application in studies of micellar systems," *Journal of the American Chemical Society*, vol. 99, no. 7, pp. 2039–2044, 1977.

[61] S. Pankasem, J. K. Thomas, M. J. Snowden, and B. Vincent, "Photophysical studies of poly(n-isopropylacrylamide) microgel structures," *Langmuir*, vol. 10, pp. 3023–3026, 1994.

[62] N. J. Flint, S. Gardebrecht, and L. Swanson, "Fluorescence investigations of smart microgel systems," *Journal of Fluorescence*, vol. 8, no. 4, pp. 343–353, 1998.

[63] C. Pietsch, A. Vollrath, R. Hoogenboom, and U. S. Schubert, "A fluorescent thermometer based on a pyrene-labeled thermoresponsive polymer," *Sensors*, vol. 10, no. 9, p. 7979, 2010.

[64] K. Hara and W. R. Ware, "Influence of solvent perturbation on the radiative transition probability from the $^1b_{1u}$ state of pyrene," *Chemical Physics*, vol. 51, no. 1, pp. 61 – 68, 1980.

[65] F. M. Winnik, H. Ringsdorf, and J. Venzmer, "Interactions of surfactants with hydrophobically-modified poly(*N*-isopropylacrylamides). 1. fluorescence probe studies," *Langmuir*, vol. 7, no. 5, pp. 905–911, 1991.

Chapter 3

The Role of anionic surfactants

Role of anionic surfactants in the synthesis of smart microgels based on different acrylamides

Bastian Wedel, Timo Brändel, Johannes Bookhold, Thomas Hellweg

Published in **ACS Omega**

Volume:2 Issue:1

Year:2017

DOI:0.1021/acsomega.6b00424

http://pubs.acs.org/doi/abs/10.1021/acsomega.6b00424

3.1 Abstract

We investigated the influence of two anionic surfactants, namely sodium dodecyl sulfate (SDS) and sodium decyl sulfate (SDeS) on acrylamide based microgels consisting of *N*-*n*-propylacrylamide (NnPAM). In this context the main focus was on the influence of the surfactant addition on the size of the microgels. The surfactant was added to the reaction mixture, before or during the polymerization at different points in time. Microgels were characterized via photon correlation spectroscopy and atomic force microscopy (AFM). All results were compared to other more common acrylamide based microgels, consisting of N-isopropylacrylamide (NIPAM) and *N*-isopropylmethacrylamide (NIPMAM). A significant difference between the three microgels and a strong dependence on the surface activity of the surfactant was found.

3.2 Introduction

Several acrylamide based microgels exhibit changes in size triggered by external stimuli as temperature and pH, for instance. This interesting behavior granted them the name smart microgels [1, 2, 3, 4, 5]. Due to their stimulus response they are considered for a lot of different applications ranging from the biomedical field [6, 7, 8, 9], to photonics [10, 11, 12, 13, 14, 15], surface modification [16, 17], nanoparticle container [18, 19] or uptake and release [20, 21]. More information can be found in recent reviews [6, 22, 23, 24]. Especially in the context of applications concerning optical properties of hybrid systems it is important to control and tune the size of the microgels during the synthesis. A very distinguished example for this importance was given by Serpe et al. They described the design of etalons from gold coated substrates[25]. Additionally tuning the particle size of acrylamide microgels broadens their scope of applicability [2]. Pelton et al. have shown in 1993 how the size of microgels based on poly (*N*-isopropylacrylamide) (PNIPAM) can be influenced by the addition of SDS [26]. For particles based on poly (*N*-isopropylmethacrylamide) (PNIPMAM) the influence of several surfactants on the size of the obtained colloidal microgels was studied by von Nessen et al. [27]. Recently, we started to study microgels based on the monomer *N*-*n*-propylacrylamide [28, 29] (NnPAM). This monomer yields microgels with a very sharp and steep change in size upon changes in temperature [29] and might therefore be used for more precise sensors, compared to the other mentioned systems. From a physical chemistry point of view this steep change in size might indicate a discontinuous phase transition in these microgels. However, this issue will be addressed in a different work. Moreover, NnPAM can be copolymerized with NIPMAM leading to a tuneability of the phase transition temperature between 21 ° (lower critical solution temperature (LCST) of PNnPAM) and 44 ° (LCST of PNIPMAM) [28]. Due to these promising properties it is of interest to achieve size control also in the synthesis of these non-NIPAM based microgels. One of the most prominent anionic surfactants for microgel synthesis is sodium dodecyl sulfate (SDS). The main aim of this study was the investigation of the influence of SDS on the synthesis of NnPAM microgels. Therefore, we synthesized NnPAM microgels in presence of different amounts of SDS. Moreover, we also used sodium decyl sulfate (SDeS) aiming at scrutinizing changes in the obtained particle properties caused by the different length of the alkyl chain of the surfactant. The results for PNnPAM microgels are compared to data for PNIPAM and PNIPMAM particles.

3.3 Materials and Methods

3.3.1 Chemicals

N-isopropylacrylamide (Sigma-Aldrich Chemie GmbH, Munich, Germany, 97 %) and *N*-isopropylmeth-acrylamide (Sigma-Aldrich Chemie GmbH, Munich, Germany, 97 %) were recrystallized from $n-$hexane. Acryloylchloride (Sigma-AldrichChemie GmbH, Munich, Germany, 98 %), $n-$propylamine (Fluka, Buchs, Switzerland 99 %), triethylamine (Grüssing, Filsum, Germany 99 %), dichloromethane (p.A.), Ammonium persulfate (Sigma-Aldrich Chemie GmbH, Munich, Germany, $\geq$ 98 %) *N,N'*-methylenebisacrylamide (Sigma-Aldrich Chemie GmbH, Munich, Germany, 99 %), Sodium dodecyl sulfate (Sigma-Aldrich Chemie GmbH, Munich, Germany, $\geq$ 99 %) and Sodium decyl sulfate (Sigma-Aldrich Munich, Germany, $\geq$ 99 %) were used without purification. Water was purified using an Arium ®pro VF system (Sartorius Stedim Systems GmbH, Göttingen, Germany). [28, 29, 30]

3.3.2 Synthesis of the Homopolymer Microgels

All microgels were synthesized via precipitation polymerization following the first published PNIPAM microgel synthesis [31]. All syntheses were performed in a 250 mL three-neck flask equipped with a reflux condenser, mechanical stirrer and a nitrogen inlet. The respective monomers (total amount 11.55 $mmol$) and the cross linker (N,N'-methylenebisacrylamide (BIS), 0.6 $mmol$, 5.4 $mol\%$) were dissolved in 150 mL purified water. After heating up to 70 $^\circ$ the solution was purged with nitrogen for one hour. The respective surfactant was added 10 min before the initiation of the polymerization. In case of SDS concentrations of 0 mM, 0.17 mM, 0.35 mM, 0.69 mM, 1.11 mM, 1.68 mM and 2.08 mM were used. The employed SDeS concentrations in the synthesis were 1.11 mM, 3.75 mM, 7.5 mM and 12.5 mM. Furthermore samples were prepared, in which SDS was added shortly after the initiation. The exact addition times were 15 s, 30 s, 60 s, 90 s, 120 s, 210 s, 300 s and 900 s. After the initiation the reaction mixture was stirred for four hours at 70 $^\circ$, then cooled to room temperature and stirred overnight. The resulting microgels were cleaned by five consecutive centrifugation, decantation and redispersion cycles using purified water. After the first centrifugation cycle the supernatant of each synthesis batch was dried and the remaining mass was analyzed gravimetrically.

3.3.3 PCS measurements

Particle sizes were determined using photon correlation spectroscopy applied to highly diluted samples ($c \leq 0.001$ wt%). Measurements of the particle size as a function of the temperature were performed using a diode laser (wave length λ =661.4 nm, Toptica Photonics, Graefelfing, Germany) and an ALV-6010 multiple-τ-correlator (ALV-GmbH, Langen, Germany). We used a scattering angle of 60 $^\circ$ to avoid the observation of internal contributions. At higher scattering angles one may also approach the form factor minimum, which is typically in the range of 90 $^\circ$ for microgels. The scattered light was collected by a single mode fiber connected to the photomultiplier tubes of an ALV detection unit and the temperature was controlled by a thermostated decaline bath. At each temperature the samples were allowed to equilibrate for 20 min. The hydrodynamic radii in the collapsed state were determined via angle-dependent PCS measurements with an ALV goniometer setup using an argon ion LASER (λ =514.5 nm, Spectra Physics 2017, Darmstadt, Germany)

operated with a constant output power and an ALV-5000/E multiple-τ-digital correlator (ALV-GmbH, Langen, Germany). In all cases the obtained time-correlation-functions of the scattered intensity were converted into the field correlation function $g^1(t)$ using the SIEGERT relation.

The different $g^1(t)$ curves were subsequently analyzed using inverse Laplace transformations by means of CONTIN [32]. This is based on the following description of $g^1(t)$.

$$g^1(t) = \int G(\Gamma) exp(-\Gamma t) d\Gamma \tag{3.1}$$

Hence, Laplace inversion yields the relaxation rate distribution $G(\Gamma)$ and the average relaxation rate $\overline{\Gamma}$. The average relaxation rate $\overline{\Gamma}$can be plotted versus q^2 leading to a linear dependence with the translational diffusion coefficient as slope.

$$\overline{\Gamma} = D^{\mathrm{T}} \cdot q^2 \tag{3.2}$$

The magnitude of the scattering vector q can be described by $q = 4\pi n/\lambda \cdot \sin(\theta/2)$ with the refractive index n of the solvent and the scattering angle θ. Deviations from the linear behavior might indicate additional dynamic contributions to the decay of the $g^1(t)$ curves by several different particle species, rotation or internal modes, for instance. [33]

3.3.4 Atomic force microscopy

AFM measurements were performed on a Nanoscope III microscope (Digital Instruments, now Bruker, Karlsruhe, Germany) at room temperature in tapping mode. The cantilevers (Tap300 Al-G, Budget Sensors, Innovative Solutions Bulgaria Ltd., Sofia, Bulgaria) had a radius $\leq 10\,nm$ and a frequency of 300 kHz and a spring constant of 40 N/m. For the sample preparation a silicon wafer (Siegert Wafer GmbH, Aachen, Germany) was coated with 50 μL of a diluted microgel suspension and dried at room temperature in the air.

3.4 Results and Discussion

3.4.1 Influence of surfactant on the particle size

We used photon correlation spectroscopy to study the swelling behavior and the size of PNnPAM microgels prepared in presence of increasing amounts of SDS between $0\,mM$ and $2.08\,mM$. All SDS concentrations were far below the bulk cmc value of SDS. [34] These results were subsequently compared to the behavior of PNIPAM and PNIPMAM microgels. Figure 3.1 shows some examplary swelling curves of the obtained PNnPAM microgels. These swelling curves are very similar to other responsive microgels [27, 35] but in contrast the transition is very steep and sharp. Especially the PNnPAM microgels synthesized without surfactant show a very rapid change in the hydrodynamic radius. The broadening of the phase transition for higher SDS concentrations could indicate a different cross-linker distribution. However, PNnPAM microgels might exhibit a discontinuous phase transition. Such a behavior was not yet observed in other microgels.

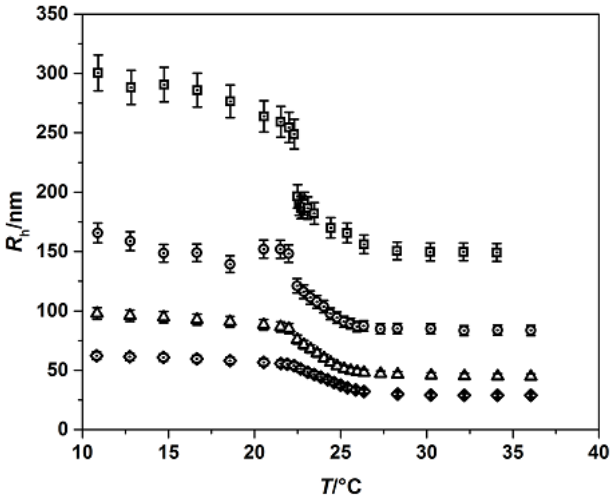

FIGURE 3.1: Swelling curves of PNnPAM microgels synthesized in presence of different SDS concentrations (squares) $\widehat{=}$ 0 mM, circles $\widehat{=}$ 0.17 mM, triangles $\widehat{=}$ 0.69 mM, diamonds $\widehat{=}$ 2.08 mM

We observed a decrease in particle radius from 150 nm to 30 nm in the collapsed state (see Fig.3.2). The relation between PNnPAM particle size and surfactant concentration was similar to the results previously published for PNIPAM and PNIPMAM microgels [26, 27] with a remarkably great difference in the reduction of the hydrodynamic radius. We synthesized PNIPAM and PNIPMAM microgels under identical conditions to compare the influence of SDS on the particle size in the collapsed state. While the radius of PNnPAM microgels decreased by around 81 % upon addition of increasing amounts of SDS the size reduction for PNIPAM microgels is 70 %. The size reduction for PNIPMAM microgels was only about 53 %. In addition, it should be noted that for SDS concentrations of 0.69 mM and 2.08 mM SDS PNnPAM nanogels were obtained despite of the fact that the "classical" Pelton synthesis was used and no functionalized comonomers were added.

We assume that the structural difference of the side chains between PNIPAM, PNIPMAM and PNnPAM gives rise to a more pronounced influence of the surfactant on the stabilization of the precursor particles during an early stage of the microgel formation. Due to the higher hydrophobicity of small PNnPAM oligomer chains compared to PNIPAM, the stabilization of the mentioned precursors starts at lower chain lengths of the oligomers. Therefore, the number of growing particles in the early stage of the process is probably substantially higher for PNnPAM compared to PNIPAM and PNIPMAM microgels. The resulting particles are consequently smaller. This assumption is confirmed when the influence of smaller amounts of surfactant is studied. The effect of the SDS is modest for PNIPAM microgels at low concentrations, e.g. 0.17 mM, whereas PNnPAM microgels become significantly smaller in presence of 0.17 mM SDS. Given the results for the influence of SDS on the hydrodynamic radius of PNnPAM microgels we expected the same trend for the addition of SDeS to the microgel reaction mixture. The results are plotted in Figure 3.3. The influence of SDeS on the particle size was, taking the lower surface activity of SDeS into account, equal to the effect of SDS addition. The inferior surface activity of SDeS can be quantified if the cmc of SDeS is compared with the cmc of SDS. (33 mM

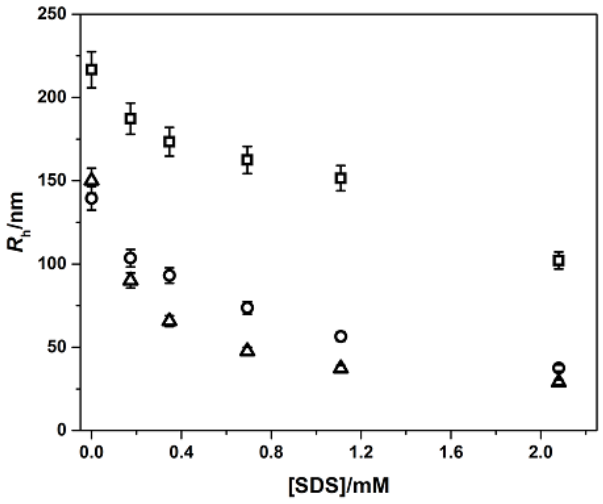

FIGURE 3.2: Hydrodynamic radius of fully collapsed PNIPMAM(squares), PNIPAM(circles) and PNnPAM (triangles) microgels as a function of SDS concentration, present during the microgel synthesis. The hydrodynamic radius was measured and calculated via angle dependent photon correlation spectroscopy

vs. 8.3 mM). [34] It was not possible to normalize the particle size, when the surfactant concentrations are divided with the cmc, though. The reason for this is that the addition of large amounts of SDeS, that lead to particles comparable in size with particles synthesized with the rather moderate SDS concentrations, cause a substantial higher ionic strength in the batch synthesis. This also influences the particle size, as it leads to a higher aggregation rate in the early synthesis phase. Therefore, we obtain smaller particles when SDS is used as surfactant in the emulsion polymerization.

3.4.2 Influence of the moment of surfactant addition

Up to this point the presented results focused on the influence of anionic surfactants on the formation and swelling behavior if the surfactant is added before the initiation of the polymerization. However, it is well known that the process of microgel formation has different steps. It is still under investigation, at which stage of the microgel formation the surfactant has the greatest influence. Two possibilities appear to be most likely. The first possibility is the stabilization of early precursor particles as mentioned above due to the surface activity of anionic surfactants. The second possibility is the action of a surfactant at a later stage of the reaction, where the surfactant molecules influence the interfacial tension between the growing microgel particles and the monomer solution and control the incorporation of monomer units and small oligomer chains. We investigated these phenomena by adding SDS to the proceeding synthesis of PNnPAM at different points in time. As shown before [29] NnPAM has a polymerization velocity compareable to NIPAM [36]. The particle formation seems to be finished after approximately 20 min. Therefore, we choose the following points in time for the addition of SDS to the ongoing synthesis: 15 s, 30 s, 60 s, 90 s, 120 s, 210 s, 300 s and 900 s. The resulting particle dispersions were investigated by angle-dependent photon correlation spectroscopy. The averaged relaxation

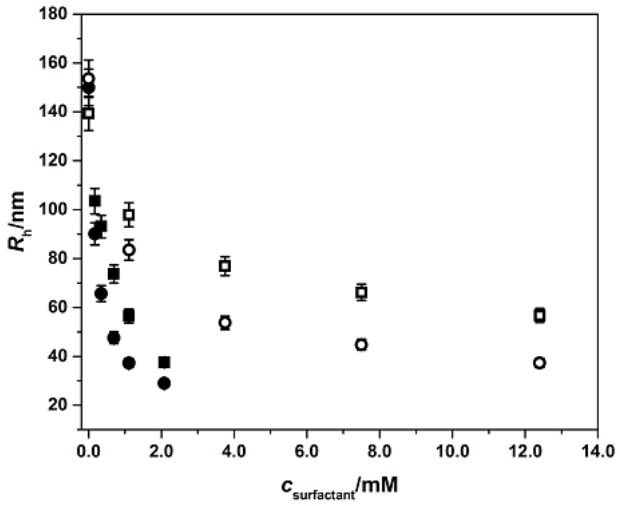

FIGURE 3.3: Hydrodynamic radius of fully collapsed PNnPAM (circles) and PNIPAM (squares) particles as a function of the surfactant concentration during the synthesis: SDS (filled symbols) and SDeS (hollow symbols)

rates Γ, which were obtained for the 8 different synthesis batches, are plotted vs. the square of the magnitude of the scattering vector q in Figure 3.4. For a system with only one population of particles in solution a linear dependence between Γ and q^2 should be detected(see eq. 3.2). Even for the sample where SDS was added 15 safter initiation a slight deviation from the expected linear dependence is observed. This effect increases for the following points of time and the maximal deviation is reached when SDS is added 210 s after starting the polymerization. Hence, it is evident that the addition time of SDS has a drastic influence on the obtained results. An SDS addition after 300 s and 900 s seems to have a minor influence on the resulting particles compared to the previous points in time. We conclude that the influence of SDS during the aggregation phase in the early synthesis procedure is more important than the influence of the surface tension during the growth of the collapsed microgel particles.

The influence of SDS is very pronounced for the addition time points from 30 s up to 210 s as during this period initiation and oligomer formation occur and precursor particles are formed. SDS stabilizes oligomers to new precursor particles at lower chain length and precursor particles, which were formed before the surfactant addition, due to a high surface charge, as well. Therefore we expect two types of particles in the reaction, differing in size. One small particle species representing the precursors that were formed after the addition of SDS at lower chain lengths and a large particle species representing the precursors that were formed before the SDS addition and are stabilized by SDS after their collapse. Concerning the time point of SDS addition the fraction of the 2nd particle species should be higher when the interval between initiation and SDS addition is increased. To verify this assumption we used atomic force microscopy (AFM). As an example Figure 3.5 shows the AFM height profiles for the representative addition times 60 s, 120 s and 300 s. The obtained results confirm the idea that an addition of SDS at different time points during the synthesis leads to the formation of two particle species, as we obtain two noticeably different particle sizes in the AFM images for the addition times of 60 s

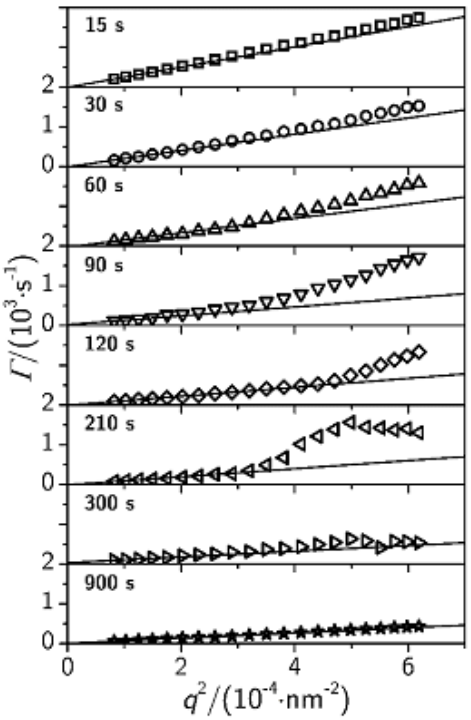

FIGURE 3.4: Relaxation rates of PNnPAM microgels against the square of the magnitude of the scattering vector. The microgels were synthesised with SDS addition to the proceeding reaction after the mentioned times.

and 120 s. The nucleation phase seems to be finished early in the synthesis process, as there is only one species left in the AFM images of the PNnPAM microgels with an addition time of 300 s.

The data clearly reveal the importance of SDS addition during the nucleation process of the PNnPAM microgel synthesis. The size distribution of the resulting particles is controlled by the time interval between initiation of the reaction and the SDS addition. To investigate the influence of SDS in the secondary particle growth later during the synthesis process, we analyzed the size of the 2nd particle species, which seems to be formed before SDS has a crucial influence on the particle nucleation. The particle size of these microgels was extracted from the height profiles of the AFM measurements and can be compared to the particle sizes obtained from an analogous surfactant free synthesis. Figure 3.6 shows the results we obtained for SDS addition during the synthesis. Clearly the interfacial tension of the growing particles plays an important role for the particle size as well. Compared with the particle size obtained by surfactant free synthesis (solid line in Figure 3.6) all PNnPAM microgels are substantially smaller. After an addition time of 120 s a plateau is reached. Even if the particle nucleation phase is finished before the addition of SDS, the particle size is only about one third of the size, that the particles have when no SDS is added to the polymerization.

A possible explanation for the limit in size might be the assembly of surfactant molecules on the microgel surface or in the microgel (see supplementary information). The surface charge of the growing particles is increased and small oligomer chains and monomers cannot be adsorbed onto the particles. Therefore, important amounts of water soluble, small polymers are produced as side products, by chain

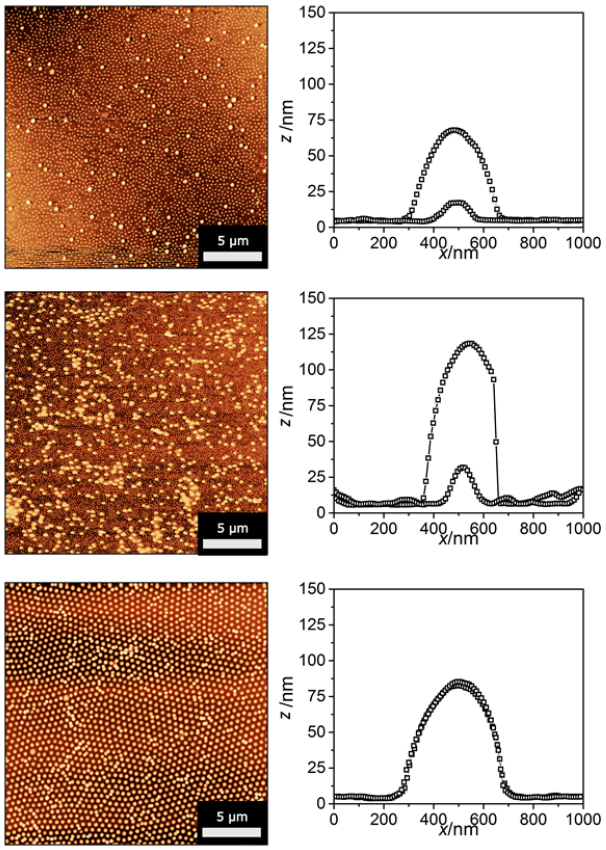

FIGURE 3.5: AFM images of PNnPAM microgels synthesized with SDS addition after 60 s (top), 120 s (middle) and 300 s (bottom). Additionally the respective hight profile of the measured particles (denoted as z-value) is given as a function of the measured x-direction. The images were recorded in tapping mode.

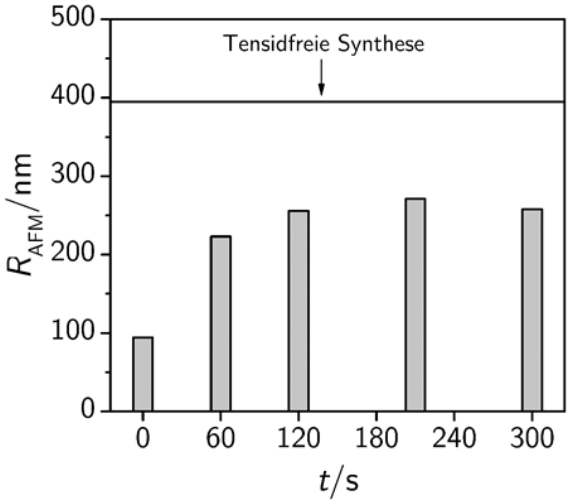

FIGURE 3.6: Particle size of PNnPAM microgels that were synthesized by adding SDS during the synthesis at the points in time given on the t-axis. The particle sizes were obtained from AFM hight profiles as shown in Fig. 3.5

termination reactions. These small polymer chains were not found to precipitate during the reaction. The resulting water soluble polymers can be analyzed during the purification process by a gravimetrical determination of the mass of PNnPAM in the supernatant of the first centrifugation cycle. Compared to PNIPAM, in the reaction mixture of the PNnPAM particles a higher amount of water soluble uncrosslinked polymer is present at the end of the synthesis. This is in accordance with the results we obtained for the VPTT shift and the particle size, because the interaction of surfactant molecules and microgel particles is stronger for PNnPAM. Consequently, the influence of SDS on the size of PNIPAM particles after the nucleation phase seems to be less pronounced or even does not exist. To confirm our observations we studied the influence of SDS and SDeS on the VPTT of premade microgels. [37, 38] The volume phase transition temperature of the purified particles changes upon addition of anionic surfactant. [38] These changes can be described by a mastercurve, which we obtained by normalization of the VPTT data by the surfactant cmc (see supplementary information).

3.5 Conclusions

This study shows the influence of anionic surfactants on the precipitation polymerization process of PNnPAM microgels. In the first part we focused on the particle size. Good control of the PNnPAM particle size was achieved by changing the SDS or SDeS concentration. At high amounts of surfactant nanogels were obtained. The results were compared to the data obtained for homologous microgels based on PNIPAM and PNIPMAM. We found that the influence of anionic surfactants on the formation of PNnPAM microgels is stronger than for PNIPAM and PNIPMAM particles. This can be explained by the very strong interaction between the amphiphilic surfactant molecules and the PNnPAM particles. In the early reaction phase smaller particles, with a substantially lower surface charge can be stabilized. In addition there is an important interaction between SDS and the growing particles during the secondary growth phase that limits the size of PNnPAM microgels. The difference between the *n*-propyl group and the isopropyl group in the side chains seems to have a crucial influence on the hydrophobicity of the resulting particles. But not only the chemical structure of the monomers plays an important role for the interaction between surfactant and microgel during and after the synthesis. The chain length of the anionic surfactant and hence the strength of the surface activity is important, too.

References

[1] R. Pelton, "Temperature-sensitive aqueous microgels," *Adv. Colloid Interf. Sci.*, vol. 85, pp. 1–33, 2000. review.

[2] S. Nayak and L. A. Lyon, "Soft nanotechnology with soft nanoparticles," *Angew. Chem. Int. Ed.*, vol. 44, pp. 7686–7708, 2005. Review.

[3] B. R. Saunders and B. Vincent, "Microgel particles as model colloids: theory, properties, and applications," *Adv. Colloid Interf. Sci.*, vol. 80, pp. 1–25, 1999.

[4] A. Imaz and J. Forcada, "N-vinylcaprolactam-based microgels: Effect of the concentration and type of cross-linker," *J. Polym. Sci.: Part A: Polym. Chem.*, vol. 46, pp. 2766–2775, 2008.

[5] A. Fernandez-Nieves, A. Fernandez-Barbero, B. Vincent, and F. J. de las Nieves, "Reversible aggregation of soft particles," *Langmuir*, vol. 17, pp. 1841–1846, 2001.

[6] W. Richtering and B. R. Saunders, "Gel architectures and their complexity," *Soft Matter*, vol. 10, pp. 3695–3702, 2014. Review.

[7] B. Sung, C. Kim, and M.-H. Kim, "Biodegradable colloidal microgels with tunable thermosensitive volume phase transitions for controllable drug delivery," *J. Colloid Interface Sci.*, vol. 450, pp. 26–33, 2015.

[8] H. Wang, Y. Hewa, and G. L. Rempel, "Preparation of polyacrylamide based microgels with different charges for drug encapsulation," *Eur. Polym. J.*, vol. 49, pp. 1110–1116, 2013.

[9] K. Uhlig, T. Wegener, J. He, M. Zeiser, J. Bookhold, I. Dewald, N. Godino, M. Jaeger, T. Hellweg, A. Fery, and C. Duschl, "Patterned thermoresponsive microgel coatings for noninvasive processing of adherent cells," *Biomacromolecules*, vol. 17, no. 3, pp. 1110–1116, 2016.

[10] R. Contreras-Cáceres, A. Sánchez-Iglesia, M. Karg, I. Pastoriza-Santos, J. Pérez-Juste, J. Pacifico, T. Hellweg, A. Fernández-Barbero, and L. M. Liz-Marzán, "Encapsulation and growth of gold nanoparticles in thermoresponsive microgels," *Adv. Mater.*, vol. 20, pp. 1666–1670, 2008.

[11] Z. H. Farooqi and M. Siddiq, "emperature-responsive poly(n-isopropylacrylamide-acrylamide-phenylboronic acid) microgels for stabilization of silver nanoparticles," *J. Dispersion Sci. Technol.*, vol. 36, pp. 423–429, 2014.

[12] M. Dulle, S. Jaber, S. Rosenfeldt, A. Radulescu, S. Förster, P. Mulvaney, and M. Karg, "Plasmonic gold-poly(n-isopropylacrylamide) core-shell colloids with homogeneous density profiles: A small angle scattering study.," *Phys. Chem. Chem. Phys.*, vol. 17, pp. 1354–1367, 2015.

[13] M. Karg, S. Jaber, T. Hellweg, and P. Mulvaney, "Surface plasmon spectroscopy of gold-pnipam core-shell nanocrystals," *Langmuir*, vol. 27, pp. 820–827, 2011.

[14] M. Das, N. Sanson, D. Fava, and E. Kumacheva, "Microgels loaded with gold nanorods: Photothermally triggered volume phase transition under physiological conditions," *Langmuir*, vol. 23, pp. 196–201, 2007.

[15] N. Hantzschel, F. Z. Z. Eckert, A. Pich, and M. A. Winnik, "Poly(*N*-vinylcaprolactam-*co*-glycidyl methacrylate) aqueous microgels labeled with fluorescent laf3:eu nanoparticles," *Langmuir the ACS journal of surfaces and colloids*, vol. 23, pp. 10793–10800, 2007.

[16] J. Wiedemair, M. J. Serpe, J. Kim, J. F. Masson, L. A. Lyon, B. Mizaikoff, and C. Kranz, "In-situ afm studies of the phase-transition behavior of single thermoresponsive hydrogel particles," *Langmuir*, vol. 23, pp. 130–137, 2007.

[17] S. Schmidt, T. Hellweg, and R. von Klitzing, "Packing density control in p(nipam-*co*-aac) microgel monolayers: Effect of surface charge, ph, and preparation technique," *Langmuir*, vol. 24, pp. 12595–12602, 2008.

[18] A. Pich, Y. Lu, V. Boyko, K.-F. Arndt, and H.-J. P. Adler, "Thermo-sensitive poly(*N*-vinylcaprolactam-*co*-acetoacetoxyethyl methacrylate) microgels: 3. incorporation of polypyrrole by selective microgel swelling in ethanol–water mixtures," *Polymer*, vol. 45, pp. 1079–1087, 2004.

[19] A. Pich, A. Karak, Y. Lu, A. K. Ghosh, and H.-J. P. Adler, "Preparation of hybrid microgels functionalized by silver nanoparticles," *Macromol. Rapid Commun.*, vol. 27, pp. 344–350, 2006.

[20] M. Bradley, B. Vincent, and G. Burnett, "Uptake and release of anionic surfactant into and from cationic core-shell microgel particles," *Langmuir the ACS journal of surfaces and colloids*, vol. 23, pp. 9237–9241, 2007.

[21] M. Bradley and B. Vincent, "Poly(vinylpyridine) core/poly(*N*-isopropylacrylamide) shell microgel particles: their characterization and the uptake and release of an anionic surfactant.," *Langmuir the ACS journal of surfaces and colloids*, vol. 24, pp. 2421–2425, 2008.

[22] Y. Hertle and T. Hellweg, "Thermoresponsive copolymer microgels," *Journal of Materials Chemistry B*, vol. 43, pp. 5874–5885, 2013.

[23] A. Pich and W. Richtering, "Precipitation polymerization: Synthesis, characterization, and functionalization," in *Chemical Design of Responsive Microgels*, Springer-Verlag Berlin Heidelberg: Berlin, Heidelberg, 2011.

[24] S. Wellert, M. Richter, T. Hellweg, R. von Klitzing, and Y. Hertle, "Responsive microgels at surfaces and interfaces," *Zeitschrift f. Phys. Chem.*, vol. 229, pp. 1225–1250, 2015.

[25] C. D. Sorrell, M. C. D. Carter, and M. J. Serpe, "Color tunable poly(*N*-isopropylacrylamide)-*co*-acrylic acid microgel-au hybrid assemblies," *Adv. Func. Mater.*, vol. 21, pp. 425–433, 2011.

[26] W. McPhee, K. C. Tam, and R. Pelton, "Poly(*N*-isopropylacrylamide) latices prepared with sodium dodecyl sulfate," *J. Colloid Interface Sci.*, vol. 156, pp. 24–30, 1993.

[27] K. v. Nessen, M. Karg, and T. Hellweg, "Thermoresponsive poly-(*N*-isopropylmethacrylamide) microgels: Tailoring particle size by interfacial tension control," *Polymer*, vol. 54, no. 21, pp. 5499–5510, 2013.

[28] B. Wedel, M. Zeiser, and T. Hellweg, "Non nipam based smart microgels: Systematic variation of the volume phase transition temperature by copolymerization," *Zeitschrift f. Phys. Chem.*, vol. 227, pp. 00–12, 2012.

[29] B. Wedel, Y. Hertle, O. Wrede, J. Bookhold, and T. Hellweg, "Smart homopolymer microgels: Influence of the monomer structure on the particle properties," *Polymers*, vol. 8, no. 162, 2016.

[30] T. Hirano, K. Nakamura, T. Kamikubo, S. Ishii, K. Tani, T. Mori, and T. Sato, "Hydrogen-bond-assisted syndiotactic-specific radical polymerizations of *N*-alkylacrylamides: the effect of the *N*-substituents on the stereospecificities and unusual large hysteresis in the phase-transition behavior of aqueous solution of syndiotactic poly(*N*-*n*-propylacrylamide)," *J. Polym. Sci. Part A: Polymer Chemistry*, vol. 46 (13), pp. 4575–4583, 2008.

[31] R. H. Pelton and P. Chibante, "Preparation of aqueous latices with n-isopropylacrylamide," *Colloids and Surfaces*, vol. 20, pp. 247–256, 1986. keine Kopie im Archiv.

[32] S. W. Provencher, "Contin: a general purpose constrained regularization program for inverting noisy linear algebraic and integral equations," *Computer Physics Com.*, vol. 27, pp. 229–242, 1982.

[33] B. J. Berne and R. Pecora, *Dynamic Light Scattering: With Applications to Chemistry, Biology and Physics*. Dover Publications Newburyport, 2013.

[34] P. Mukerjee and K. J. Mysels, "Critical micelle concentrations of aqueous surfactant system," tech. rep., National Bureau of Standards of NSRDS-NBS 36, 1971.

[35] K. Kratz and W. Eimer, "Swelling properties of colloidal poly(n-isopropylacrylamide) microgels in solution," *Ber. Bunsenges. Phys. Chem.*, vol. 102, pp. 848–854, 1998.

[36] X. Wu, R. H. Pelton, A. E. Hamielec, D. R. Woods, and W. McPhee, "The kinetics of poly(*N*-isopropylacrylamide) microgel latex formationx," *Colloid Polym. Sci.*, vol. 272, pp. 467–477, 1994.

[37] C. Wu and S. Zhou, "Effects of surfactants on the phase transition of poly(n-isopropylacrylamide) in water," *J. Polym. Sci. B Polym. Phys*, vol. 34, pp. 1597–1604, 1996.

[38] S. J. Mears, Y. Deng, T. Cosgrove, and R. Pelton, "Structure of sodium dodecyl sulfate bound to a poly(nipam) microgel particle," *Langmuir*, vol. 13, p. 1901, 1997.

Chapter 4

Patterned microgel coatings

Patterned thermoresponsive microgel coatings for noninvasive processing of adherent cells

Katja Uhlig, Thomas Wegener, Jian He, Michael Zeiser, Johannes Bookhold, Inna Dewald, Neus Godino, Magnus Jaeger, Thomas Hellweg, Andreas Ferye, Claus Duschl

Published in **Biomacromolecules**

Volume:17 Issue:3

Year:2016

DOI:10.1021/acs.biomac.5b01728

http://pubs.acs.org/doi/abs/10.1021/acs.biomac.5b01728

4.1 Abstract

Cultivation of adherently growing cells in artificial environments is of utmost importance in medicine and biotechnology to accomplish *in vitro* drug screening or to investigate disease mechanisms. Precise cell manipulation, like localized control over adhesion, is required to expand cells, to establish cell models for novel therapies and to perform non-invasive cell experiments. To this end, we developed a method of gentle, local lift-off of mammalian cells using polymer surfaces which are reversibly and repeatedly switchable between a cell-attractive and a cell-repellent state. This property was introduced through micropatterned thermoresponsive polymer coatings formed from colloidal microgels. Patterning was obtained through automated nanodispensing or microcontact printing, making use of unspecific electrostatic interactions between microgels and substrates. This process is much more robust against ambient conditions than covalent coupling, thus lending itself to up-scaling. As an example, wound healing assays were accomplished at 37 °C with highly increased precision in microfluidic environments.

4.2 Introduction

The promises of novel therapeutic approaches, diagnostic tools and test systems that utilize cells for assessing the efficacy or the toxicity of compounds are about to show their first benefits [1, 2]. However, substantial obstacles are still limiting a broad application of cell-based systems. These limitations do not necessarily lie in a limited understanding of basic aspects of the biological context. They rather result from an inability to ensure and maintain the quality and reliability levels of cell material that are mandatory for clinical applications and pharmaceutical research. A key aspect in this context is the non-invasive treatment and reliable and reproducible processing of adherent cells. For improving the reliability and accuracy of cell assays as well as for cell expansion, the control of cell adhesion is crucial. This includes the thorough detachment of cells from their substrate. Crude mechanical scratching or the use of enzyme solutions, which both heavily impair cell viability [3], are still standard methods for removing adherent cells from the culture surface. A much more gentle approach that does not affect the quality of the cells makes use of surface coatings from thermoresponsive polymers [4, 5]. Such coatings mediate protein- and therefore cell adhesion above the lower critical solution temperature (LCST), where the polymer is in a collapsed state. Below the LCST, the polymer changes to a hydrated and expanded configuration, thus disallowing protein binding and resulting in cell repulsion [6, 7, 8, 9, 10]. The most popular thermoresponsive polymer poly(*N*-isopropylacrylamide) (PNIPAM) has a LCST of 32 °C. Hence, cell cultivation on PNIPAM coatings is straightforward at 37 °C and decreasing the temperature below the LCST initiates cell detachment from the substrate for further use. Okano et al. pioneered this concept over the last two decades, focusing on applications in regenerative medicine. Various coating techniques have been reported using grafting-from approaches, like surface-initiated ATRP (atom transfer radical polymerization) or electron beam-induced graft polymerization [11, 12], or grafting-to approaches using covalent coupling on gold substrates [13]. However, the fabrication of these coatings requires expensive equipment, e. g. specialized gaseous atmospheres, and lacks the flexibility necessary for adapting the coating properties to the wide range of adhesion behaviors of the cell types of interest. Recently, we introduced thermoresponsive PNIPAM microgels as a coating material [14]. Thermoresponsive microgel

coatings show a number of advantages over layer formats where the polymer is tethered directly to the substrate [15, 16]. The microgel that we employed for coating has a diameter of several hundreds of nanometers. This size is sufficient to ensure firm immobilization to common surface materials through nonspecific electrostatic and van der Waals interaction. A thin poly(ethyleneimine) (PEI) base serves to stabilize the layer. This allows the use of very simple immobilization methods, such as dipping the substrate into a microgel solution, spraying or spin-coating suitable solutions, and hence increases the flexibility for producing a wide range of coating patterns. As an example, we address one challenging requirement for establishing new cell assays: enabling the localized and reproducible control of cell adhesion without inflicting cell injury. This need is very prominent for popular cell tests like the wound healing assay [17]. Here, collective cell migration is studied under a variety of conditions, e.g. the effect of drug candidates [18, 19]. A cell-free area representing the wound is generated within a cell monolayer to observe its resettlement. Next to standard procedures, like local cell scratching, several protocols for selective cell detachment have been suggested: Kolesnikova et al. applied a laser-induced patterning of a confluent cell layer growing on gold nanoparticles [20]. Pasparakis et al. exposed a cell layer to light through a structured mask to locally ablate a cell adhesion-mediating coating [21]. Besides light-triggered cell detachment, electrochemical triggers were also reported. Surfaces of Raghavan et al. for example can be switched from a cell-repellent to a cell-attractive state [22]. Although these cell detachments were localized, they are not reversible and partly cell invasive. Here, we demonstrate the fabrication of patterned thermoresponsive microgel coatings employing automated nanodispensing and microcontact printing (μCP). We utilized both methods to generate spots with a feature size of 200 μL and show the selective control of cell adhesion on coated versus uncoated areas. In contrast to other methods, clear boundaries between cell-populated and bare areas can be produced with high definition and without producing ill-defined cell debris. Finally a cell assay is described that assesses the migration activity of cells, thus demonstrating the considerable potential of patterned thermoresponsive microgel coatings for designing novel tools for the analysis of adherent cells.

4.3 Materials and Methods

4.3.1 Microgel synthesis

N-isopropylacrylamide (NIPAM; Sigma Aldrich 97 %) was recrystallized in *n*-hexane. Acrylic acid (AA; Merck 99 %) was freed from the stabilizer 4-methoxyphenol using a column packed with aluminum oxide, basic (Alox B, Macherey & Nagel). The radical initiator ammonium persulfate (APS; Sigma-Aldrich, $\geq$ 99 %) and the cross-linker N,N'-methylenebisacrylamide (BIS; Sigma-Aldrich, 99 %) were used without further purification. Water was purified using an Arium®pro VF system (Satorius Stedim). The homopolymer microgel of NIPAM (MZ140) and the copolymer microgel of NIPAM and acrylic acid (MZ160) with a monomer ratio of 99 : 1 were synthesized through a precipitation reaction. All syntheses were performed in a 250 mL three-neck flask equipped with a reflux condenser, a mechanical stirrer and a nitrogen inlet. For the synthesis of the homopolymer microgel MZ140 and the copolymer microgel MZ160, the thermoresponsive compounds NIPAM (10.568 mmol, 1.196 g) and BIS (0.98 mmol, 0.151 g) (total amount of thermoresponsive compounds 11.548 mmol) were dissolved in 150 mL purified water. The solution was heated up to 70 °C under continuous stirring and purged with nitrogen. In case of the copolymer synthesis,

1 mol% acrylic acid (0.116 mmol, 0.036 g) was added after 50 min. All polymerization reactions were initiated after 1 h of heating and stirring under nitrogen gas flow by the addition of APS (0.41 mmol, 0.096 g) dissolved in 1 mL water. The polymerization reaction proceeded for 4 h at 70 °C. Afterwards, the reaction medium was cooled to room temperature and stirred overnight. Both microgels were cleaned from reaction by-products and impurities through five successive centrifugation, decantation and redispersion steps using purified water. The sample names and the related chemical composition of the microgels are shown in Table 4.1.

TABLE 4.1: Monomer content of themicrogels.

Sample name	m_{NIPAM}/g	m_{BIS}/g	c_{BIS}/mol%	m_{AA}/g	c_{AA}/mol%
MZ140	1.196	0.151	8.486	0	0
MZ160	1.196	0.151	8.486	0.0096	1.133

4.3.2 Photon Correlation Spectroscopy (PCS)

Particle sizes and volume phase transition temperatures were measured at a fixed scattering angle of $\theta = 60°$ using a diode LASER (Toptica Photonics AG) with a wavelength of λ = 661.4 nm and a fast correlator (ALV-6010, ALV GmbH) with a thermostat bath (Haake Phoenix II, Thermo Scientific). All measurements were performed on a highly diluted sample with a concentration of $c \leq 0.001$ wt% in cylindrical quartz cuvettes (Hellma GmbH & Co. KG) with an outer diameter of 10 mm. The samples were thermally equilibrated for 15 min prior to the measurement.

4.3.3 Local microgel coating

Ink-jet printing

The microgel spots were deposited using a nano-plotter (NP2.1, GeSiM, Germany) equipped with a piezo dispenser (Nano-Tip A, GeSiM, Germany). For each spot, 300 pL were dispensed with a distance of 500 μm to cover an area of 1 cm^2. Two different kinds of target substrates were used for microgel dispensing: 1) Glass cover slips (20 x 20 mm^2, Menzel, Germany) were cleaned with 5 % Hellmanex III (Hellmanex Analytics, Germany) for 5 h followed by rinsing with deionized water. Subsequently, the glass substrates were dipped into 1 % poly(ethylenimine) solution (PEI, Sigma Aldrich, Germany) for 10 s followed by a drying step using an air stream. 2) Cyclo olefin polymer substrates (COP or Zeonex) were purchased from ibidi (ibiTreat COP). The COP substrates were modified by the manufacturer for cell culture purposes. The static contact angles of COP and PEI-modified glass substrates were measured with a contact angle measuring system G10 (Krüss Surface Science, Germany).

Microcontact printing

The microcontact printing of the microgel was performed using the μCP3 in combination with a poly(dimethylsiloxane) stamp (all GeSiM, Germany). The stamp structure consisted of a pillar array with 200 μm diameter each and a pillar-to-pillar distance of 83 μm. For inking, the stamp was put into a reservoir with 1.4 wt% microgel suspension and incubated for 300 s. Afterwards, the stamp was dried with an air stream and then pressed to a PEI-modified glass substrate for 120 s.

4.3.4 AFM analysis

Atomic force microscopy (AFM) images of dried samples were obtained using a commercial AFM (Dimension 3100 equipped with a NanoScope V controller from Bruker AXS Inc., USA) operating in tapping mode using standard Si_3N_4 cantilevers from Olympus with a typical spring constant of $\tilde{4}2\,Nm^{-}1$ and a typical resonance frequency of 300 kHz (OTESPA, Bruker). All images were processed and analyzed using NanoScope software (Version 7.30).

4.3.5 Microfluidic device

The microchannels were self-produced by assembling a sandwich consisting of a 3 mm thick poly(methyl methacrylate) (PMMA, Modulor, Germany) plate, a structured double-side sticky PSA foil (Pressure-sensitive adhesive, 3M, U.S.A.) and for sealing a glass substrate with microgel patterns as bottom. Due to the huge pattering area of $1\,cm^2$, an accurate positioning of the channel and the patterns was not needed. A micromill (MDX-40A, Roland DG, Germany) was used to drill the holes for the corresponding tubing connection into the PMMA plate of 40 x 22 mm. The microfluidic features were created by cutting the 86 μm thick PSA foil with a cutting plotter (CE5000-40 Graphtec CraftRobo Pro, U.S.A.). PMMA, PSA and microgel-modified glass substrate were assembled and laminated at 60 °C (DH-360, laminator, Linea, Germany). The channel was 500 μm wide, 1 cm long and had three inlets. The tubing (Teflon FEP, ID 0,020 x 10, Techlab, Germany) was connected to the channel, valves (Omnifit, CHM, Germany) and a 1 mL syringe (ILS, Germany).

4.3.6 Cell culture

L929 mouse fibroblasts (ACC 2, DSMZ, Germany) were cultivated in DMEM containing HEPES (25 mM), FCS (10 %), penicillin / streptomycin (1 %) and L-glutamine (2 mM, all Biochrom, Germany) and CHO-K1 (ACC 110, DSMZ Germany) were cultivated in Ham's F12 supplemented with FCS (10 %) and penicillin / streptomycin (1 %, all Biochrom, Germany) at 37 °C and 5 % CO_2. About $3 \cdot 10^4$ cells/cm^2 were seeded on the thermoresponsive microgel surface. The samples were stored in the incubator for one or two days. After this time, the substrates were cooled down to room temperature ($\sim$22 °C), i. e. below the LCST of the microgels, which made the pattern cell-repellent. To observe the morphology of the cells, the samples were quickly transferred from the incubator to an optical microscope at room temperature, equipped with a 10 x / 0.25 objective and a Nikon Digital Sight DS-L1 (Nikon, Germany). After 30 min under microscopic observation, the cells were gently rinsed with a 1 mL pipette.

4.3.7 Cell assays in microfluidic set-up

The microsystems were incubated with cell medium overnight. Afterwards, air bubbles were flushed out of the system with additional medium. $2 \cdot 10^6$ L929 mouse fibroblasts ml$^{-}1$ were injected through a side channel and cultivated in situ for one day in an incubator. After 30 min under microscopic observation at $\sim$22 °C different flow velocities were applied through the main channel using a 1 mL glass syringe (ILS, Germany) driven by a syringe pump (SP230IWZ, WPI, UK).

4.3.8 Cell migration observation

All cell migration observations were performed with a fully automated set-up (Cell-R, Olympus, Germany) equipped with a 10 x / 0.3 objective and an incubation chamber (Air Conditioning Unit, Evotec, Germany). For assaying the inhibition, locally defined areas were first created by cooling and rinsing a cell monolayer on a polymer substrate as described above. Subsequently, locostatin (dissolved in DMSO, both Sigma Aldrich, Germany) was added to a final concentration of 42 μM resulting in 1.2 % DMSO. As a control an identical substrate was incubated with 1.2 % pure DMSO to preclude an effect on the cell behavior. For analyzing the cell survival rate in samples treated with and without locostatin, a propidium iodide staining (Sigma Aldrich, Germany) using 42 μg/mL was performed after 400 min.

4.4 Results and Discussions

For non-invasive processing of adherent cells, we locally deposited two different thermoresponsive microgels which were negatively charged. The colloidal microgels MZ140 and MZ160 have cross sections of approximately 300 nm above the LCST and 150 nm below the LCST. They differ in the content of acrylic acid. MZ160 has more negative charges due to the presence of 1.1 mol% acrylic acid. The presence of acrylic acid resulted in a LCST of $\sim$35 °C for MZ160 which was two degrees higher than the LCST of MZ140 at $\sim$33 °C. First, we established two different protocols to pattern surfaces with microgels using either spotting or microcontact printing. Structured thermoresponsive coatings were created by dispensing 300 pL droplets of MZ140 microgel suspension (0.5 wt%) on PEI-modified glass and on COP substrates in a 350 μm grid using an ink-jet printer. The deposited microgel spots were visualized by phase contrast microscopy. On PEI-modified glass the spots were approximately 200 μm in diameter (Figure 4.1 A) while on COP they were 25 wt% smaller (Figure 4.1 E). The difference in size of the microgel spots is related to the wettability of the substrate. Water contact angle measurements on COP substrates resulted in (68 $\pm$2 °) and in (31 $\pm$1 °) on PEI-modified glass substrates. COP is more hydrophobic than PEI-modified surfaces; therefore, the contact area of the aqueous microgel suspension is smaller, leading to smaller microgel spots. The distance of the spots was arbitrary and the dispensing volume, i. e. spot size, can be varied depending on the application. Alternatively, the microgels were locally deposited by microcontact printing. We employed a PDMS stamp structured with 200 μm diameter pillars arranged in a 283 μm grid. Various patterns can be obtained, depending on the stamp design. The stamp had been wetted with a 1.4 wt% microgel suspension of MZ140 and was transferred to a PEI-modified glass cover slide. The printed microgel pattern corresponded well with the employed stamp design (Figure 4.1 I). To investigate the cell adhesion on the thermoresponsive spots, L929 mouse fibroblasts and CHO epithelial cells were cultured for 2 d on either spotted or printed surfaces while the cell morphology was monitored (Figure 5.2 B, F, J and Si Figure B.1 A). The cells grew homogeneously, establishing a monolayer throughout the whole surface. After the temperature had been decreased below the LCST to 22 °C for 30 min, the microgel spots could be identified due to the local change in the morphology of the fibroblasts (Figure 4.1 C, K and Si Figure B.1 B). The fibroblasts rounded up on the microgel spots, induced by changes in physico-chemical properties of the microgel as it cooled below its LCST14. Cells on the PEI-modified glass remained in the elongated morphology, indicating that the loss of adherence was not simply due to a direct temperature effect on the cells. In contrast to the cell behavior of L929 mouse

fibroblasts on the microgel coating, the CHO epithelial cells on the microgel spots remained in the elongated state, despite the temperature reduction to 22 °C (Figure 4.1 G). Subsequently, the surfaces were gently rinsed using a 1 mL pipette. As a result, both the fibroblasts and the epithelial cells were flushed only from the microgel spots (Figure 4.1 D, H, L and Si Figure B.1 C). Cells on the COP and on the PEI-coated glass remained on the substrate after rinsing and maintained their spread morphology. Remarkably, the CHO cells were also detached locally upon rinsing, although there had been no visible change in the morphology of these cells on the microgel spots. A possible explanation is that cell-cell contacts between the epithelial cells preserved the cell layer in spite of the overall loss of adhesion to the then repellent microgel substrate. This stabilization was, however, insufficient to withstand the shear force generated by rinsing. In contrast, fibroblasts do not develop cell-cell contacts, thus the morphology change was clearly observable. There was no apparent difference between the microgels MZ140 and MZ160. The use of both microgel suspensions resulted in efficient local cell detachment of fibroblasts and epithelial cells. Therefore, we used both microgels for the following experiments. Both techniques, spotting and printing, resulted in coatings that were fully functional with regard to controlling cell adhesion. Spotting is a very robust method that yields a high reproducibility of surface functionality. It is, however, necessarily limited in the geometric features that can be obtained. In contrast, microcontact-printed microgel patterns not always resulted in functional coatings, indicating a lower reproducibility (data not shown).

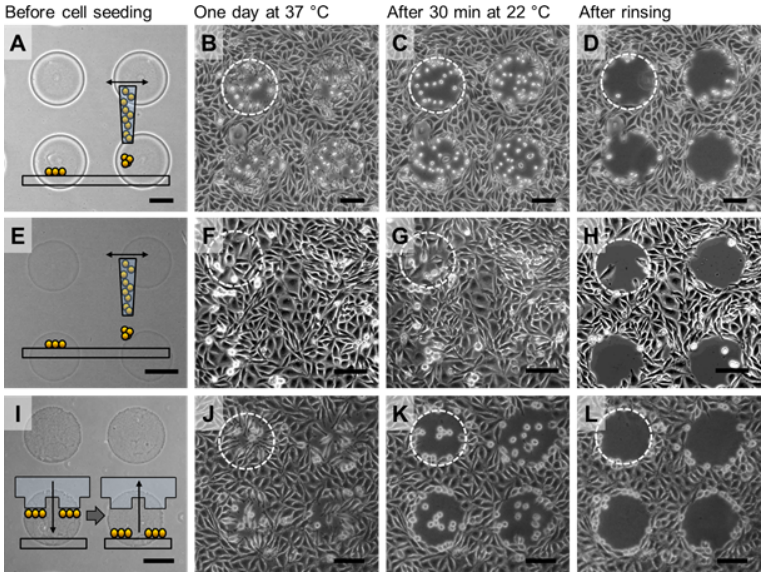

FIGURE 4.1: Phase contrast images of (A,E) spotted and (I) printed (μ-CP) thermoresponsive microgel suspensions (MZ140) on PEI-coated glass cover slides (A,I) and COP (E). For (A-H) 0.5 wt% and for (I-L) 1.4 wt% microgel suspensions were employed. The position of one microgel spot is indicated exemplarily by dashed white circles. After 2 d at 37 °C, L929 mouse fibroblasts (B, J) and CHO-K1 epithelial cells (F) adhered homogeneously on the surface. After having been exposed to room temperature (˜[22]°C) for 30 min, the fibroblasts on the microgel spots changed their morphology from an elongated to a round shape (C,K) while cells on the surrounding PEI-coated regions remained in the elongated shape. The CHO cells maintained their elongated morphology on both the microgel coating and the COP substrate (G). All cells could locally be removed from the microgel patterns by rinsing (D,H,L). The scale bars are 100 μm.

Cell detachment requires a certain minimum microgel density on the surface. In order to quantify this, the surface topography was investigated by AFM. The concentration of the microgel MZ160 suspensions used for spotting were varied (0.2 wt%, 0.1 wt% to 0.05 wt%). As mentioned above, this microgel has the same diameter as MZ140. Afterwards, cell tests and AFM measurements were performed to correlate the microgel density with cell detachment functionality (Si Figure B.1). The results were then related to AFM measurements of a substrate generated by microcontact printing. Representative AFM images obtained from both coating techniques are shown in Figure 4.2. Spotting a 0.2 wt% microgel suspension resulted in a mixture of multi- and monolayers. The microgels were heterogeneously distributed. Due to the high concentration of the microgel suspension, the particles tended to form aggregates configured in multilayers. These aggregates are visible as regions with high topography in the micrometer range (Figure 4.2, upper row). Less concentrated suspensions mostly produced monolayers. The average microgel distance was found to be dμgel = 0.914 $\pm$ 0.001 μm for 0.1 wt% and dμgel = 0.961 $\pm$ 0.001 μm for 0.05 wt%. Although these values merely differ by 5 %, the cell tests remarkably revealed that the cell detachment functionality upon temperature reduction was substantially decreased for a concentration of 0.05 wt% (Si Figure B.1). In contrast to the multilayer formation at high microgel concentrations achieved by spotting, microcontact printing of MZ140 led to the generation of microgel monolayers. Reducing microgel vacancies again requires a minimum microgel density. Using 1.4 wt% resulted in an average microparticle distance of dμgel = 832 pm1 nm. This surface coverage was found to be sufficient for successful cell detachment after cooling of the substrate to room temperature (Figure 4.1 F-H). Repeated microgel hydration and dehydration caused by temperature shifts below and above the LCST did not influence the microgel distribution on the surface as shown by Schmidt et al. [15, 16].

To demonstrate the broad applicability of patterned thermoresponsive coatings, we integrated them into a microfluidic cell assay. First, we seeded L929 mouse fibroblasts for one day in a microchannel at 37 °C (Figure 4.3, first row). The cells grew homogenously as a monolayer throughout the channel. Subsequently, we reduced the temperature to 22 °C for 30 min. Cells on the microgel spots decreased their cell adhesion area and assumed a rounded morphology. Cells on the PEI coating remained in the adhered state and maintained a spread morphology. Application of a laminar shear flow flushed away cells from microgel patterns, resulting in defined cell-free areas. In an additional experiment, the cell medium was supplemented with a viability marker (calcein AM) after local cell detachment (Si Figure B.3). Almost all cells were stained, indicating an unimpaired viability and thus a particularly gentle local cell patterning.

The temperature-dependent cell adhesion-mediating properties of thermoresponsive polymers enable a reversible switching from a cell-attractive to a cell-repellent and back to cell-attractive state. For validation, we incubated the microchannel with the previously patterned cell sheets at 37 °C and observed the cell behavior (Figure 4.3, second row and Si Figure B.3). Within 15 h, the mouse fibroblasts resettled the cell-free areas and formed a homogenous monolayer. Using the recovered cell layer, the temperature was again decreased to 37 °C (Figure 4.3, third row). The cells did not round up after 30 min. This may have been due to the increased cell number. Thus, the L929 fibroblasts started to form cell-cell contacts contrary to their native behavior and were able to maintain their spread morphology. Nevertheless, application of a shear flow locally detached the fibroblasts from the microgel spots. Finally, we increased the temperature once more to 37 °C and again observed a cell overgrowth of the spots (Figure 4.3, fourth row).

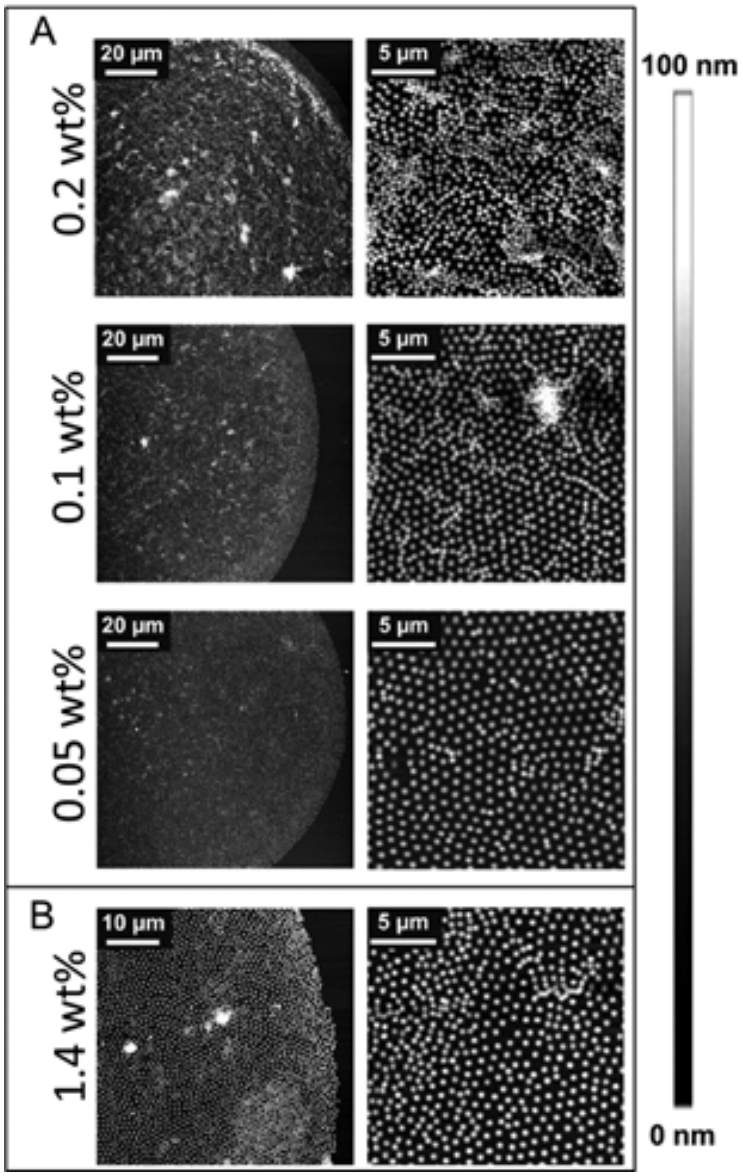

FIGURE 4.2: A) AFM images of thermoresponsive microgel spots deposited on PEI-coated glass cover slides using an ink-jet spotter. The concentration of the microgel (MZ160) suspension was reduced from 0.2 wt% (top row) to 0.1 wt% (middle row) and 0.05 wt% (bottom row). A concentration of 0.2 wt% resulted in a heterogeneous microgel coating composed of microgel multilayers and monolayers. At lower concentrations (0.1 wt% and 0.05 wt%), homogenous monolayers were obtained with an average microgel distance of dμgel = 0.914 ± 0.001 μm for 0.1 wt% and dμgel = 0.961 ± 0.001 μm for 0.05 wt%. B) AFM images of thermoresponsive microgel (MZ140) spots deposited on PEI-coated glass cover slides using microcontact printing. The inking suspension had a concentration of 1.4 wt%. For large parts, homogenous monolayers with an average microgel distance of dμgel=832 ± 1 nm were obtained.

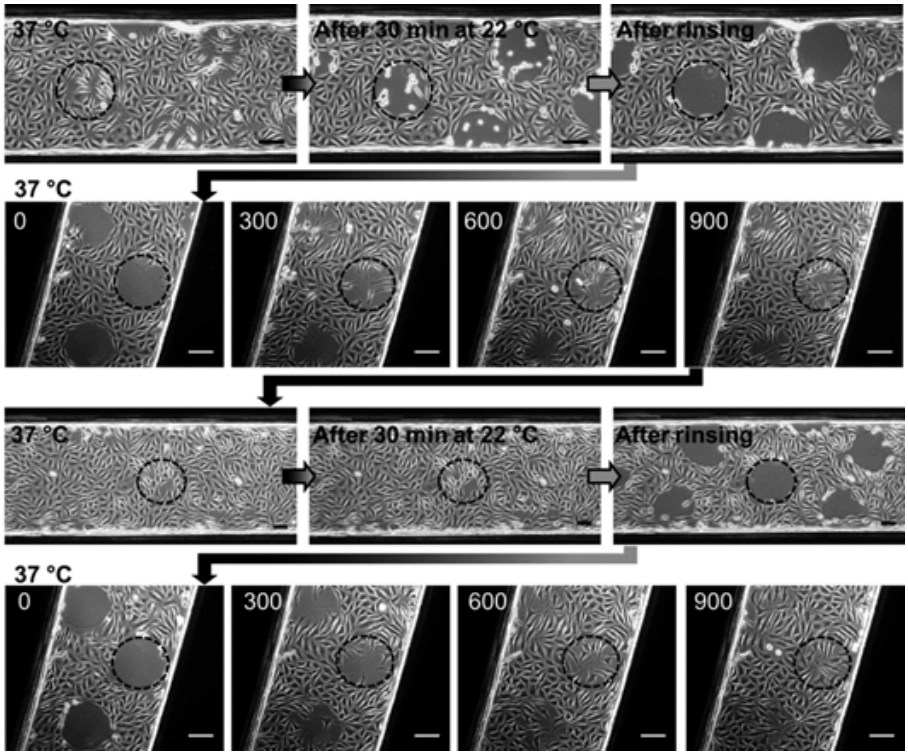

FIGURE 4.3: Phase contrast images of L929 mouse fibroblasts cultivated in a microchannel on a PEI-coated glass slide with microgel spots (MZ160, $c = 0.5$ wt%). All images correspond to one continuous experiment. Exemplary, one microgel-coated area per picture is indicated by a dashed black circle. The scale bars are 100 μm. First row) Mouse fibroblasts exposed to (left) 37 °C, (center) 30 min at 22 °C and (right) after exposure to a shear flow. Cells were locally removed from the microgel spots. Second row) Time lapse at 37 °C of the cells migrating onto the previously created cell-free thermoresponsive microgel spots at 0 min, 300 min, 600 min and 900 min. When the temperature was increased to 37 °C, cells started to migrate to the newly generated open space and form a closed cell monolayer after 900 min. Third row) Temperature decrease from 37 °C (left) to 22 °C (center) and application of a shear flow again removed the cells from the microgel spots (right). Fourth row) Resettlement of the initially cell-free spots over a course of 900 min after temperature increase to 37 °C. Brightness has been adjusted of the images in the second and forth lines for better visualization.

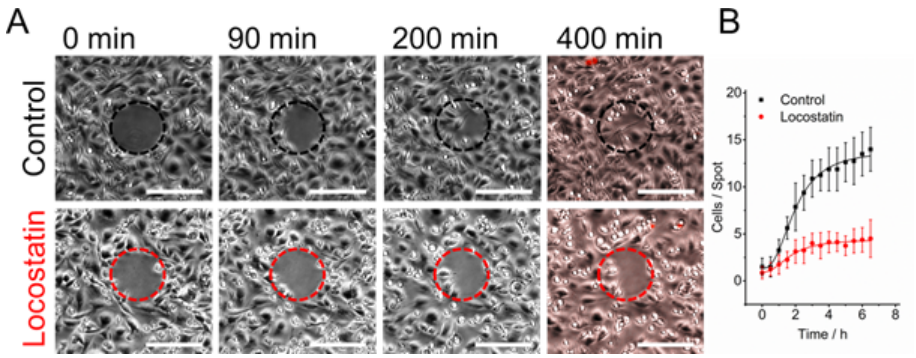

FIGURE 4.4: A) Time lapse microscopy of CHO epithelial cells migrating on thermoresponsive microgel spots (MZ140, $c = 0.5$ wt%, indicated by a dashed circle) without (first row) and with 42 μM locostatin (second row). Before recording the resettlement of the free areas through migration, the cells were locally removed from the spots by rinsing after 30 min at to 37 °C and the temperature was increased to 37 °C again. After 400 min, the dead cells were stained with propidium iodide. A merge of the phase contrast image and the fluorescence image is shown in the last column. There is no observable difference of dead cell (red staining) numbers with regard to no addition and locostatin addition. The scale bars are 200 μm. B) With locostatin, the number of cells on the functional spots was significantly lower than in the control without locostatin at every time point beyond 1 h (B, evaluation of $n = 8$ spots).

To prove the claim just outlined, a wound healing assay was performed using a cell migration-inhibiting compound, viz. locostatin. This small, organic and cell permeable molecule acts on the Raf kinase inhibitor protein (RKIP) and, thus, inhibits the cell migration of epithelial cells [23]. We cultured CHO-K1 epithelial cells on substrates with locally structured thermoresponsive polymers, removed cells from the spots by temperature reduction below the LCST and rinsing as detailed above. Subsequently, we observed the resettlement of the spots at 37 °C in samples with and without locostatin (Figure 4.4). A nearly complete coverage of the cell monolayer was achieved after 400 min on the control surface, whereas the samples treated with locostatin showed still plenty of free space on the spots at this time. The extent of cell recovery was analyzed by quantification of cells on the spots as a function of time (Figure 4.4 B). The decelerating effect of locostatin could be measured after 90 min at the earliest. Locostatin also induced a change in the cell morphology in comparison to the control: The CHO cells started to round up during the incubation. To quantify toxic effects of locostatin, a propidium iodid staining was performed after 400 min, to visualize the dead cells. In both samples, the survival rates were similar, i. e. about 95 %, suggesting that locostatin had no toxic effect under the given experimental conditions. In summary, we show that thermoresponsive microgel coatings are highly suitable for wound healing assays. The surface-induced cell detachment is a very mild procedure. Cells that were either detached or remained on the surface showed no signs of stress induced by the thermoresponsive microgel, as verified by calcein live staining (data not shown). Furthermore, our patterning techniques allow for a well-defined geometry with sharp microgel coating edges as visualized in Figure 4.2. This enables a precise local cell detachment and, thus, strongly improves assay-to-assay comparability. These benefits set our method apart from other wound-forming techniques using destructive approaches,

e. g. electric current or laser ablation of cells. These procedures inevitably also damage cells near to the detaching area, thus influencing the test result. Cell scratching similarly harms cells and results in undefined removal. In particular, our combination of thermoresponsive microgels with microfluidics enables an easy exchange of medium and test compounds, evidently also in an alternating manner to allow for time-depending dosing.

4.5 Conclusions

We established an easy-to-process, robust and flexible locally structured thermoresponsive polymer coating for defined spatially resolved cell detachment that can be induced by a temperature trigger. The coating principle is based on electrostatic interactions of a negatively charged microgel with a positively charged substrate like PEI-coated glass or synthetic materials like COP. For locally patterned deposition, spotting of microgel suspensions of picoliter volumes or microcontact printing were successfully applied. Both coating strategies resulted in a spatially defined cell detachment upon temperature shifting. We identified a lower limit of surface coverage by systematically varying the average microgel distance and correlating it with cell detachment efficiency. The establishment of a wound healing assay and its integration into microfluidics indicates the versatility and practicality of thermoresponsive microgels. As a future perspective, we plan to also establish co-cultures of different cell lines based on locally patterned thermoresponsive coatings. Due to the flexibility in designing different geometries and dimensions, we believe that microgel-based thermoresponsive coatings may become a crucial element in novel powerful assays.

References

[1] R. J. Wade, E. J. Bassin, W. M. Gramlich, and J. A. Burdick, "Nanofibrous hydrogels with spacially patterned biochemical signals to control cell behavior," *Advanced Materials*, vol. 27, pp. 1356–1362, 2015.

[2] K. Saha, Y. Mei, C. M. Reisterer, N. K. Pyzocha, J. Yang, J. Muffat, M. C. Davies, M. R. Alexander, R. Langer, D. G. Anderson, and R. Jaenisch, "Surface-engineered substrates for improved human pluripotent stem cell culture under fully defined conditions," *PNAS*, vol. 108 (46), pp. 18714–18719, 2011.

[3] G. M. Hodges, D. C. Livingston, and L. M. Franks, "The localization of trypsin in cultured mammalian cells," *J Cell Sci.*, vol. 12 (3), pp. 887–902, 1973.

[4] C. R. B. Mendon, C. I. D. Bica, E. F. Simó-Alfonso, G. Ramis-Ramos, and C. M. S. Piatnicki, "Physical chemical properties and kinetics of redox processes in water/soybean oil microemulsions," *J. Braz. Chem. Soc.*, vol. 19, no. 4, pp. 775–781, 2008.

[5] R. M. da Silva, J. F. Mano, and R. L. Reis, "Smart thermoresponsive coatings and surfaces for tissue engineering: switching cell-material boundries," *Trends Biotechnol.*, vol. 25 (12), pp. 577–583, 2007.

[6] J.-F. Lutz, K. Weichenhan, O. Akdemir, and A. Hoth, "About the phase transitions in aqueous solutions of thermoresponsive copolymers and hydrogels based on 2-(2-methoxyethoxy)ethyl methacrylate and oligo(ethylene glycol) methacrylate," *Macromolecules*, vol. 40, no. 7, pp. 2503–2508, 2007.

[7] T. Okano, N. Yamada, H. Sakai, and Y. Sakurai, "A novel recovery system for cultured cells using plasma-treated polystyrene dishes grafted with poly(n-isopropylacrylamide)," *J. Biomed. Mater. Res.*, vol. 27 (10), pp. 1243– 1251, 1993.

[8] T. Okano, N. Yamada, M. Okuhara, H. Sakai, and Y. Sakurai, "Mechanism of cell detachment from temperature-modulated, hydrophilic-hydrophobic polymer surfaces.," *Biomaterials*, vol. 16 (4), pp. 297–303, 1995.

[9] E. Wischerhoff, K. Uhlig, A. Lankenau, H. G. Börner, A. Laschewsky, C. Duschl, and J.-F. Lutz, "Controlled cell adhesion on peg-based switchable surfaces," *Angew. Chem. Int. Ed.*, vol. 47 (30), pp. 5666–5668, 2008.

[10] K. Uhlig, E. Wischerhoff, J.-F. Lutz, A. Laschewsky, M. S. Jaeger, A. Lankenau, and C. Duschl, "Monitoring cell detachment on peg-based thermoresponsive surfaces using tirf microscopy," *Soft Matter*, vol. 6, pp. 4262–4267, 2010.

[11] A. Mizutani, A. Kikuchi, M. Yamato, H. Kanazawa, and T. Okano, "Preparation of thermoresponsive polymer brush surfaces and their interaction with cells," *Biomaterials*, vol. 29 (13), pp. 2073–2081, 2008.

[12] N. Idota, T. Tsukahara, K. Sato, T. Okano, and T. Kitamori, "The use of electron beam lithographic graft-polymerization on thermoresponsive polymers for regulating the directionality of cell attachment and detachment," *Biomaterials*, vol. 30, no. 11, pp. 2095 – 2101, 2009.

[13] K. Uhlig, H. G. Boerner, E. Wischerhoff, J.-F. Lutz, M. S. Jaeger, A. Laschewsky, and C. Duschl, "On the interaction of adherent cells with thermoresponsive polymer coatings," *Polymers*, vol. 6, no. 4, pp. 1164–1177, 2014.

[14] S. Schmidt, M. Zeiser, T. Hellweg, C. Duschl, A. Fery, and H. Möhwald, "Adhesion and mechanical properties of pnipam microgel films and their potential use as switchable cell culture substrates," *Adv. Func. Mater.*, vol. 20, no. 19, pp. 3235–3243, 2010.

[15] S. Schmidt, H. Motschmann, T. Hellweg, and R. von Klitzing, "Thermoresponsive surfaces by spin-coating of pnipam-co-paa microgels. a combined afm and ellipsometry study," *POLYMER*, vol. 49, pp. 749–756, 2008.

[16] S. Schmidt, T. Hellweg, and R. von Klitzing, "Packing density control in p(nipam-*co*-aac) microgel monolayers: Effect of surface charge, ph, and preparation technique," *Langmuir*, vol. 24, pp. 12595–12602, 2008.

[17] X. Yao, R. Peng, and J. Ding, "Cell-material interactions revealed via material techniques of surface patterning," *Advanced Materials*, vol. 4;25 (37), pp. 5257–5286, 2013.

[18] P. Friedl and D. Gilmour, "Collective cell migration in morphogenesis, regeneration and cancer," *Nat. Rev. Mol.Cell Biol.*, vol. 10 (7), pp. 445–457, 2009.

[19] R. Rørth, "Collective cell migration," *Annu. Rev. of Cell Dev. Biol.*, vol. 25, pp. 407–429, 2009.

[20] T. A. Kolesnikova, D. Kohler, A. G. Skirtach, and H. Möhwald, "Laser-induced cell detachment, patterning, and regrowth on gold nanoparticle functionalized surfaces," *ACS Nano*, vol. 6, no. 11, pp. 9585–9595, 2012. PMID: 23066742.

[21] G. Pasparakis, T. Manouras, A. Selimis, M. Vamvakaki, and P. Argitis, "Laser-induced cell detachment and patterning with photodegradable polymer substrates," *Angewandte Chemie*, vol. 123, no. 18, pp. 4228–4231, 2011.

[22] S. Raghavan, R. A. Desai, Y. Kwon, M. Mrksich, and C. S. Chen, "Micropatterned dynamically adhesive substrates for cell migration," *Langmuir*, vol. 26, no. 22, pp. 17733–17738, 2010. PMID: 20886900.

[23] W. M. Bement, "A role for rkip in cell motility," *Chem. Biol.*, vol. 12 (9), pp. 953–954, 2005.

Chapter 5

Smart membranes

Smart membranes by electron beam cross-linking of copolymer microgels

Johannes Bookhold, Lars Wiehemeier, Maxim Dirksen, Sebastian Knust, Florian Paneff, Xinaghui Zhang, Tilman Kottke, Dario Anselmetti, Armin Gölzhäuser, Thomas Hellweg

Manuscript submitted

Year:2017

5.1 Abstract

Poly(*N*-isopropylacrylamide) (pNIPAM) based copolymer microgels were used to create free-standing, transferable, thermoresponsive membranes. The microgels were synthesized by copolymerization of NIPAM with *N*-benzylhydrylacrylamide (NBHAM). Monolayers of these colloidal gels were subsequently cross-linked using an electron gun leading to the formation of a connected monolayer. Furthermore, the cross-linked microgel layer is detached from the supporting material by dissolving the substrate. These unique systems can be used as transferable, thermoresponsive coatings and as thermoresponsive membranes. As a proof of principle for the use of such membranes we studied the ion transport through them at different temperatures revealing drastic changes when the lower critical solution temperature of the copolymer microgels is reached.

5.2 Introduction

In recent years interest in responsive materials [1, 2, 3, 4, 5, 6] has grown steadily. This is due to the plethora of possible applications for these materials ranging from sensors [7, 8, 9] and photonic materials [10, 11], via smart surfaces [12, 13] and carriers for catalysts [14] to nano-actuators [15]. At present, most of the studied microgels are based on poly-(*N*-isopropylacrylamide) (pNIPAM) [1] which can easily be copolymerized [16, 17] with other monomers to generate e.g. pH sensitivity [18] or to shift the lower critical solution temperature. The use of (*N*-isopropylacrylamide-*co*-acrylic acid microgels [18] as smart surface coatings has lead to very promising results in cell culture applications for vertebrate cells [12, 19]. However, at present microgel coatings are prepared on the substrate they are intended to be used on [20]. Despite of the wide variety of applications for these simple coatings, it is desirable to make them transferable to arbitrarily shaped surfaces.

Hence, in the present work we will address this issue and describe an approach leading to free standing linked microgel films which can be transfered on different substrates or which can be used as responsive membrane. To our knowledge at present smart membranes are made predominantly by modification of porous inorganic or organic precursor e.g. with p(NIPAM). [21, 22]

Such transferable, thermoresponsive coatings have a lot of obvious advantages in terms of surface modification. The ability to coat three dimensional substrates, gratings and wells would definitely prove to be an advantage for a number of research fields. Using pNIPAM based microgels, biological[23, 24, 25, 26] and medical [12] applications are also possible. PNIPAM is known to be water soluble at temperatures below 32 °C and with increasing temperature hydrophobicity gradually increases. [1, 5, 27] As part of this transition pNIPAM microgels undergo a microphase-separation which leads to a transition between the swollen ($T < 32\,^{\circ}C$) and the collapsed ($T > 32\,^{\circ}C$) state. [1, 5, 27] The only possibility to form a free-standing microgel monolayer[9] is to irreversibly link the microgel particles to each other. Recently published work from Gölzhäuser et al. showed the possibility to form free-standing carbon nano membranes by electron beam irradiation of self-assembled aromatic molecules. [28, 29] The durability and strength of these materials is astonishing and based on the bonds formed between the aromatic moieties during the irradiation.

Therefore, we have chosen a similar approach to cross-link microgel particles in a monolayer. For this purpose various possible comonomers containing an aromatic

moiety suitable for a radical precipitation polymerization were tested for applicability. The microgel particles have been prepared by precipitation polymerization of different amounts of comonomers with NIPAM and the best results have been obtained using *N*-benzylhydrylacrylamide (NBHAM) [30].

A number of publications in the past years have shown, that the incorporation of comonomers into a microgel network adds additional chemical functionalities and changes its phase behavior as well as the responsivity. [17, 18, 31, 32] Hydrophilic comonomers such as acrylic acid shift the volume phase transition (VPTT) to higher values [17, 18] whereas microgels with hydrophobic comonomers like *N-tert*-butylacrylamide tend to exhibit a slightly lower VPTT [33]. Therefore, a comonomer with a large aromatic moiety like NBHAM is expected to shift the VPTT towards lower temperatures. Nonetheless, the aromatic funcionality is needed in order to subsequently cross-link the particles. [28, 29]

As mentioned before, the free-standing microgel membranes are build up by electron beam cross-linking of a monolayer of such copolymer microgels. We achieved to make microscopic membranes using this approach. These membranes are still thermoresponsive. They can be transferred to e.g. porous supports and we show that these microgel based free-standing membranes can be used to regulate ion flow. Such membranes could in fact be the basis for self regulating fuel cells or smart osmotic membranes.

5.3 Materials and Methods

5.3.1 Chemicals

N-isopropylacrylamide (NIPAM, Sigma Aldrich Chemie GmbH, München, Germany; purity 97 %) was recrystallized from *n*-hexane. *N*-benzylhydrylacrylamide (NBHAM, Sigma Aldrich Chemie GmbH, München, Germany; purity 96 %), the radical initiator ammonium persulfate (APS, Sigma Aldrich Chemie GmbH, München, Germany; purity $\geq$ 99 %) and the cross-linker *N*,*N*'-methylenbisacrylamide (BIS, Sigma Aldrich Chemie GmbH, München, Germany; purity 99 %) were used without further purification. Water was purified using an Arium® pro VF system (Satorius AG, Göttingen, Germany).

5.3.2 Synthesis of the copolymer microgels

The copolymer microgels pNIPAM-*co*-NBHAM were synthesized via surfactant-free precipitation polymerization. [1] For all synthesis the amount of the thermoresponsive monomer NIPAM was kept constant and the aromatic monomer NBHAM was used with different molar amounts with respect to NIPAM. The chemical structures of the used monomers are depicted in Fig.5.1. All the synthesis were performed in a 250 mL three-neck-flask equipped with a reflux condenser, mechanical stirrer and a nitrogen inlet. The thermoresponsive monomer (NIPAM, 1.307 g, 11.55 mmol) and the cross-linker (BIS, 0.089 g, 0.578 mmol) were dissolved in 149 mL of purified water.

The solution was heated up to 70 °C under continuous stirring and purged with nitrogen for 55 min. Then, the aromatic comonomer (NBHAM, total amounts depicted in Tab. 5.1) was added. After 5 min equilibration time the polymerization was initiated by the addition of APS (0.093 g, 0.41 mmol) dissolved in 1 mL purified water. The concentrations of the cross-linker was 5 mol%, in respect to PNIPAM. The polymerization proceeded for 4 h at 70 °C. Afterwards, the reaction mixture was

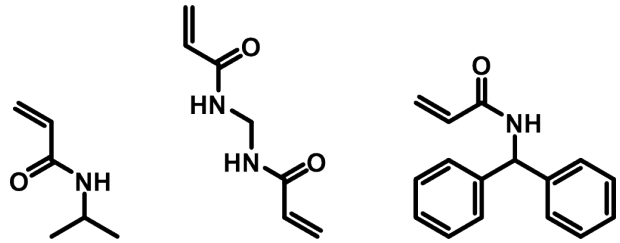

FIGURE 5.1: Structures of the used compounds. (left to right: NIPAM, NBHAM, BIS)

TABLE 5.1: Sample names, mass, molar amount and molar concentrations of the aromatic monomer NBHAM in respect to the amount of the thermoresponsive monomer NIPAM

Sample Name	m NBHAM / g	n NBHAM / mmol	c NBHAM / mol%
NcBH 5	0.137	0.5775	5
NcBH 10	0.274	1.155	10
NcBH 15	0.411	1.733	15
NcBH 20	0.548	2.310	20
NcBH 30	0.822	3.456	30

cooled down to room temperature and stirred over night. All microgels were cleaned by five successive centrifugation, decantation and redisperion cycles with purified water. The sample names, the numbers corresponding to the nominal amount of aromatic comonomer in the microgel synthesis, used monomer masses and the related molar amount are summarized in Tab. 5.1.

5.3.3 Photon Correlation Spectroscopy (PCS)

Particle sizes were determined using photon correlation spectroscopy (PCS) [34] on highly diluted samples (c $\leq$ 0.0001 wt%). Measurements of the particle size as a function of the temperature were performed using a classical goniometer setup equipped with a multiple-τ digital correlator ALV-5000/E (ALV-Laser Vertriebsgesellschaft mbH, Langen, Germany) and an argon-ion laser (Spectra Physics Stabilite 2017, Newport Spectra-Physics GmbH, Darmstadt, Germany; $\lambda = 514.5$ nm) as light source. The temperature was adjusted using a temperature controlled index matching bath. The concentration of the solution was below 0.0001 wt% in order to avoid multiple scattering effects. The measured autocorrelation functions were analyzed by applying inverse Laplace transformation (CONTIN) [35, 36] and using the method of cumulants [37] that provides the mean relaxation rate of the relaxation rate distribution functions. From this the translational diffusion coefficient D^T for diluted particle solutions can be calculated via $\overline{\Gamma} = D^T \cdot q^2$ with q, the magnitude of the scattering vector ($q = 4\pi n/\lambda \cdot \sin(\theta/2)$) with λ the wavelength, n the refractive index and θ the scattering angle. Using the Stokes-Einstein relation, the hydrodynamic radius R_h of the microgel particles can be calculated:

$$D^T = \frac{k_B T}{6\pi\eta R_h} \tag{5.1}$$

with k_B the Boltzmann constant, T the temperature and η the corresponding viscosity of the solvent. The values of the viscosity and the refractive index have been

corrected with respect to the temperature during the measurement.

The volume phase transition temperature (VPTT) and the temperature dependent phase behavior was studied using a HeNe LASER with an ALV-6010 multiple-τ correlator at a constant scattering angle of 60 °. The temperature was adjusted using a thermostated index matching bath. The microgel solutions where highly diluted ($c \leq 0.0001$ wt%). In order to analyze the temperature dependent phase behavior, the sample was heated from 10 °C to 50 °C in steps of 1 °C, at each temperature the sample was allowed to equilibrate for 50 min. The temperature depended measurements were used to obtain the swelling curves of the microgel (hydrodynamic radius vs. Temperature) and to determine the VPTT.

5.3.4 Atomic Force Microscopy (AFM)

Particle sizes of dried microgel particles on a surface and homogeneity analysis of microgel monolayers and detached films were conducted through atomic force microscopy (AFM). [38, 39, 40, 41] Measurements were performed with a DI Nanoscope IIIa (Digital Instruments, now Bruker, Karlsruhe, Germany)mounted on a Zeiss Axiovert 135 inverted optical microscope (Carl Zeiss Microscopy GmbH, Jena, Germany) in tapping mode using BudgetSensors (Innovative Solutions Bulgaria Ltd., Sofia, Bulgaria) Al-Reflex Tap300Al-G cantilevers with a tip radius of <10 nm, a resonance frequency of about 300 kHz and a spring constant of 40 N/m. To measure the size of single microgel particles a diluted solution ($c \leq 0.0001$ wt%) of the sample was deposited on a cleaned silicon wafer and dried at ambient temperature in air and several measurements in tapping mode were performed in order to obtain reliable statistics. Prior to the deposition of the sample the wafers were cleaned with ethanol and treated with oxygen plasma for 10 min. The microgel particle size was determined utilizing the cross-section function in the AFM analysis software Gwyddion [42]. The monolayers and free-standing thin films were prepared as described in the section "Preparation and characterization of free-standing microgel membranes". The prepared monolayers were analyzed in tapping mode, measurements were performed in order to ensure the homogeneity of the monolayers. The analysis of the obtained membranes was also performed in tapping mode. Measurements along the edges were done to determine the thickness of the membrane and scans on the membrane were performed to test for inhomogeneities and structual changes in the membrane compared to the monolayer.

5.3.5 Fourier Transform Infra-Red Spectroscopy (FT-IRS)

Fourier transform infra-red spectroscopy (FT-IR) was performed using a IFS 66 (Bruker, Ettlingen, Germany) FT-IR spectrometer equipped with a nine reflection diamond attenuated total reflection cell (DuraSamp IR, Smiths) and a mercury cadmium telluride detector. The microgel suspensions 10 μL were deposited on top of the ATR crystal and dried to a film using air flow for at least 10 min. The spectra were recorded using a resolution of 2 cm^{-1} with 1024 scans in a spectral range of 0 to 7899 cm^{-1}. The acquired absorbance data were multiplied by the corresponding wavenumber to correct the wavenumber dependent penetration depth and normalized to the absorption amide-band at 1643 cm^{-1}.

Scanning Electron Microscopy (SEM)

Scanning electron microscopy (SEM) investigations were performed on an ESEM-FEG (Philips XL30, Philips, Eindhoven, Netherlands) with an acceleration voltage of 3 kV and a working distance of 10 mm. For the sample preparation 25 μL of microgel solution ($c \leq 0.0001$ wt%) were deposited on cleaned silicon wafers and dried at ambient temperature in air. The wafers were cleaned as described in the section "Atomic Force Microscopy" and sputtered with palladium with a Polaron Equiqment (Polaron Equipment Ltd., now Quorum Technologies Ltd., Puslinch, Ontario, Canada) SEM Coating Unit E5000 . Particle diameters were analyzed to support the AFM Images using the program ImageJ (Wayne Rasband, National Institutes of Health, USA).

5.3.6 Preparation and Characterization of free-standing microgel membranes

Microgel monolayers were prepared via spin-coating 10 x 10 mm gold sputtered wafer using a spin-coater (Süss MicroTec Lithography GmbH, Garching, Germany). Prior to the gold sputtering the wafers were cleaned with ethanol, treated with oxygen plasma for 10 min and for high purity treated with a solution of H_2O:NH_3:H_2O_2 in a ratio 5:1:1. Afterwards the wafers were sputtered with gold for 999 s in an argon plasma using a BAL-TEC MED20 coating system with a BAL-TEC MSC010 multi control cystem (BAL-TEC AG (since 2008 Leica BAL-TEC), Balzers, Liechtenstein). The gold sputtered wafers were treated with oxygen plasma for 30 s in order to increase the hydrophilicity of the gold surface. A diluted microgel solution (1 mL; 0.35 wt%) was spin-coated onto the gold sputtered wafers at 1000 rpm for 300 s. The so produced microgel monolayers were characterized using AFM.

In order to produce free-standing cross-linked microgel membranes the microgel monolayers were cross-linked with an electron beam in high vacuum ($5 \cdot 10^{-8}$ mbar) using an electron flood gun at an energy of 100 eV and an electron dose of 70 mC/cm^2 being applied. The substrate with the cross-linked microgel layer was than placed in a bath containing diluted aqua regia (HCl:HNO_3 in a ratio of 6:1) in order to dissolve the gold layer. During the removal of the gold layer the microgel film detaches from the substrate and drifts towards the air/liquid interface were it could be picked up with any other substrate. For reference measurements the film was transferred to another piece of silicon wafer and again characterized using AFM.

5.3.7 Resistance Measurements

Free-standing microgel membranes from the samples NcBH5, NcBH10 and NcBH15 were cut into small pieces ($\sim$ 2 mm^2) and picked up out of the solution with a (3 mm^2)Si_3N_4-chip with a (70 μm^2)funnel hole. This chip was placed in a microfluidic array in a temperature controlled acrylic glass block. On each end of the chip with the microgel membrane a silver electrode was embedded in the microfluidic array. This setup was used to determine the change in resistance as a function of the temperature if a voltage was applied to the electrodes. As medium for the current to flow between the electrodes a ferrocyanide solution with phosphate-buffer (20 mM KCl, 20 mM monosodium phosphate (NaH_2PO_4)) at pH 7.0 was employed. The resistance of the microgel membranes was measured in a range of 17 °C to 34 °C with an increment of 1 °C and a voltage of $\pm$5 mV with an increment of 1 mV / 1 °C was applied with an Axopatch 200B Amplifier (Molecular Devices, Sunnyvale CA, USA). The resistance was recorded as a function of the temperature.

5.4 Results and Discussion

5.4.1 Photon Correlation Spectroscopy (PCS) results

A copolymerization of NIPAM with the comonomer NBHAM in a standard surfactant free radical precipitation polymerization was successfully performed. In order to characterize the hydrodynamic dimensions, the polydispersity and the temperature response of the obtained copolymer microgels temperature dependent PCS measurements were performed. Moreover, the PCS experiments also yield the VPTT.

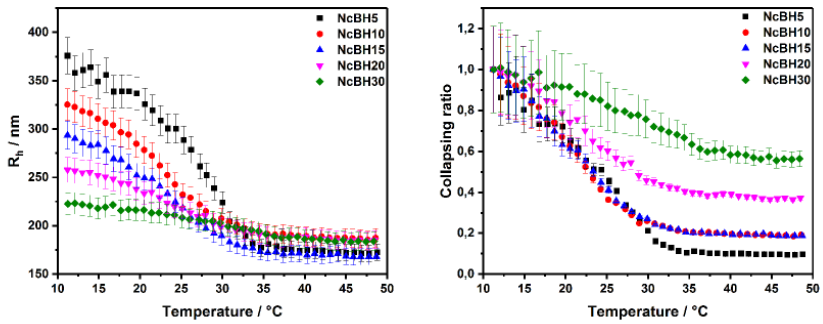

FIGURE 5.2: (left) The swelling curves show the change in the hydrodynamic radius of the microgel particles with increasing temperature. The inflection point is the VPTT of the system. Due to the broadening of the phase transition with increasing NBHAM content this point cannot be defined precisely for all systems. (right) Collapsing ratio of the microgel particles as a function of the temperature.

From the Stokes-Einstein equation the hydrodynamic radius R_h was calculated and the results for the microgels in swollen state (T = 10 °C) and the collapsed state (T = 50 °C) are listed in Tab. 5.2. The hydrodynamic radii of the microgel particles as a function of the temperature curves and the collapsing ratio as a function of the temperature are depicted in Fig. 5.2. From the microgel size the maximum collapsing ratio α_{max} can be determined via eq 1 using the particle volume in the swollen state $V_{swollen}$ and the volume in the collapsed state $V_{collapsed}$ with the assumption of spherical particles. All obtained values are summarized in Tab. 5.2.

$$\alpha_{max} = \frac{V_{h,collapsed}}{V_{h,swollen}} = \frac{R^3_{h,collapsed}}{R^3_{h,swollen}} \tag{5.2}$$

Looking at Tab. 5.2 it is obvious that the size of the microgel particles in the swollen state (T = 10 °C) decreases with increasing NBHAM content, while the size in the collapsed state (T = 50 °C) is similar for all NBAHM contents. A similar behavior was observed in pNIPAM-*co*-*N*-*tert*-butylacrylamide copolymer microgels. [33] *N*-*tert*-butylacrylamide and NBHAM both are hydrophobic, which leads to a decrease in swelling capacity and a shift of the lower critical solution temperature (LCST) towards lower temperatures. With NBHAM this effect is even more pronounced compared to *N*-*tert*-butylacrylamide. Hence, it is straightforward to assign the strong shift of LCST and the slow diminishing of the transition at 20 mol% NBHAM and above to the highly hydrophobic aromatic comonomer. Therefore the swelling curves already indicate the successful incorporation of the NBHAM into the synthesized particles.

TABLE 5.2: Hydrodynamic radii of the copolymer microgels in the swollen and collapsed state and the maximum collapsing ratio α_{max}.The error of the radii corresponds to an estimation of 5%. Included in this estimation is not only the inacuracy of the measurement but also the polydispersity of the sample.

Sample Name	$R_{h,swollen}$/ nm	$R_{h,collapsed}$/ nm	α_{max}
NcBH 5	379±19	167±8	0.08±0.005
NcBH 10	335±17	177±9	0.15±0.01
NcBH 15	304±16	152±8	0.13±0.01
NcBH 20	270±14	174±9	0.27±0.02
NcBH 30	213±11	177±9	0.58±0.03

At first glance it is obvious, that with increasing temperature the solubility of the polymer network decreases which leads to a collapse of the microgel particles and a reduction of particle size. Additionally, with increasing NBHAM content this behavior alters. It can clearly be seen that with increasing NBHAM content the size of the microgels in the swollen state is continuously reduced. If the collapsing ratio is plotted as a function of temperature (see Fig.5.2) the magnitude of this effect becomes more prominent. However, it also can be seen, that samples NcBH10 and NcBH15 have a very similar collapsing ratio despite their difference in size. This could be the result of a different morphology that occurs when a certain amount of hydrophobic comonomer is present during the syntheis. In p(NIPAM-*co*-*N*-*tert*-butylacrylamide) copolymer microgels it was observed that the maximum nominal amount of *N*-*tert*-butylacrylamide that could be used in the synthesis was 15 mol%. [33] It is conceivable that this represents a threshold for the incorporation of hydrophobic molecules in the polymer network. This issue will be investigated in further research on this topic. Regardless of this observation the values from the temperature dependent PCS measurements are in good agreement with the data from the angular dependent PCS measurements. In addition it can be seen from the swelling curves that the VPTT decreases to lower values with increasing NBHAM content.

All these effects are a direct consequence of the hydrophobic aromatic moieties in the polymer network. The more hydrophobic material is present inside the polymer network, the poorer the solubility of the particle will be and the less it is able to swell under otherwise good solvent conditions. Therefore, the hydrophobic NBHAM lowers the solubility of the whole particle to the point (NcBH 30, 30 mol% nominal) where the microgel particles are constantly in the collapsed state and are no longer thermoresponsive.

5.4.2 Fourier Transformation Infrared Spectroscopy (FT-IR) results

To determine the actual amount of comonomer which is incorporated into the polymer network FT-IR spectroscopy is used. This technique is fast, non-invasive and especially reliable for identifying functional groups with a high sensitivity. Reference measurements of the pure comonomer NBHAM in acetone and quantum chemical calculations revealed absorption bands at 760, 742 and 700 cm^{-1} as characteristic bands for vibrations of the aromatic rings in the comonomer NBHAM. FT-IR spectra of pNIPAM-*co*-NBHAM copolymers show an increasing absorption at the respective wavenumber with increasing content Fig.5.3. However the specimen with 30 mol% nominal NBHAM amount exhibits an absorption comparable to that of the 20 mol% specimen.

In addition, a shift of the amide band at 1520 cm^{-1} to lower wavenumbers can be observed with increasing NBHAM content. To further analyse this effect, Fourier self deconvolution (FSD) [43] was applied Fig. 5.3. The deconvolution of the bands shows this shift more clearly. A comparison of the change of absorption and shift of the deconvoluted bands Fig. 5.3 shows that both methods yield comparable results for the copolymerization of NBHAM and NIPAM. For NBHAM amounts utilized during the synthesis between 0 mol% and 30 mol% the influence on the spectra is proportional to the utilized amount.

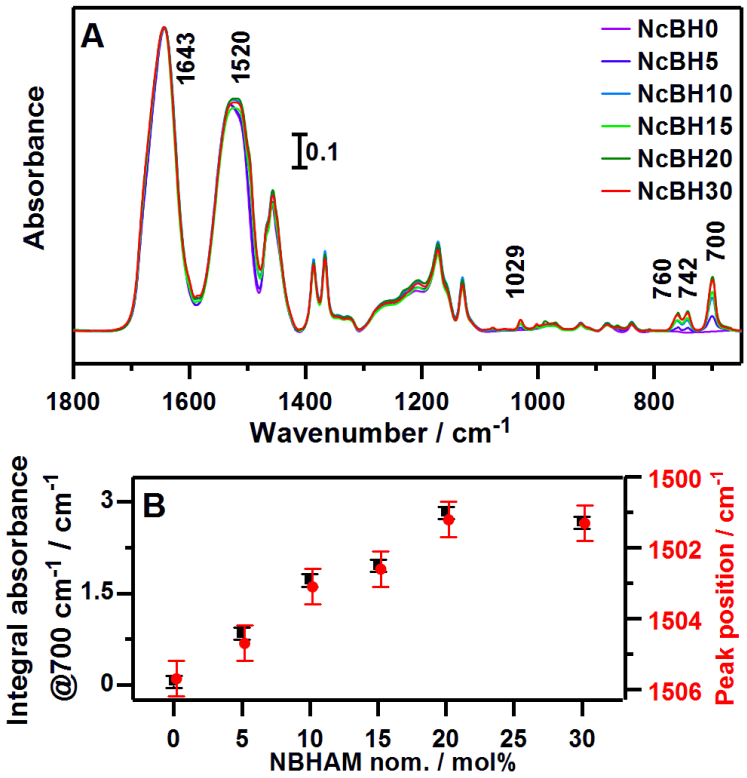

FIGURE 5.3: (A) FT-IR spectra of dried microgel films. The absorbance of the bands typical for NBHAM at 760, 742 and 700 cm^{-1} increase with increasing NBHAM amount. (B) FT-IR spectra of microgel in solution. (C and D) Dependence of absorbance and peak position after FSD on the NBHAM content during the synthesis.

5.4.3 Imaging techniques

Atomic Force Microscopy (AFM) results

The different copolymer microgels were deposited on silicon wafers and characterized using AFM in tapping mode. The recorded images of the totally collapsed particles in dried state are shown in Fig. 5.4 and a summary of the obtained results is given in Tab. 5.3. The AFM images clearly show that the dried microgel particles exhibit a circular form in top view with a narrow size distribution. An analysis of around 100 imaged particles obtained comparable particle diameters. The size determined from AFM measurements deviates from the PCS measurements due to the fact that dried particles on a surface are investigated here instead of free particles in solution. The size observed in the AFM images is a result of the particle behavior upon drying. The amount of aromatic comonomer has a strong influence on the

TABLE 5.3: Mean diameter and radii of the copolymer microgel particles obtained from analysis of AFM Images. The given error values is standard deviation of the diameter and radii, respectively.

Sample Name	Diameter / nm	Radius / nm
NcBH 5	599±42	299±21
NcBH 10	620±41	309±20
NcBH 15	670±39	335±19
NcBH 20	718±44	359±22
NcBH 30	792±40	396±20

particles which becomes obvious in the comparison of the size of the dried particles. From Tab. 5.3 it can be seen that with increasing NBHAM amount the particles tend to be significantly larger in the dried state. Additional measurements were performed with a scanning electron microscope (SEM) (see Supporting Information: Appendix C) These measurements confirm the results gathered from AFM.

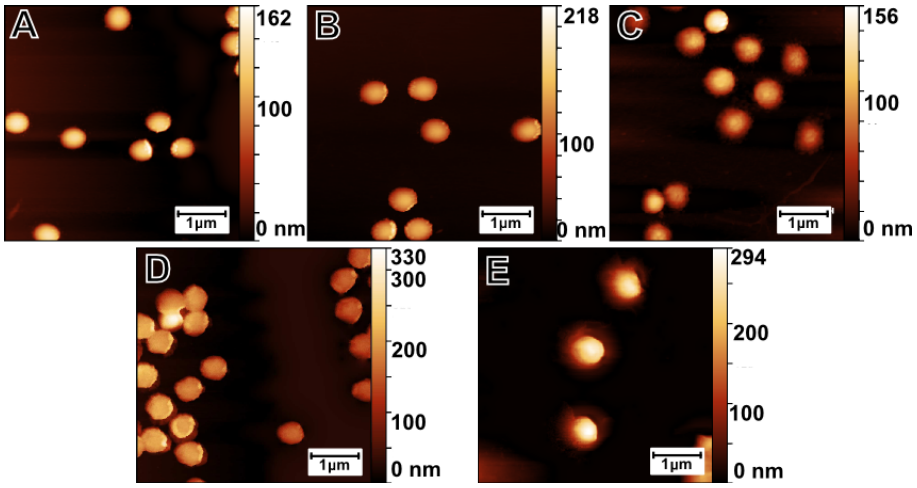

FIGURE 5.4: AFM images (5 μm^2)of the different copolymer microgel particles. Microgel solution (c $\leq$ 0.0001 wt%) evaporated in air at ambient temperatures. (A) NcBH5, (B) NcBH10, (C) NcBH15, (D) NcBH20 and (E) NcBH30. Various AFM images of microgel particles on silicon wafers were used to study the morphology and determine the size of the dried microgels on a flat, smooth surface.

5.4.4 Free-standing membranes and membrane resistance

For the fabrication of the free standing microgel membranes the particles have to be deposited in densely packed monolayers on a suitable surface. Due to the strong decrease of the thermoresponsive behavior with increasing NBHAM content, only the microgel systems which are still significantly temperature responsive were used for the electron-beam cross-linking procedure. The samples used were NcBH5, NcBH10 and NcBH15.

In order to obtain homogenous monolayers of microgels a diluted microgel solution was spin-coated onto 10 mm^2 gold sputtered silicon wafers. These layers were analyzed with respect to their homogeneity using AFM in tapping mode at multiple spots on the surface. Fig. 5.5 shows typical AFM images of such spin-coated monolayers.

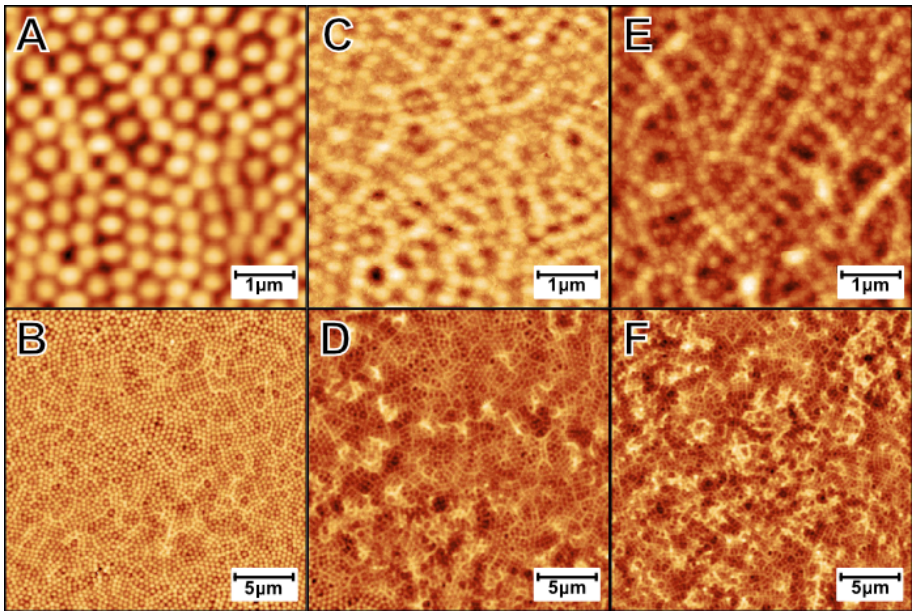

FIGURE 5.5: AFM images ($5\,\mu m^2$ and $25\,\mu m^2$) of microgel monolayers. (A,B) Images of a spin-coated microgel layer from the sample NcBH5, (C,D) images of a spin-coated layer from the sample NcBH10 and (E,F) images of a spin coated layer from the sample NcBH15. All layers were produced using the same spin-coating parameters.

The AFM images show that the produced layers consist of densely packed microgel particles with nearly no defects.We assume that the rotational forces during the spin-coating and the very dense packing of the microgel particles result in a deformation of the microgel network. As a consequence, the contact area between individual particles is enlarged and favors an inter-particle cross-linking during electron beam treatment. The increased overlapping of the microgel particles is reflected in the roughness of the densely packed microgel monolayers. After the cross-linking procedure at ($5 \cdot 10^{-8}$ mbar) using an electron flood gun at an energy of 100 eV and an electron dose of $70\,mC/cm^2$ the microgel coated wafers were placed in a 6:1 mixture of hydrochloric acid and nitric acid. This mixture was chosen to dissolve the gold coating in a more gentle way compared to standard aqua regia and to avoid rapid gas formation, which could disrupt the membrane. During the dissolution process of the gold layer, the microgel membrane detaches slowly from the wafer and floats towards the air/liquid interface

At this point the membrane can be picked up at the liquid interface with another silicon wafer and placed in a water bath to remove traces of acid in the polymer network. From the water bath the microgel membrane can be transferred to any substrate. The transfer process is carried out in a simple manner utilizing polymer scale pans for dissolving the gold and washing the film. The substrates to pick up the microgel films are handled with tweezers. When comparing the microgel layers after deposition (Fig 5.5 to the detached films (Fig 5.7) using AFM, it is obvious that the morphology of the films has changed. While the films from the samples NcBH5 and NcBH15 are still clearly showing that these films are composed of microgel particles the film from the sample NcBH10 has completely changed in morphology. The microgel particles can hardly be identified and the layer appears to be composed of worm-like structures. This distortion seems to significantly influence the film structure as subsequent experiments have shown. The membranes from

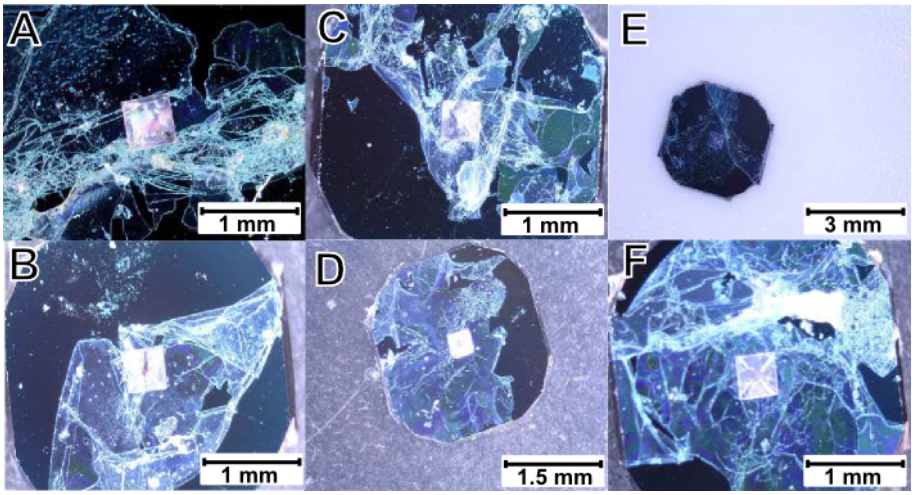

FIGURE 5.6: Photograph of microgel monolayers deposited on a silicon chip with a silicon-nitrate (Si_3N_4) membrane with a funnel hole after detachment from the original gold coated substrate. A and B are membranes made from the NcBH5 microgel, C and D are made from NcBH10 and E and F are made from NcBH15. The membranes on the Si_3N_4 chips where used in this form for the conductivity measurements.

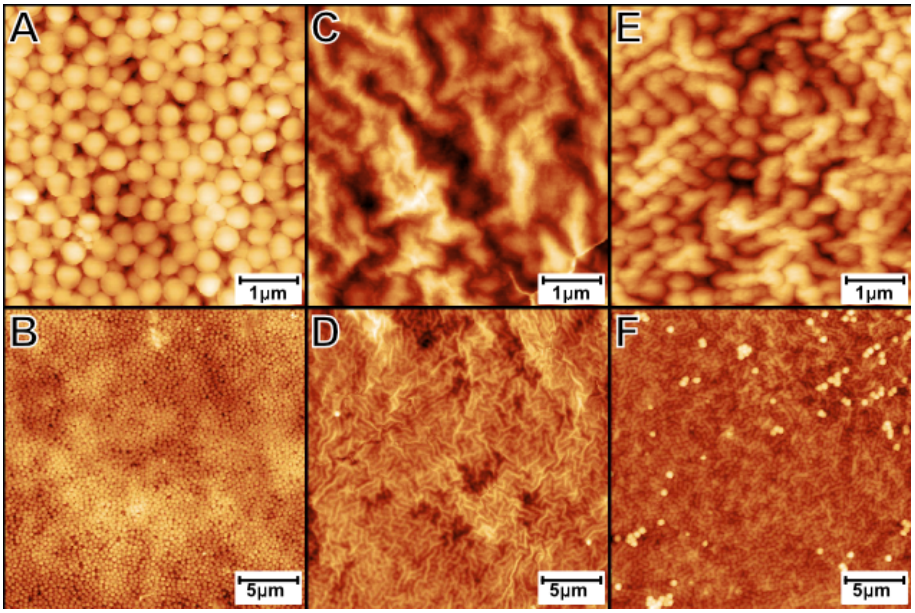

FIGURE 5.7: AFM Images (5 μm^2 and 25 μm^2) of cross-linked microgel membranes deposited on silicon chip with a silicon-nitrate (Si_3N_4) membrane with a funnel hole after detachment from the original gold coated substrate. A and B are membranes made from the NcBH5 microgel, C and D are made from NcBH10 and E and F are made from NcBH15.

the sample NcBH10 show a significantly higher resistivity than the films from the samples NcBH5 and NcBH15.

As an experiment which reveals the possibilities arising from these free-standing membranes we have transferred pieces of membranes ($\sim 2\,mm^2$) to a $3\,mm^2$ silicon chip with a Si_3N_4-membrane with a ($70\,\mu m^2$) funnel hole. These chips with the membrane covered funnel holes were placed in a temperature controlled microfluidic device as described in the experimental part. The resistance as a function of the temperature was determined by measuring the current between two platinum electrodes through a phosphate-buffer 20 mM KCl, 20 mM monosodium phosphate (NaH_2PO_4) solution at pH 7.0. The results for a measurement with two of the membranes are depicted in Fig. 5.8.

This figure (Fig. 5.8) shows the resistivity increases with increasing temperature with a steep increase around the VPTT of the microgels. This clearly reveals the dependence of the conductivity on the temperature induced shrinking of the microgel membrane. Hence, the temperature response of the microgels is preserved in the electron beam cross-linking process and responsive transferable membranes are obtained. This way of utilizing a polymer network as a switchable filtration device is even different from previously published work in which nano-porous materials were coated with thermoresponsive microgels by Menne et al.[44]. In the mentioned work the microgels open the pores upon collapse and therefore enable a higher molecular flux at higher temperatures. Whereas our membrane enables a higher molecular flux upon swelling at low temperatures. The functionality is in principle similar to the thermoresponsive ultrafiltration membranes fabricated by Frost and Ulbricht [21]. However the microgel membrane presented in this paper has the major additional advantage of transferability to any desired solid or porous substrate and therefore increasing the range of possible applications significantly.

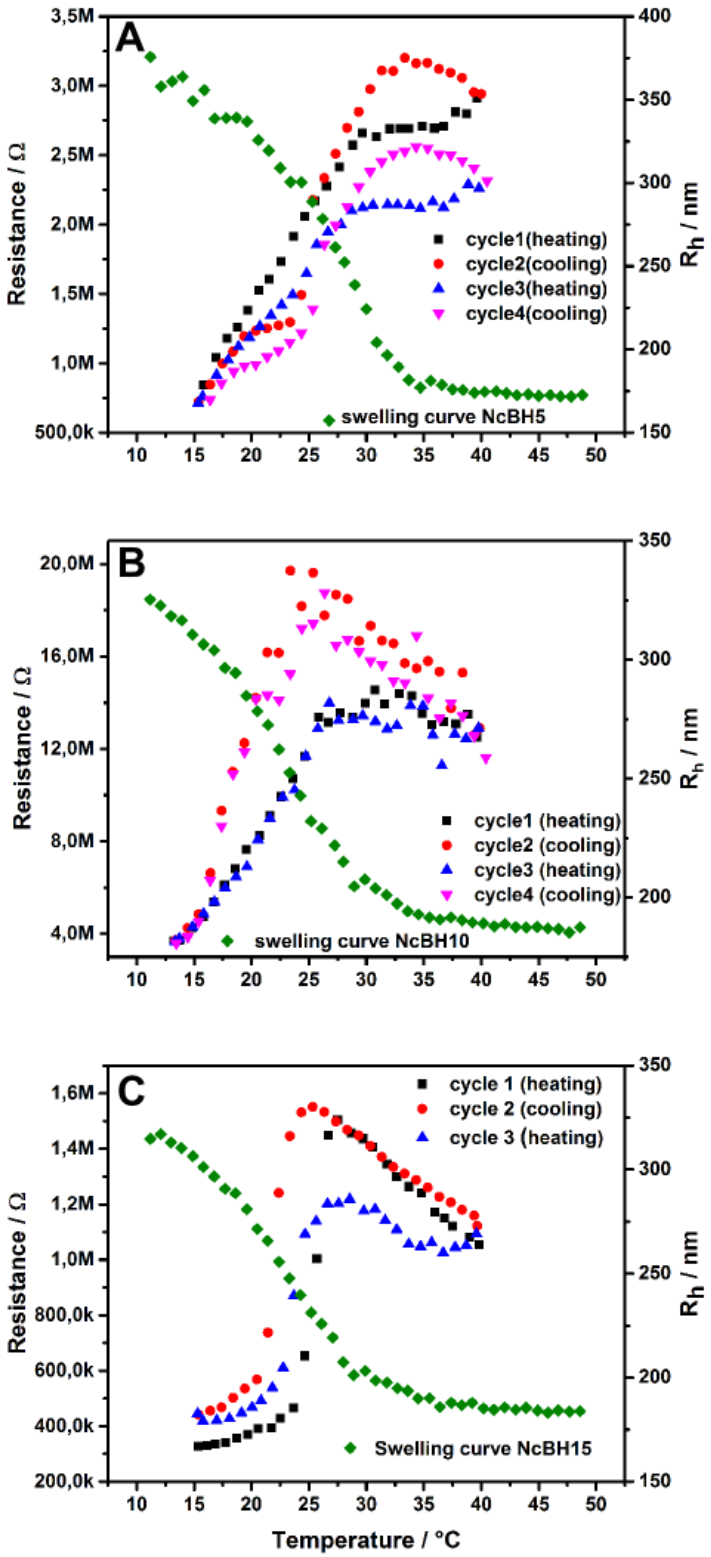

FIGURE 5.8: Resistivity for membranes from the microgel samples NcBH5 (A), NcBH10 (B) and NcBH15 (C) for a phosphate-buffer 20 mM KCl, 20 mM monosodium phosphate (NaH_2PO_4) solution at pH 7.0 and the swelling curves of the corresponding microgels obtained from PCS measurements.

5.5 Conclusions

In this work we have synthesized and characterized NIPAM copolymer microgels with NBHAM as an aromatic comonomer. The particles exhibit a spherical and homogenous shape with a narrow size distribution confirmed by PCS, AFM and SEM. A further characterization of these particles revealed that these copolymer microgels are only thermoresponsive up to a comonomer content of 20 mol%. Beyond this amount the swelling and deswelling is simply of osmotic nature. The comonomer allows electron beam cross-linking of microgel monolayers and hence the production of free-standing, responsive and transferable microgel membranes. For the creation of these thermoresponsive free-standing films the copolymer microgels which are still thermoresponsive, NcBH5, NcBH10 and NcBH15, have been chosen. The spin-coated microgel monolayers were cross-linked via electron beam irradiation in high vacuum using an electron flood gun. Subsequently the cross-linked microgel monolayers were detached from the substrate by dissolving the supporting gold film in aqua regia. In first experiments the free-standing, thermoresponsive microgel membranes were used as coatings for Si_3N_4-Chips with a ($70\,\mu m^2$) funnel hole. The membranes were found to modulate the ion flow as a function of temperature.

In contrast to existing rigid polymer membranes[22] where the filtration properties are determined by the pore size which is fixed and determined by the fabrication process, our membranes provide a tunable mesh or pore size that is determined by the swelling ratio of the polymer network. The presented approach for membrane modification is versatile and the microgel membranes can be used to coat and surface functionalize a broad variety of structures and due to the mechanical properties might also be useful as free-standing membranes. Furthermore these free-standing microgel films can be utilized to modify other types of membranes[22, 44] in order to tune their filtration properties.

References

[1] R. Pelton, "Temperature-sensitive aqueous microgels," *Adv. Colloid Interf. Sci.*, vol. 85, pp. 1–33, 2000. review.

[2] W. Richtering and B. R. Saunders, "Gel architectures and their complexity," *Soft Matter*, vol. 10, pp. 3695–3702, 2014. Review.

[3] A. Z. Pich and H.-J. P. Adler, "Composite aqueous microgels: an overview of recent advances in synthesis, characterization and application," *Polym. Int.*, vol. 56, pp. 291–307, 2007. Review.

[4] B. R. Saunders, "On the structure of poly(*N*-isopropylacrylamide) microgel particles," *Langmuir*, vol. 20, pp. 3925–3932, 2004.

[5] S. Nayak and L. A. Lyon, "Soft nanotechnology with soft nanoparticles," *Angew. Chem. Int. Ed.*, vol. 44, pp. 7686–7708, 2005. Review.

[6] V. S. Shinde, M. V. Badiger, A. K. Lele, and R. A. Mashelkar, "Core-shell morphology in poly(n-isopropyl acrylamide) copolymer gels induced by restricted diffusion of surfactant," *Langmuir*, vol. 17, pp. 2585–2588, 2001.

[7] J. D. Debord and L. A. Lyon, "Thermoresponsive photonic crystals," *J. Phys. Chem. B*, vol. 104, no. 27, pp. 6327–6331, 2000.

[8] M. Karg, Y. Lu, E. Carb*ó*-Argibay, I. Pastoriza-Santos, J. P*é*rez-Juste, L. M. Liz-Marz*á*n, and T. Hellweg, "Multi-responsive hybrid colloids based on gold nanorods and poly-(nipam-*co*-allyl-acetic acid) microgels:
temperature- and ph-tunable plasmon resonance," *Langmuir*, vol. 25, pp. 3163–3167, 2009.

[9] Y. Gao and M. J. Serpe, "Light-induced color changes of microgel-based etalons," *ACS Applied Materials & Interfaces*, vol. 6, no. 11, pp. 8461–8466, 2014.

[10] G. Kumaraswamy, A. M. Dibaj, and F. Caruso, "Photonic materials from self-assembly of tolerant core-shell coated colloids," *Langmuir*, vol. 18, pp. 4150–4154, 2002.

[11] M. Karg, S. Jaber, T. Hellweg, and P. Mulvaney, "Surface plasmon spectroscopy of gold-pnipam core-shell nanocrystals," *Langmuir*, vol. 27, pp. 820–827, 2011.

[12] K. Uhlig, T. Wegener, J. He, M. Zeiser, J. Bookhold, I. Dewald, N. Godino, M. Jaeger, T. Hellweg, A. Fery, and C. Duschl, "Patterned thermoresponsive microgel coatings for noninvasive processing of adherent cells," *Biomacromolecules*, vol. 17, no. 3, pp. 1110–1116, 2016.

[13] M. J. Serpe, C. D. Jones, and L. A. Lyon, "Layer-by-layer deposition of thermoresponsive microgel thin films," *Langmuir*, vol. 19, pp. 8759–8764, 2003.

[14] Y. Lu, Y. Mei, M. Drechsler, and M. Ballauff, "Thermoresponsive core-shell particles as carriers for ag nanoparticles: Modulating the catalytic activity by a phase transition in networks," *Angew. Chem. Int. Ed.*, vol. 45, pp. 813–816, 2006.

[15] M. Zeiser, I. Freudensprung, and T. Hellweg, "Linearly thermoresponsive core-shell microgels: Towards a new class of nanoactuators," *Polymer*, vol. 53, pp. 6096–6101, 2012.

[16] A. Balaceanu, V. Mayorga, W. Lin, M.-P. Schürings, D. E. Demco, A. Böker, M. A. Winnik, and A. Pich, "Copolymer microgels by precipitaion polymerization of *N*-isopropylacrylamides in aqueous medium," *Colloid Poly. Sci.*, vol. 291, pp. 21–31, 2013.

[17] M. J. Snowden, B. Z. Chowdhry, B. Vincentb, and G. E. Morris, "Colloidal copolymer microgels of *N*-isopropylacrylamide and acrylic acid: ph, ionic strength and temperature effects," *Journal of the Chemical Society, Faraday Transactions*, vol. 92, pp. 5013–5016, 1996.

[18] J. D. Debord and L. A. Lyon, "Synthesis and characterization of ph-responsive copolymer microgels with tunable volume phase transition temperatures," *Langmuir*, vol. 19, pp. 7662–7664, 2003.

[19] S. Schmidt, M. Zeiser, T. Hellweg, C. Duschl, A. Fery, and H. Möhwald, "Adhesion and mechanical properties of pnipam microgel films and their potential use as switchable cell culture substrates," *Adv. Func. Mater.*, vol. 20, no. 19, pp. 3235–3243, 2010.

[20] S. Schmidt, H. Motschmann, T. Hellweg, and R. von Klitzing, "Thermoresponsive surfaces by spin-coating of pnipam-co-paa microgels. a combined afm and ellipsometry study," *POLYMER*, vol. 49, pp. 749–756, 2008.

[21] S. Frost and M. Ulbricht, "Thermoresponsive ultrafiltration membranes for the switchable permeation and fractionation of nanoparticles," *Journal of Membrane Science*, vol. 448, pp. 1 – 11, 2013.

[22] R. Bernstein, E. Anton, and M. Ulbricht, "Tuning the nanofiltration performance of thin film strong polyelectrolyte hydrogel composite membranes by photografting," *J. Membrane Sci.*, vol. 427, pp. 129–138, 2013.

[23] K. Nagase, A. Kimura, T. Shimizu, K. Matsuura, M. Yamato, N. Takedab, and T. Okano, "Dynamically cell separating thermo-functional biointerfaces with densely packed polymer brushes," *J. Matter. Chem.*, vol. 22, pp. 19514–19522, 2012.

[24] K. Saha, J. Kim, E. Irwin, J. Yoon, F. Momin, V. Trujillo, D. V. Schaffer, K. E. Healy, and R. C. Hayward, "Surface creasing instability of soft polyacrylamide cell culture substrates," *Biophysical Journal*, vol. 99, pp. L94–L96, 2010.

[25] R. Steitz, V. Leiner, K. Tauer, V. Khrenov, and R. von Klitzing, "Temperature induced changes in polyelectrolyte films at the solid-liquid interface," *Appl. Phys. A*, vol. 74, pp. S519–S521, 2002.

[26] K. Nagase, J. Kobayashi, and T. Okano, "Temprature-responsive intellignet interfaces for biomolecular separation and cell sheet engineering," *J. Royal Soc. Interface*, vol. 6, pp. S293–S309, 2009.

[27] F. A. Plamper and W. Richtering, "Functional microgels and microgel systems," *Acc. Chem. Res.*, vol. 50, pp. 131–140, 2017. 10.1021/acs.accounts.6b00544.

[28] W. Geyer, V. Stadler, W. Eck, M. Zharnikov, A. Gözhäuser, and M. Grunze, "Electron-induced crosslinking of aromatic self-assembled monolayers: Negative resists for nanolithography," *Applied Physics Letters*, vol. 75, no. 16, pp. 2401–2403, 1999.

[29] C. T. Nottbohm, A. Beyer, A. S. Sologubenko, I. Ennen, A. Hütten, H. Rösner, W. Eck, J. Mayer, and A. Gölzhäuser, "Novel carbon nanosheets as support for ultrahigh-resolution structural analysis of nanoparticles," *Ultramicroscopy*, vol. 108, no. 9, pp. 885 – 892, 2008.

[30] S. Khaksar, E. Fattahi, and E. Fattahi, "Organocatalytic synthesis of amides from nitriles via the ritter reaction," *Tetrahedron Letters*, vol. 52, no. 45, pp. 5943 – 5946, 2011.

[31] M. Karg, I. Pastoriza-Santos, B. Rodriguez-González, R. von Klitzing, S. Wellert, and T. Hellweg, "Temperature, ph, and ionic strength induced changes of the swelling behavior of pnipam-poly(allylacetic acid) copolymer microgels," *Langmuir*, vol. 24, no. 12, pp. 6300–6306, 2008.

[32] B. Wedel, M. Zeiser, and T. Hellweg, "Non nipam based smart microgels: Systematic variation of the volume phase transition temperature by copolymerization," *Zeitschrift f. Phys. Chem.*, vol. 227, pp. 00–12, 2012.

[33] Y. Hertle, M. Zeiser, C. Hasenöhrl, P. Busch, and T. Hellweg, "Responsive p(nipam-*co*-ntbam) microgels: Flory–rehner description of the swelling behaviour," *Colloid and Polymer Science*, vol. 288, pp. 1047–1059, 2010.

[34] B. J. Berne and R. Pecora, *Dynamic Light Scattering*. New York: John Wiley & sons, Inc., 1976.

[35] S. W. Provencher, "A constrained regularization method for inverting data represented by linear algebraic or integral equations," *Computer Physics Com.*, vol. 27, pp. 213–217, 1982.

[36] S. W. Provencher, "Contin: a general purpose constrained regularization program for inverting noisy linear algebraic and integral equations," *Computer Physics Com.*, vol. 27, pp. 229–242, 1982.

[37] D. E. Koppel, "Analysis of macromolecular polydispersity in intensity correlation spectroscopy: the method of cumulants," *The Journal of Chemical Physics*, vol. 57, pp. 4814–4820, 1972.

[38] P. A. FitzGerald, D. Dupin, S. P. Armes, and E. J. Wanless, "In situ observations of adsorbed microgel particles," *Soft Matter*, vol. 3, pp. 580–586, 2007. no copy.

[39] C. D. Sorrell and L. A. Lyon, "Bimodal swelling responses in microgel thin films," *J. Phys. Chem. B*, vol. 111, pp. 4060–4066, 2007.

[40] S. Höfl, L. Zitzler, T. Hellweg, S. Herminghaus, and F. Mugele, "Volume phase transition of smart microgels in bulk solution and adsorbed at an interface: A combined afm, dynamic light, and small angle neutron scattering study," *Polymer*, vol. 48, pp. 245–254, 2007.

[41] A. Burmistrova, M. Richter, C. Uzum, and R. von Klitzing, "Effect of cross-linker density of p(nipam-*co*-aac) microgels at solid surfaces on the swelling/shrinking behaviour and the youngs modulus," *Colloid Poly. Sci.*, vol. 289, pp. 613–624, 2011.

[42] D. Necas and P. Klapetek, "Gwyddion: an open-source software for (spm) data analysis," *Central European Journal of Physics*, vol. 10, pp. 181–188, 2012.

[43] J. K. Kauppinen, D. J. Moffatt, H. H. Mantsch, and D. G. Cameron, "Fourier self-deconvolution: A method for resolving intrinsically overlapped bands," *Appl. Spectrosc.*, vol. 35, pp. 271–276, 1981.

[44] D. Menne, F. Pitsch, J. E. Wong, A. Pichj, and M. Wessling, "Temperature-modulated water filtration using microgel-functionalized hollow-fiber membranes," *Angewandte Chemie International Edition*, vol. 53, no. 22, pp. 5706–5710, 2014.

Chapter 6

Conclusion and perspective

Smart surfaces are a useful tool for numerous applications as it has been shown by the research performed during this work. The ability to alter the properties of a surface is a key aspect for the creation of surfaces with extraordinary properties.

This study has revealed interesting aspects of microgels adsorbed at an interface. Atomic force microscopy measurements of microgels have shown the structure of single microgels of different architecture when attached to a solid surface. These measurements are necessary when it comes to the understanding of certain aspects of the behavior of microgels in an adsorbed state and it provides crucial knowledge for the production of homogeneous microgel coatings. It has been shown that microgels that are made from different monomers like NIPAM, NNPAM and NIPMAM behave different when adsorbed on a surface though they seem similar in a lot of ways. All three monomers are very similar to each other in terms of the chemical structure and they all form microgels under the same reaction condition which all are spherical in shape and do not differ significantly in size. The major difference between these monomers is the lower critical solution temperature (LCST) and the behavior around that temperature of the polymers they form. AFM measurements have revealed that these microgel particles exhibit a significantly different morphology when adsorbed to a surface. While pNNPAM and pNIPAM microgels show a very pronounced core-shell structure, which is more prominent in pNNPAM microgels, pNIPMAM microgels show a homogeneous morphology. These findings hint at a different mechanism during the polymerization process leading to an entirely different particle morphology. Observation of this was possible due to the ability to detect differences in surface morphology and its physical properties by measuring the phase in an AFM experiment performed in tapping mode. Using electron microscopy it would not have been possible to detect the thin stretched polymer chains originating from the microgel particles core that surrounded the same. This occurrence, which is a few nm thick polymer disk would not deflect a sufficient amount of electrons to be clearly visible in an electron microscopy image and could therefore be easily missed. These results demonstrate the usefulness of AFM for investigating microgel morphology and architecture. Especially when taken into consideration, that it is possible to probe samples with AFM in their native state and environment. The sample does not need to be coated with a metal film or to be introduced to a vacuum to be characterized. Such procedures can be a disadvantage due to the fact that the sample might be altered through these. (Chapter 2)

Being able to investigate microgel particle morphology in their native state and environment in such detail, AFM was used to study the morphology of particles that were synthesized with surfactant addition at different times after initiation of the reaction. AFM analysis revealed, that two species were formed during the synthesis. Further, these measurements showed that the ratio of the two species depends strongly on the point of time at which the surfactant is added. From a certain point

of time on only one species can be detected. In the case of the presence of multiple microgel species the PCS analysis is not possible in an easy manner and therefore the determination of the size of the two species is a challenging task. Atomic force microscopy provides a tool which in this case can be used to estimate the particle sizes and their ratio to one another. (Chapter 3)

Preceding AFM imaging experiments with microgels adsorbed at a solid interface led to a better understanding of these particles and their behavior when they adsorb. These experiments provided information about the capability of the microgel particles to deform, the influence of the microgels architecture and their morphology. When designing smart surface coatings based on these particles the results obtained offered useful insights on the deposition behavior of microgel particles. Numerous experiments were performed with microgels of divers architecture in order to investigate the formation of a microgel layer under different conditions using different coating techniques like spin-coating, dip-coating and spray-coating. (Appendix E)

In the course of the cooperation with different institutes and companies during the BMBF funded project "ThermoCell" this information proved valuable when it came to the question what material to use for advanced cell culture substrates. Here microgels proved to be superior to other materials like coatings with linear polymers and PEG microgels not only in their deposition behavior but most of all in their applicability for the project goals. The size, LCST, architecture and morphology of pNIPAM based microgels are easily tunable to achieve the desired characteristics. Furthermore the synthesis can be up-scaled and is reproducible every time. Deposition experiments in which homogeneous microgel monolayers where produced using spin-coating were a foundation on which further experiments were based. The main information taken from the experiments were the deposition behavior of the microgels and the structure, roughness and durability of the resulting microgel coating. Coating experiments have been mainly performed with pNIPAM based copolymer microgels copolymerized with acrylic acid (AA). These microgel particles originated from works by Michael Zeiser. In addition a pNIPAM homopolymer was tested for applicability resulting in the finding that this homopolymer microgel with 5 mol% cross-linker BIS and the copolymer microgel with the lowest AA content (1.1 mol%) are the most suitable. The microgels from these samples were found to have the best characteristics in terms of volume phase transition temperature (VPTT) and layer roughness in the collapsed state and therefore were ideal for the cell culture experiments. From the deposition experiments performed by us a routine for printing those microgels with inkjet printers and stamps was developed. This led to the development of the advanced wound-healing assays developed from this project. (Chapter 4)

During the experiments with microgel surface coatings and cell culture substrates the idea was formed that it would be of great advantage if such a smart microgel coating would be transferable. The major disadvantage of modifying surface properties with smart microgels is, that this can solely be done by direct deposition on the substrate. This limitation excludes three dimensional substrates and gratings since they can't be directly coated with these particles. Therefore a technique was developed to make microgel coatings transferable to any desired substrate. Novel copolymer microgels have been developed with this application in mind. These new microgel copolymer particles contain aromatic moieties in order to cross-link the particles in a microgel layer using electron-beam irradiation. After the irradiation process the gold layer underneath the microgels was dissolved in aqua regia and a

free-standing microgel layer could be obtained from the process. In order to investigate the thermoresponsive properties of these free-standing microgel film a conductivity measurement procedure was developed in cooperation with the physics department of Bielefeld University. For this the microgel film was deposited on a silicon chip with a nano-porous funnel hole and introduced to a micro-fluidic device. In this device the electric current through a phosphate-buffer solution was measured between two electrodes. Therefore the conductivity of the buffer solution was measured. The microgel film on the funnel hole was placed between the two electrodes in the buffer solution and the change in current was measured in dependence of the temperature. By measuring the change in current the resistivity of the film was measured indirectly. It has been found that the resistivity of the microgel film increases with decreasing temperature. This showed not only that the cross-linked microgel film was still thermoresponsive but that it also could be used as a temperature controlled membrane. Upon collapse of the microgels the permeability of ions through the membrane was reduced. In the performed experiments we have not only realized a transferable microgel coating that can be used to coat three dimensional substrates, we additionally have discovered and shown that these transferable microgel films can be used as temperature controllable membranes. (Chapter 5)

The presented research in this work has shown that microgel coatings can be utilized as cell culture substrates and that these smart surface coatings can be made transferable and even be used as a smart membrane. Here we present two of many possible applications that these smart surface coatings can be utilized for. Especially the transferability of such coatings enables numerous applications in membrane technology [1, 2, 3], biological and medical science [4, 5, 6], photonic materials [7, 8] and sensors [9]. All these research fields can profit from transferable smart coatings, therefore the applicability of these novel microgel membranes in these fields has to be investigated. First and foremost the process of producing the free-standing microgel films has to be optimized. The dissolving process of the supporting gold layer displays many flaws. In some cases the membrane reattaches itself to the silicon wafer beneath the gold layer and does not float towards the surface and in addition aqua regia is a very strong and aggressive acid which might hydrolyze the polymer leading to possible blemishes. A more gentle approach should be investigated in the course of which the whole supporting substrate is dissolved and the microgel film has therefore nothing to reattach itself to. Since it is only possible up to now to isolate small pieces of free-standing film due to the named flaws it is desirable to optimize the process to the point where larger films can be obtained from the process in order to be able to perform coating experiments with various three dimensional shapes. In recent conductivity experiments only phosphate buffer solution was used to investigate the membrane capabilities of the microgel films. This can and should be extended to experiments with a variety of charged molecules. Through this way the barrier characteristics of the microgel membrane can be investigated further. In the performed experiment the membrane was able to restrict the flow of charged molecules through it not stop it entirely. The question that needs to be answered is what characteristics and what size a molecule needs to have, so that it may not be able to pass the microgel membrane at all. Furthermore, tailoring membrane properties through by using microgels with different sizes and phase transition behavior is another interesting approach. It is unclear if a copolymerization of the aromatic co-monomer is possible with NNPAM or NIPMAM or if the membranes characteristics can be tuned in any other way either by variations in the microgel synthesis or post-synthetic. The possibilities are manifold and this work has proven the concepts feasibility and has opened a path to numerous possible applications.

References

[1] R. Bernstein, E. Anton, and M. Ulbricht, "Tuning the nanofiltration performance of thin film strong polyelectrolyte hydrogel composite membranes by photografting," *J. Membrane Sci.*, vol. 427, pp. 129–138, 2013.

[2] D. Menne, F. Pitsch, J. E. Wong, A. Pichj, and M. Wessling, "Temperature-modulated water filtration using microgel-functionalized hollow-fiber membranes," *Angewandte Chemie International Edition*, vol. 53, no. 22, pp. 5706–5710, 2014.

[3] S. Frost and M. Ulbricht, "Thermoresponsive ultrafiltration membranes for the switchable permeation and fractionation of nanoparticles," *Journal of Membrane Science*, vol. 448, pp. 1 – 11, 2013.

[4] K. Nagase, A. Kimura, T. Shimizu, K. Matsuura, M. Yamato, N. Takedab, and T. Okano, "Dynamically cell separating thermo-functional biointerfaces with densely packed polymer brushes," *J. Matter. Chem.*, vol. 22, pp. 19514–19522, 2012.

[5] K. Uhlig, T. Wegener, J. He, M. Zeiser, J. Bookhold, I. Dewald, N. Godino, M. Jaeger, T. Hellweg, A. Fery, and C. Duschl, "Patterned thermoresponsive microgel coatings for noninvasive processing of adherent cells," *Biomacromolecules*, vol. 17, no. 3, pp. 1110–1116, 2016.

[6] S. Schmidt, M. Zeiser, T. Hellweg, C. Duschl, A. Fery, and H. Möhwald, "Adhesion and mechanical properties of pnipam microgel films and their potential use as switchable cell culture substrates," *Adv. Func. Mater.*, vol. 20, no. 19, pp. 3235–3243, 2010.

[7] G. Kumaraswamy, A. M. Dibaj, and F. Caruso, "Photonic materials from self-assembly of tolerant core-shell coated colloids," *Langmuir*, vol. 18, pp. 4150–4154, 2002.

[8] M. Karg, S. Jaber, T. Hellweg, and P. Mulvaney, "Surface plasmon spectroscopy of gold-pnipam core-shell nanocrystals," *Langmuir*, vol. 27, pp. 820–827, 2011.

[9] M. Zeiser, I. Freudensprung, and T. Hellweg, "Linearly thermoresponsive core-shell microgels: Towards a new class of nanoactuators," *Polymer*, vol. 53, pp. 6096–6101, 2012.

Appendix A

Supporting Information Chapter 3

The interaction of anionic surfactants with PNnPAM microgels seems to be much more pronounced than the interaction of anionic surfactants with PNIPAM microgels, concerning the early synthesis phase. Unfortunately, there are a lot of different aspects that can affect this early synthesis process in emulsion polymerizations. Therefore, the exact role of the difference in the chemical structure of the monomers NnPAM and NIPAM and NIPMAM is difficult to determine. In order to obtain more insights on the interactions of the surfactants with the polymers, we investigated the influence of SDS addition to premade PNnPAM and PNIPMAM microgel suspensions and compared the influence of SDS on the volume phase transition temperature (VPTT) of these microgel suspensions with the results for PNIPAM microgels obtained by Wu et al. [1] The increase of the VPTT can be explained by incorporation of surfactant molecules into the microgel network. This reduces the osmotic pressure and generates a higher charge density in the microgel network.[2, 3] Fig. A.1 shows the influence of SDS on the VPTT of PNnPAM, PNIPAM and PNIPMAM microgels. It is obvious, that the influence of SDS on PNIPAM microgels is much lower, than in the case of PNnPAM microgels and is lowest for PNIPMAM microgels. While the VPTT of PNIPAM only shifts a few degrees at intermediate amounts of SDS and PNIPMAM microgels are nearly unaffected, a crucial influence on the VPTT of PNnPAM is already visible at low surfactant concentrations. At the highest SDS concentration the VPTT of PNIPMAM only shifts about 16 % and in case of PNIPAM the VPTT shifts by about 37 %. In contrast, the VPTT of PNnPAM is increased by 117 %. These observations are in line with the influence of the surfactant on the obtained particle size of the microgel particles, when SDS is present in the synthesis. The interaction of SDS with PNIPAM and PNnPAM has to be different, or more precisely PNnPAM shows a considerably stronger interaction with SDS than PNIPAM. As mentioned above, this strong interaction should correlate to the assembly of SDS molecules inside the microgels internal network. We assume that this is related to a stronger hydrophobicity of PNnPAM microgels. The solvation of the *n*-propyl sidechains seems to be less favorable than the solvation of the isopropyl group of PNIPAM and causes therefore stronger interactions with the hydrophobic parts of the surfactant molecules. Additional insight into the interaction of the surfactant with the different side chains can be obtained by a variation of the surfactant structure. Therefore, we replaced the SDS with SDeS. The results of these experiments are also shown in Fig. A.1 and are compared to the results for SDS. It is obvious that the observed trends for SDS and SDeS are similar. While PNIPAM and PNIPMAM show a rather weak response to the addition of SDeS to the microgel suspension, PNnPAM has a more pronounced response. Since both, SDS and SDeS have a lot of structural motives in common, this is a result one would expect. However, a remarkable difference is that the concentrations of SDeS required to influence the VPTT are a lot higher than those for SDS. The same trend was also observed for

the influence on the particle size. A longer hydrophobic chain leads to a stronger incorporation into the microgel network and therefore shifts the VPTT already at lower concentrations.

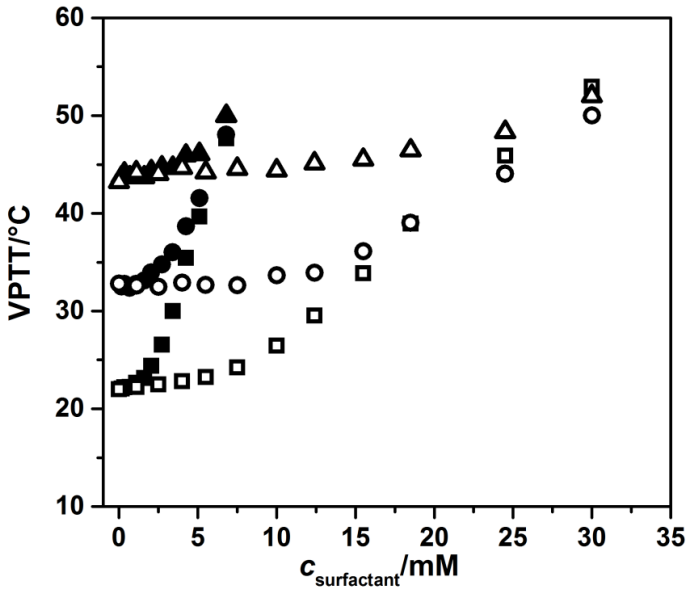

FIGURE A.1: VPTT of premade PNnPAM (squares), PNIPAM (circles) and PNIPMAM (triangles) microgel suspensions as a function of the added surfactant concentration of SDS (filled symbols) and SDeS (hollow symbols). The VPTT was determined by turbidity measurements.

A parameter which is not included in Fig. A.1 is the inferior surface activity of SDeS compared with SDS. It should be possible to normalize the obtained VPTT shifts with the cmc of the respective surfactant. The result of this normalization may allow an exact prediction of the VPTT shift of an acrylamide by addition of an anionic surfactant, if the cmc of the surfactant is quantified. Fig. A.2 shows the result of the normalization process. The data sets for all three microgels fall on a mastercurve as it was shown for PNIPMAM microgels by von Nessen et al. [4]. We expect that a prediction of the VPTT shift for sulfate surfactants of any chain length is possible, if the concentration and the cmc of the surfactant are known. But one additional important fact is, that the influence of any anionic surfactant on PNnPAM is always more pronounced compared to the influence on PNIPAM microgels or on PNIPMAM microgels.

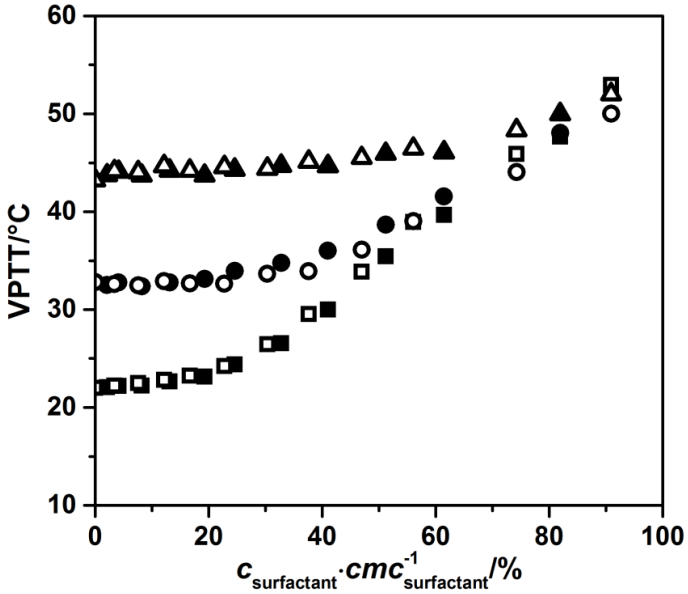

FIGURE A.2: VPTT shift of PNnPAM (squares), PNIPAM (circles) and PNIPMAM(triangles), due to addition of SDS (filled symbols) and SDeS (hollow symbols) to premade microgel suspensions. The added surfactant concentration was normalized with the respective cmc of the surfactant, to generate a mastercurve for all three microgels, respectively.

References

[1] C. Wu and S. Zhou, "Effects of surfactants on the phase transition of poly(n-isopropylacrylamide) in water," *J. Polym. Sci. B Polym. Phys*, vol. 34, pp. 1597–1604, 1996.

[2] S. J. Mears, Y. Deng, T. Cosgrove, and R. Pelton, "Structure of sodium dodecyl sulfate bound to a poly(nipam) microgel particle," *Langmuir*, vol. 13, p. 1901, 1997.

[3] K. C. Tam, S. Ragaram, and R. H. Pelton, "Interaction of surfactants with poly(n-isopropylacrylamide) microgel latexes," *Langmuir*, vol. 10, pp. 418–422, 1994.

[4] K. v. Nessen, M. Karg, and T. Hellweg, "Thermoresponsive poly-(*N*-isopropylmethacrylamide) microgels: Tailoring particle size by interfacial tension control," *Polymer*, vol. 54, no. 21, pp. 5499–5510, 2013.

Appendix B

Supporting Information Chapter 4

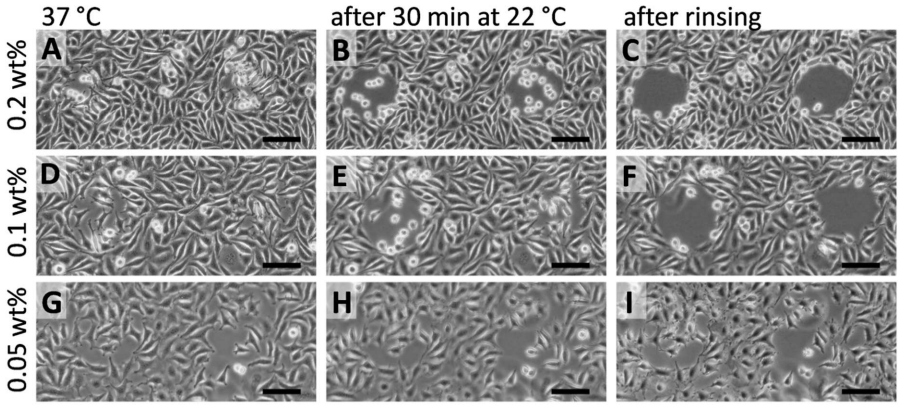

FIGURE B.1: Phase contrast images of L929 mouse fibroblasts cultivated on PEI-coated glass cover slides with thermoresponsive microgels spots (MZ160). The concentration of the microgel suspension was varied during spotting (ink-jet); from 0.2 wt% (A-C) to 0.1 wt% (D-F) and 0.05 wt%(G-I). After one day of cell culture at 37 °C, the cells adhered and spread on the PEI-coated area and on the microgel (A, D and G). When having been exposed to room temperature ($\sim$ 22 °C) for 30 min, the cells changed their morphology from an elongated to a round shape on the microgel deposited with the highest concentration of 0.2 wt%(B). On spots generated from a microgel suspension of 0.1 wt%, the cells reduced their adhesion area (E). Cells located on spotted microgel with the lowest concentration of 0.05 wt% remained spread (H). The cells could locally be removed from the microgel by rinsing (C, F), except for those on microgel spots formed from 0.05 wt%(I). These cells remained on the microgel surfaces, similar to those growing on the PEI coating. The scale bars are 100 μm.

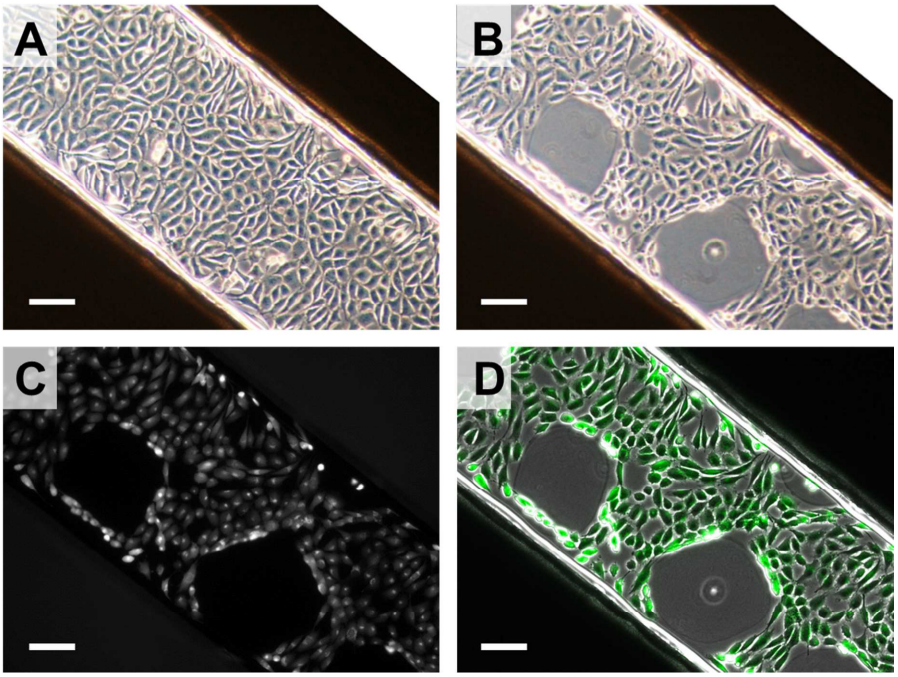

FIGURE B.2: Microscopy images of L929 mouse fibroblasts cultivated on PEI-coated glass cover slides with thermoresponsive microgels spots (MZ140, 0.5 wt%, prepared by spotting) in a microchannel. (A) After two days of cell culture at 37 °C, the cells adhered and spread on the PEI-coated area and on the microgel. (B) When having been exposed to room temperature (∼ 22 °C) for 30 min and flushing, the cells could locally be removed from the microgel. Afterwards, a life staining with calcein was performed to investigate the cell viability. All cells are stained as shown in the fluorescence image (C) and in the overlay (D), indicating a particularly gentle generation of a wound in a cell monolayer. The scale bars are 100 μm.

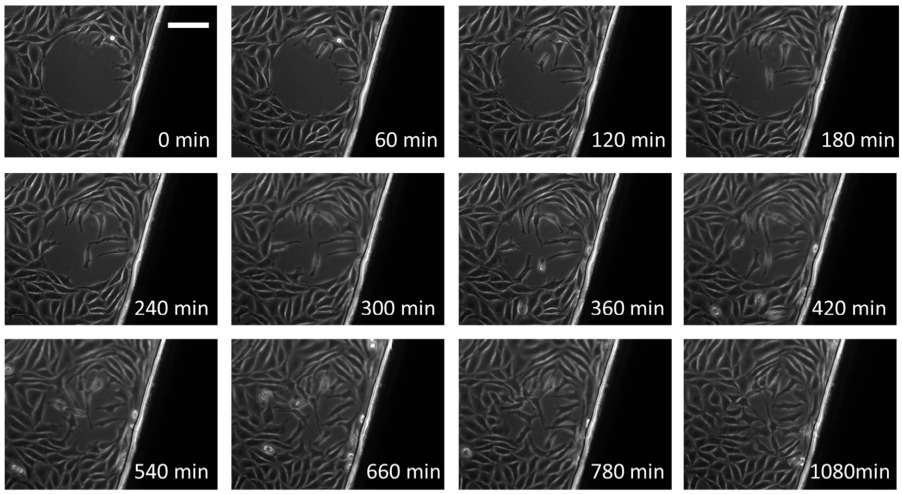

FIGURE B.3: More detailed time series of Figure 4.3, second row. Time lapse at 37 °C of the cells migrating onto the previously created cell-free thermoresponsive microgel spots at different time points within 15 h. When the temperature was increased to 37 °C, cells started to migrate to the newly generated open space and form a closed cell monolayer. The scale bar is 100 μm.

Appendix C

Supporting Information Chapter 5

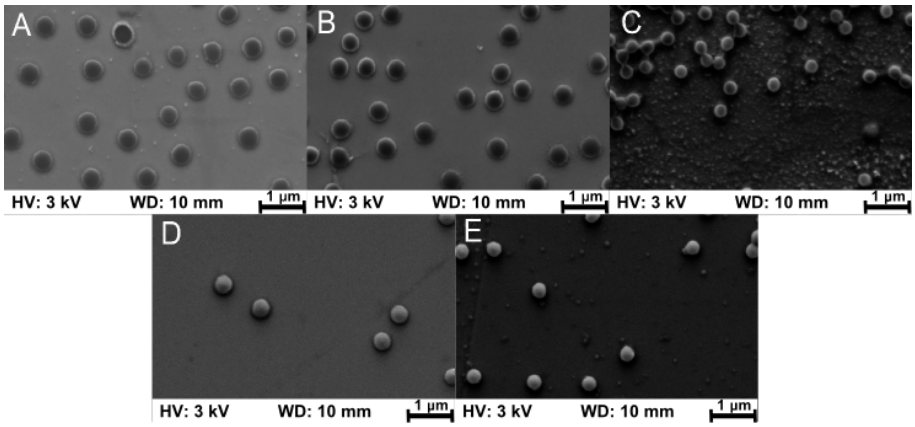

FIGURE C.1: SEM images of the copolymer microgels (A) NcBH5, (B) NcBH10, (C) NcBH15, (D) NcBH20, (E) NcBH30. The microgel particles were deposited on silicone wafers by drying of the solution at ambient conditions. The wafers with the deposited microgels were sputtered with palladium before measurement.

Fig C.1 In addition to the AFM measurements also SEM images were recorded. These images support the information gathered through the AFM measurements and also show that the synthesized microgel particles are spherical in shape and have a narrow size distribution.

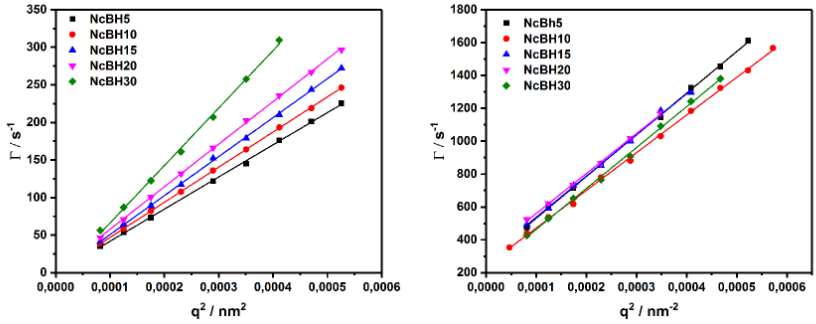

FIGURE C.2: Angular dependent PCS measurements of the copolymer microgels. From the Γ versus q^2 plots the hydrodynamic radii can be calculated via the Stokes-Einstein equation (eq.2). Measurements were performed at $10\,^{\circ}$C in the swollen state (left) and $50\,^{\circ}$C in the collapsed state (right) in order to additionally determine the maximum collapsing ratio $\boldsymbol{\alpha_{max}}$.

Fig C.2 The hydrodynamic radii of the copolymer microgels were calculated using the Stokes-Einstein equation (eq.5.1) from the data obtained in angular dependent PCS measurements. The measurements were performed using photon correlation spectroscopy (PCS) [1] on highly diluted samples (c $\leq$ 0.0001 wt%). The experimental setup is as described in the materials and methods section. The microgel solution was measured at two temperatures, in the swollen state at $10\,^{\circ}$C and in the collapsed state at $50\,^{\circ}$C. Additionally the maximum collapsing ratio $\boldsymbol{\alpha_{max}}$ was determined from this data via (eq.5.2) and is shown in table 5.1.

References

[1] B. J. Berne and R. Pecora, *Dynamic Light Scattering*. New York: John Wiley & sons, Inc., 1976.

Appendix D

Further Information on Chapter 5

This section will cover the research and experiments of the first steps of making cross-linkable microgel membranes. The initial challenge was the development of microgels suitable for cross-linking a membrane. While the number of chemical possibilities to cross-link polymer chains is plentiful, ranging from the classic cross-linker for the microgel synthesis *N*,*N*'-methylenebisacrylamide (BIS) [1], to photo cross-linkers containing a benzophenone moiety [2] and click chemistry [3], the well known industrial process of electron-beam processing has been chosen. This was due to two main reasons. First, the cross-linking process had to be done post synthesis and on microgels assembled in a monolayer on a surface. Second, recently published work from Gölzhäuser et al. showed the possibility to form free-standing carbon nano membranes by electron beam irradiation of self-assembled aromatic molecules. [4, 5] This approach offered two main advantages, the aromatic moieties can capture electrons, thereby reducing the energy needed to cross-link the microgels and the conducting metal coating beneath the polymer layer needed for this process can be dissolved in order to release the cross-linked microgel layer.

The search for suitable monomers with aromatic moieties for a radical precipitation reaction with *N*-isopropylacrylamide (NIPAM) lead to a publication from Khaksar et al. in which a catalytic reaction approach for the synthesis of amides from nitriles via the Ritter reaction was described [6]. Among the large number of molecules described in the publication were numerous exhibiting the traits needed in a suitable monomer. Three molecules deemed most promising were chosen for experiments. These molecules were *N*-(1-Phenylethyl)-acrylamide (NPhEAM), *N*-(2,3-dihydro-1H-inden-1-yl)acrylamide (NIndAM) and *N*-Benzylhydrylacrylamide (NBHAM).

Synthesis of aromatic monomers

The possible monomers for a copolymerization with NIPAM, NPhEAM, NIndAM and NBHAM selected from the publication by Khaksar et al. [6] where chosen due to similarity to NIPAM, availability of the reactants and economic effectiveness. The first approach to synthesize the monomers was done as described by Khaksar et al. [6] due to the postulated catalytic efficiency and the high proposed yield (more than 90 %).

Ritter reaction

The Ritter reaction with Pentafluorophenylammonium triflate (PFPAT) (see Fig. D.1 Z-H) as organocatalyst is a solvent free reaction of a nitrile with an alcohol. In a first step the hydroxyl group of the alcohol is protonated and after water secedes a carbenium ion emerges. In the next step the nitrile attacks in a nucleophilic reaction. The resulting nitrilium ion is hydrolysed by water which results in an amide (Fig. D.1) [7].

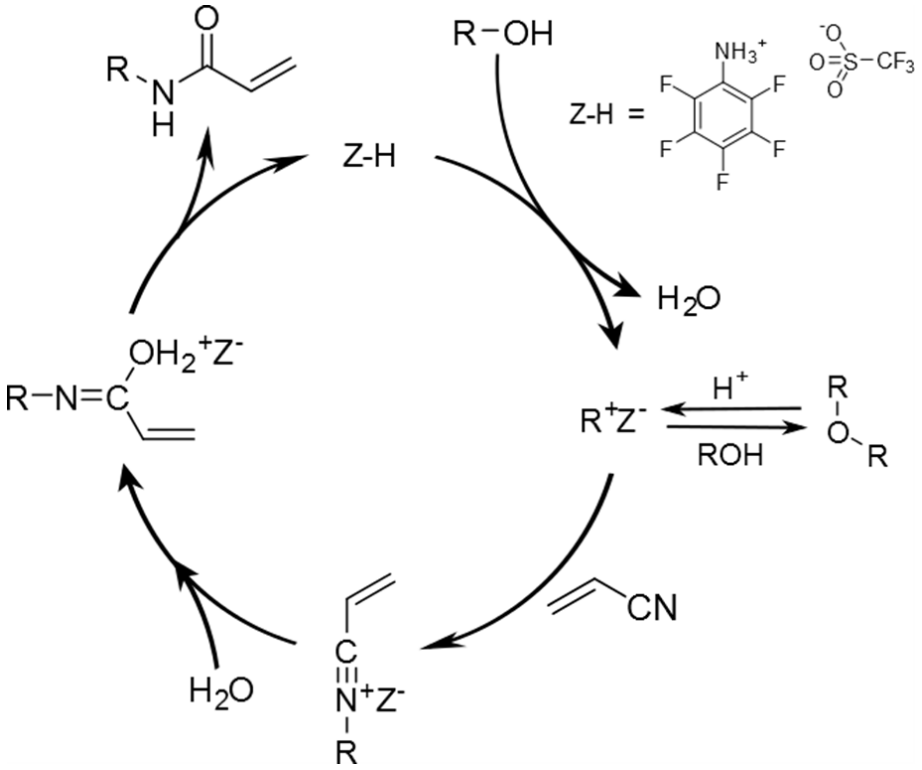

FIGURE D.1: Schematic illustration of the catalytic cycle for a Ritter reaction with PFPAT as organocatalyst (Z-H) [7]

The alcohol (2 mmol) and the nitrile (2.2 mmol) are placed into a round-bottom flask together with the catalyst PFPAT (0.21 mmol/5 mol%). The reaction solution is heated under reflux at 100 °C for at least 48 h. The reaction is finished if no more alcohol can be detected. This is done via thin-layer chromatography. After cooling the solution to ambient temperature 5 mL NaOH (1 M) is added and the water phase is extracted three times with 20 mL CH_2Cl_2. The organic phase is dried over Na_2SO_4 and the solvent is removed at 50 °C and 800 mbar. The raw product is subjected to a column chromatography with Cyclohexane/$CHCl_3$ (95 %:5 %) as solvent. From the fractions the product can be isolated by removing the solvent at 50 °C and 10 mbar.

Figure D.2 depicts the reaction schematics for the three chosen amides NPhEAM, NIndAM and BHAM.

The yield from these reactions is listed in Tab. D.1. In general we obtained a lower yield that proposed by Khaksar et al. [6] and in addition the removal of the catalyst PFPAT was a tedious effort.

In addition to the effort of the synthesis the monomers NPhEAM and NIndAM both are viscous brown liquids that is difficult to handle when subsequently used for the copolymer synthesis. NBHAM is isolated as a colorless solid.

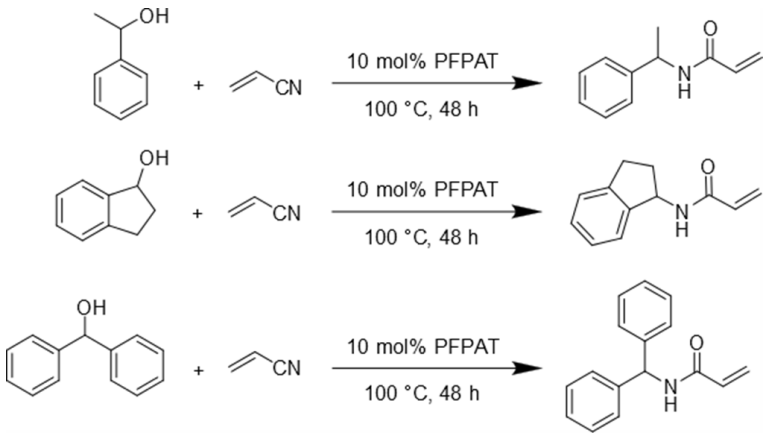

FIGURE D.2: Reactions schematics of the synthesis for the chosen amides NPhEAM (top), NIndAM (middle) and NBHAM (bottom) via the Ritter reaction with PFPAT.

TABLE D.1: Yields for the aromatic monomer NPheAM, NIndAM and NBHAM from the Ritter reaction with PFPAT as catalyst.

Product	**Yield /%**
NPhEAM	45
NIndAM	88
NBHAM	88

Schotten-Baumann reaction

Due to the Ritter reaction with PFPAT as organocatalyst proving to be inefficient in terms of effort, time and economic reasons the Schotten-Baumann reaction [8] approach was also investigated. This reaction is used to synthesize amides from amines and acid chlorides and is typically used to synthesize *N*-isopropylacrylamide (NIPAM), *N*-*n*-propylacrylamide (NNPAM) and *N*-isopropylmethacrylamide (NIPMAM) (see chapter 2). The basic reaction route is a condensation reaction of an amine with the desired aromatic moiety and acryloyl chloride. For this the amine (4 mmol) is mixed with an excess of triethylamine (1 mL) at 0 °C in CH_2Cl_2 (5 mL) and the acryloyl chloride (6 mmol) is added slowly over time. After addition of the acryloyl chloride the reaction solution is stirred at ambient temperature for 12 h. In a next step 10 mL of CH_2Cl_2 is added to the solution and it is extracted first with 20 mL saturated Na_2SO_4 solution, than 20 mL water and last with 20 mL saturated NaCl solution. The solvent from the organic phase is removed at 50 °C and 800 mbar.

TABLE D.2: Yields for the aromatic monomer NPheAM, NIndAM and NBHAM from the Schotten-Baumann reaction.

Product	**Yield /%**
NPhEAM	77
NIndAM	88
NBHAM	90

NMR-Data from aromatic monomers

In order to analyze the reaction products and confirm their purity 1H-NMR spectra where recorded.

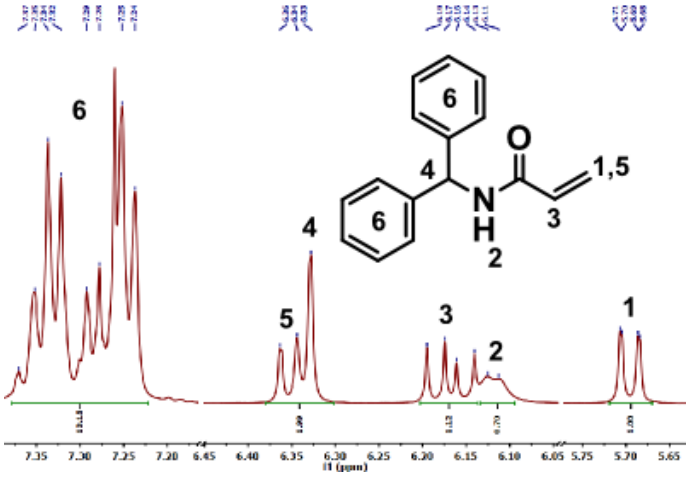

FIGURE D.3: NMR spectrum of NBHAM in $CDCl_3$. (500 MHz, $CDCl_3$) δ [ppm] = 5.70 (dd, $^2J_{gem}$H,H = 1.4 Hz, $^3J_{cis}$ = 10.3 Hz, COCH=CH_2, 1H), 6.16 (s, NH, 1H), 6.13 (m, COCH=CH_2, 1H), 6.36 (s, NCH, 1H), 6.33 (dd, $^2J_{gem}$H,H = 1.4 Hz, $^3J_{trans}$ = 17.0 Hz, COCH=CH_2, 1H), 7.30 (m, 10H).

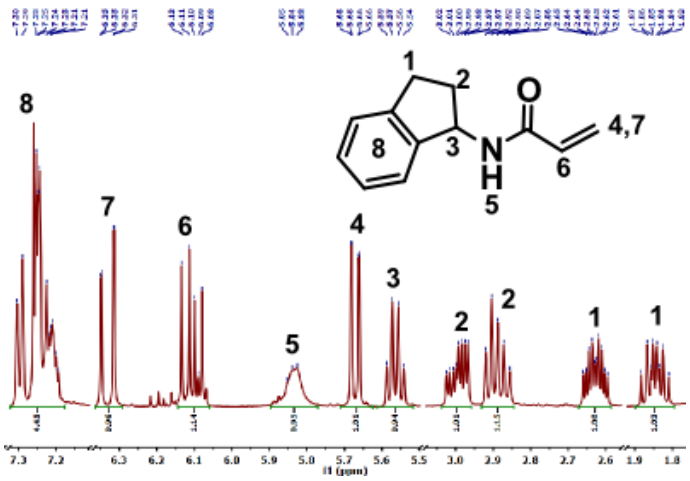

FIGURE D.4: NMR spectrum of NIndAM in $CDCl_3$. (500 MHz, $CDCl_3$) δ [ppm] = 1.85 (m, CH_2, 1H), 2.63 (m, CH_2, 1H), 2.89 (m, CH_2, 1H), 3.00 (m, CH_2, 1H), 5.5 (m, NCH, 1H), 5.67 (dd, $^2J_{gem}$H,H = 1.4 Hz, $^3J_{cis}$ = 10.3 Hz, COCH=CH_2, 1H), 5.85 (s, NH, 1H), 6.12 (m, COCH=CH_2, 1H), 6.32 (dd, $^2J_{gem}$H,H = 1.4 Hz, $^3J_{trans}$ = 17.0 Hz, COCH=CH_2, 1H), 7.25 (m, 4H).

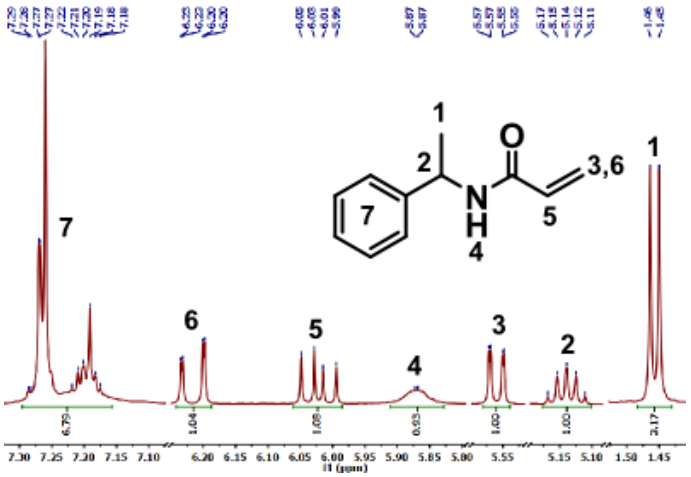

FIGURE D.5: NMR spectrum of NPheAM in $CDCl_3$. (500 MHz, $CDCl_3$) δ [ppm] = 1.45 (d, ^{3}JH,H = 6.9 Hz, $NCHCH_3$, 3H), 5.14 (m, $NCHCH_3$, 1H), 5.55 (dd, $^2J_{gem}$H,H = 1.4 Hz, $^3J_{cis}$ = 10.3 Hz, $COCH{=}CH_2$, 1H), 5.87(s, NH, 1H), 6.02 (dd, $^3J_{cis}$ = 10.3 Hz, $^3J_{trans}$ = 17.0 Hz, $COCH{=}CH_2$, 1H), 6.21 (dd, $^2J_{gem}$H,H = 1.4 Hz, $^3J_{trans}$ = 17.0 Hz, $COCH{=}CH_2$, 1H), 7.20 (m, 5H).

NPhEAM, NIndAM and NBHAM copolymer microgels

The synthesized novel monomers NPhEAM, NIndAM and NBHAM were copolymerized in a modified precipitation reaction. Due to the poor solubility in pure water a suitable solvent for the aromatic monomers had to be found. This solvent had to match certain requirements. The aromatic monomers had to exhibit a decent solubility in it. The solvent needs to be miscible with water for the precipitation reaction and should not pertubate the reaction.

The aromatic monomers exhibited a decent solubility in *t*-butanol. This solvent is interesting due to its very good miscable with water and it does not hamper the precipitation reaction. Primary and secondary alcohols such as ethanol and 2-propanol react with the initiator ammonium persulfate (APS) and thereby inhibit the reaction. *t*-Butanol as a tertiary alcohol does not react with APS. The aromatic monomers where dissolved in the smallest volume of *t*-butanol possible. This is important due to the cononsolvency effect of pNIPAM exhibits in water/alcohol mixtures [9, 10, 11]. A large amount of *t*-butanol could possibly change the reaction conditions too much and thereby alter the particle growth kinetics in an unfavorable manner.

Copolymer microgel synthesis

The copolymer microgels of PNIPAM-*co*-NPhEAM, PNIPAM-*co*-NIndAM and PNIPAM-*co*-NBHAM were synthesized in a modified precipitation polymerization without surfactant. All synthesis were performed in a 250 mL three-neck round flask equipped with a reflux condenser, mechanical stirrer and a nitrogen inlet. The monomer NIPAM (11.55 mmol) and the cross-linker *N,N'*-methylenebisacrylamide (BIS) (5 mol% in respect to the amount of NIPAM) were dissolved in 141.5 ml purified water and were heated up to 70 °C under continuous stirring and purged with nitrogen. The aromatic comoners NPhEAM, NIndAM and NBHAM (2.31 mmol, 20 mol% in respect to the amount of NIPAM) were dissolved *t*-butanol (7.5 mL). The solution was purged with nitrogen and added to the reaction solution. After 1 h the

polymerization was initiated by the addition of 1 ml of a 2.71 mM solution of APS and left to proceed for 4 h at 70 °C. After the reaction time, the solution was cooled to room temperature and stirred over night. For purification, all samples have been treated by five cycles of centrifugation, decantation and redispersion using purified water (Arium® pro VF system (Satorius AG, Göttingen, Germany)).

As a control experiment a NIPAM homopolymer microgel was synthesized in the same solvent mixture under the same conditions.

Characterization of the copolymer particles

In order to characterize the swelling behavior of the copolymer microgels and the NIPAM homopolymer microgel and to determine their VPTT, temperature dependent PCS measurements were performed. The swelling curves are depicted in Figure D.6. It can be seen that the swelling behavior of the NIPAM homopolymer is not altered. The VPTT is 33 °C, this is in good agreement with the literature [12, 13, 14, 15, 16, 17, 18]. Therefore it can be stated, that the synthesis conditions are not altered too strongly by the addition of 5 vol.-% of *t*-butanol.The copolymer microgels exhibit a different swelling behavior than the NIPAM homopolymer microgel.They are smaller in size, in the swollen and collapsed state compared to the homopolymer microgel. In addition, their swelling behavior is strongly differs from the NIPAM microgel. The phase transition is shifted to lower temperatures from the VPTT of 33 °C of the pNIPAM homopolymer. This effect increases from NPhEAM to NIndAM to NBHAM and is thereby more pronounced the more hydrophobic the co-monomer is.

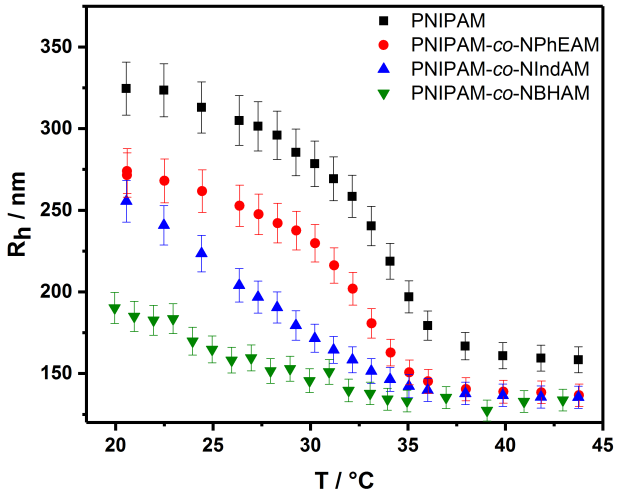

FIGURE D.6: Swelling curves of PNIPAM, PNIPAM-*co*-NPhEAM, PNIPAM-*co*-NIndAM and PNIPAM-*co*-NBHAM microgels synthesized in a water *t*-butanol mixture with 5 vol.-% of *t*-butanol. The nominal co-monomer amount of the copolymer microgels is 20 mol%.

For further characterization AFM images of these copolymer microgels were recorded (Fig. D.7). These images show that the copolymer microgels are spherical in shape but that the samples are not monodisperse. In every image two particle species can be observed where the larger microgel particles are always accompanied by smaller particles. Both species in every sample appear if considered separately

monodisperse. These satellite particles are most likely a result of the synthesis with *t*-butanol as they cannot be observed in the copolymer microgels synthesized in just water (see chapter 5). This was one reason, besides the complicated handling of *t*-butanol due to its high melting point, why the synthesis of the respective copolymer microgels in pure water was developed.

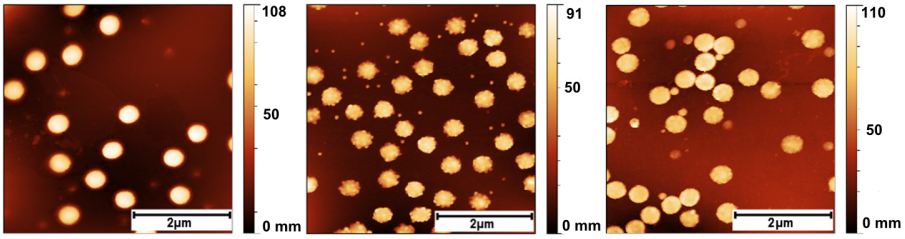

FIGURE D.7: AFM Images of single copolymer microgel particles with 20 mol% co-monomer content. PNIPAM-*co*-NPhEAM (left), PNIPAM-*co*-NIndAM (center)and PNIPAM-*co*-NBHAM (right)

Free-standing microgel film from PNIPAM-*co*-NBHAM

The synthesized homo- and co-polymer microgels were spin-coated onto a gold sputtered wafer, cross-linked with an electron beam and placed into a bath containing aqua regia in order to dissolve the gold layer and retrieve the microgel film. The procedure was done as described in chapter 5. The layers produced from the PNIPAM-*co*-NPhEAM and PNIPAM-*co*-NIndAM microgel sample dissolved totally like the homopolymer layer, no free-standing microgel film could be retrieved from these samples. The layer produced from the sample PNIPAM-*co*-NBHAM detached from the carrier substrate, floated toward the surface but broke up into numerous smaller fragments. One of the larger fragments, about ($\sim 2\,mm^2$), could be picked up from the solution with a piece of silicon wafer. A photograph and AFM image of this film can be seen in Figure D.8.

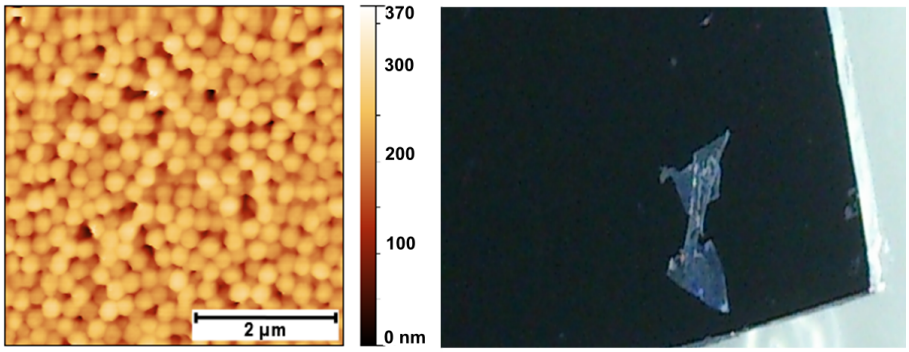

FIGURE D.8: (left) AFM Image of the first isolated microgel film that was detached in aqua regia after electron-beam cross-linking. (right) Photograph of the isolated microgel film that was detached in aqua regia after electron-beam cross-linking. The depicted film was made from PNIPAM-*co*-NBHAM copolymer microgels with 20 mol% synthesized in *t*-butanol.

These experiments led to the decision to continue the research effort for a free standing microgel film with PNIPAM-*co*-NBHAM copolymer microgels. The modified precipitation reaction with a mixture of water and *t*-butanol was droped and a synthesis route in pure water was developed. Due to the weak solubility of NBHAM in water the monomer has to be dispersed finely by placing it prior to the reaction in 20 mL of water and shaking the dispersion at 3000 rpm for 30 min or placing the dispersion in an ultra sonic bath for 1 min. Following this route the reaction is feasible in pure water and only one species of particles is produced in this manner.

References

[1] R. Pelton, "Temperature-sensitive aqueous microgels," *Adv. Colloid Interf. Sci.*, vol. 85, pp. 1–33, 2000. review.

[2] G. T. Carroll, M. E. Sojka, X. Lei, N. J. Turro, and J. T. Koberstein, "Photoactive additives for cross-linking polymer films: Inhibition of dewetting in thin polymer films," *Langmuir*, vol. 22, no. 18, pp. 7748–7754, 2006. PMID: 16922559.

[3] H. C. Kolb, M. G. Finn, and K. B. Sharpless, "Click chemistry: Diverse chemical function from a few good reactions," *Angewandte Chemie International Edition*, vol. 40, pp. 2004–2021, 2001.

[4] W. Geyer, V. Stadler, W. Eck, M. Zharnikov, A. Gözhäuser, and M. Grunze, "Electron-induced crosslinking of aromatic self-assembled monolayers: Negative resists for nanolithography," *Applied Physics Letters*, vol. 75, no. 16, pp. 2401–2403, 1999.

[5] C. T. Nottbohm, A. Beyer, A. S. Sologubenko, I. Ennen, A. Hütten, H. Rösner, W. Eck, J. Mayer, and A. Gölzhäuser, "Novel carbon nanosheets as support for ultrahigh-resolution structural analysis of nanoparticles," *Ultramicroscopy*, vol. 108, no. 9, pp. 885 – 892, 2008.

[6] S. Khaksar, E. Fattahi, and E. Fattahi, "Organocatalytic synthesis of amides from nitriles via the ritter reaction," *Tetrahedron Letters*, vol. 52, no. 45, pp. 5943 – 5946, 2011.

[7] M. Barbero, S. Bazzi, S. Cadamuro, and S. A. Dughera, "o-benzenedisulfonimide as a reusable brønsted acid catalyst for ritter-type reactions," *Eur. J. Org. Chem.*, vol. 2009, pp. 430–436, 2009.

[8] L. Kürti and B.Czakó, *Strategic Applications of Named Reactions in Organic Synthesis: Background and Detailed Mechanisms*. Elsevier Academic Press, 2005.

[9] F. M. Winnik, M. F. Ottaviani, S. H. Bossmann, W. Pan, M. Garcia-Garibay, and N. J. Turro, "Cononsolvency of poly(*N*-isopropylacrylamide): A look at spin-labeled polymers in micxtures of water and tetrahydrofuran," *Macromolecules*, vol. 26, pp. 4577–4585, 1993.

[10] H. M. Crowther and B. Vincent, "Swelling behavior of poly(n-isopropylacrylamide) microgel particles in alcoholic solutions," *Colloid Polym. Sci.*, vol. 276, pp. 46–51, 1998. Not really very interesting.

[11] C. Scherzinger, O. Holderer, D. Richter, and W. Richtering, "Polymer dynamics in responsive microgels: influence of cononsolvency and microgel architecture," *Phys. Chem. Chem. Phys.*, vol. 14, pp. 2762–2768, 2012.

[12] Y. Hertle, M. Zeiser, C. Hasenöhrl, P. Busch, and T. Hellweg, "Responsive p(nipam-*co*-ntbam) microgels: Flory–rehner description of the swelling behaviour," *Colloid and Polymer Science*, vol. 288, pp. 1047–1059, 2010.

[13] T. Hellweg, C. D. Dewhurst, E. Brückner, K. Kratz, and W. Eimer, "Colloidal crystals made of pnipa-microgel particles," *Colloid & Polymer Sci.*, vol. 278, no. 10, pp. 972–978, 2000.

[14] L. Arleth, X. Xia, R. P. Hjelm, J. Wu, and Z. Hu, "Volume transition and internal structures of small poly(*N*-isopropylacrylamide) microgels," *Journal of Polymer Science Part B: Polymer Physics*, vol. 43 (7), pp. 849–860, 2005.

[15] C. Wu, S. Zhou, S. C. F. Au-yeung, and S. Jiang, "Volume phase transition of spherical microgel particles," *Die Angewandte Makromolekulare Chemie*, vol. 240, no. 1, pp. 123–136, 1996.

[16] P. W. Zhu and D. H. Napper, "Coil-to-globule type transitions and swelling of poly(*N*-isopropylacrylamide) and poly(acrylamide) at latex interfaces in alcohol-water mixtures," *Journal of Colloid and Interface Science*, vol. 177, no. 2, pp. 343 – 352, 1996.

[17] S. Seelenmeyer, I. Deike, S. Rosenfeldt, C. Norhausen, N. Dingenouts, M. Ballauff, T. Narayanan, and P. Lindner, "Small-angle x-ray and neutron scattering studies of the volume phase transition in thermosensitive core-shell colloids," *J. Chem. Phys.*, vol. 114, no. 23, pp. 10471–10478, 2001.

[18] Y. Maeda, M. Tsubota, and I. Ikeda, "Fourier transform ir spectroscopic study on phase transitions of copolymers of *N*-isopropylacrylamide and alkyl acrylates in water," *Colloid and Polymer Science*, vol. 281, no. 1, pp. 79–83, 2003.

Appendix E

Surface Coverage by Microgels

The behavior of linear uncharged polymer chains when deposited on a surface by spin-coating is a well known and intensively studied process [1, 2, 3, 4]. The same is true for the layer-by-layer deposition via dip-coating [5, 6, 7, 8] or spray-coating [9, 10, 11] for charged polymer chains. While a theoretical description of this process is possible due to the freedom of movement of the linear polymer chains this is not as easily done for microgel particles. Microgels are cross-linked polymer particles, this means that a single microgel is build from numerous chemically and also physically linked polymer chains. These chains have a certain degree of freedom of movement but are limited in that freedom by the connection points between the chains. The chains can never move fully independent or separate from each. In addition a microgel can not be seen as an uncharged polymer particle due to the charges from the initiator APS at each end of each polymer chain [12, 13, 14]. Therefore a microgel must be viewed as a negatively charged, elastic polymer particle with the size of thousand of linear, spatially confined polymer chains. This makes a theoretical description of the deposition processes very complex if all possible factors are accounted for.

This chapter describes an empirical study of coating surfaces with microgels using different techniques such as spin-, dip- and spray-coating. The aim is to investigate the utility of each method for producing homogeneous microgel monolayers and we will show that, for spin-coating, even a change in cross-linker content will significantly change the deposition behavior. Additionally, this part is offering a guide line for surface coating with microgels of different architectures. Used for the deposition experiments described in this part where microgels with different cross-linker content. Four microgel samples pNI-Q010, pNI-Q025, pNI-Q050 and pNI-Q100 with a nominal cross-linker content of 1 mol%, 2.5 mol%, 5 mol% and 10 mol% where chosen for the empirical study. The swelling curves are depicted in Fig. E.1.

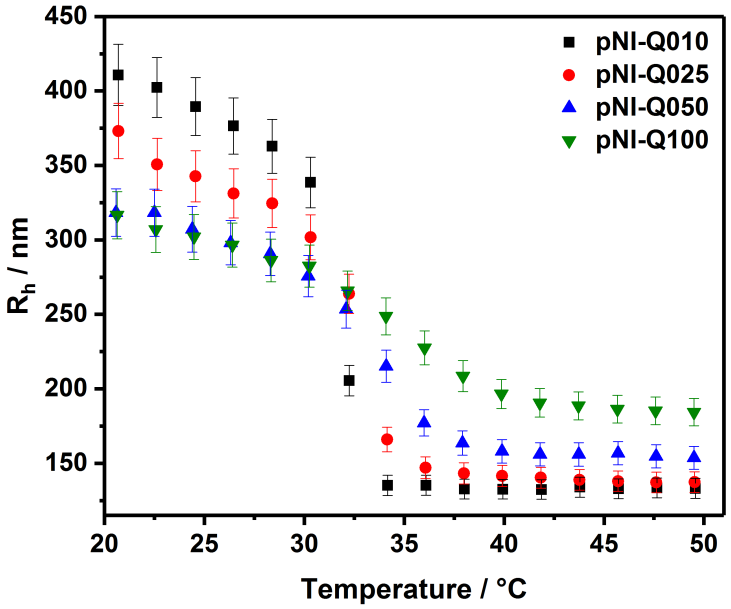

FIGURE E.1: Swelling curves of the four microgels pNI-Q010, pNI-Q025, pNI-Q050 and pNI-Q100 with a nominal cross-linker content of 1 mol%, 2.5 mol%, 5 mol% and 10 mol% used in the deposition experiments.

As it can be seen from Fig. E.1, with increasing cross-linker content the swelling behavior of the microgels changes significantly. The most prominent change is the change in size. With increasing amount of cross-linker the size in the swollen state decreases and the size in the collapsed state increases. This also means that the higher the cross-linker content is, the lower is the swelling ratio. Furthermore a broadening in the phase transition with an increasing amount of cross-linker can be observed. The effect of these obvious differences between the microgel samples on the deposition behavior of the particles has been investigated and will be displayed in the following paragraphs.

Spin-coating

Spin-coating is one of the fastest, most economic and easiest to use methods when it comes to surface coatings, especially with polymers. [1, 2, 3, 4] The amount of material needed is small and the process itself is fast when compared to other coating methods. [1, 2, 3, 4] For linear polymers this process is well known and theoretically described to a great extend. It will be shown, that there are certain similarities between microgels and linear polymers when it comes to concentration and speed of rotation and that an empirical description can be possible if all influencing parameters are known to a certain extend.

Spin-coating procedure

The spin coating process is performed with a Süss Microtechnic Labspin 6 TT equipped with a 2“ teflon chuck to fix the silicone wafer using under-inflation. For the coating process 100 oriented, N/Ph doped silicone wafers with the dimensions

of 50.8 $\pm$ 0.3 mm in diameter and a thickness of 279 $\pm$ 25 μm and a resistivity of 10-20 Ω/cm from Siegert Wafer are used. All wafers are treated with an oxygen plasma for 30 s, a RCA1 solution at 75 °C for 10 min and peroxymonosulfuric acid (caro's acid) for 30 min. The wafers are coated with a 0.25 wt% poly-(ethylene imine) (PEI) at 2000 rpm for 120 s prior to the microgel coating in order to ensure a better adsorption of the microgel particles.

The microgels used are PNIPAM homopolymer gels with varying cross-linker (BIS) content. Used are cross-linker amounts of 1 mol%, 2.5 mol%, 5 mol% and 10 mol% with respect to the amount of NIPAM. These four microgel samples are than deposited via spin-coating on the PEI-coated wafers in different concentrations (0.25 wt%, 0.5 wt% an 0.75 wt%) and with varying speeds of rotation (500 rpm, 1000 rpm, 1500 rpm and 2000 rpm) for every microgel sample at every concentration.

Characterization

Microgel monolayers were characterized using ellipsometry [15, 16, 17, 18] for probing the layer thickness in dried state and AFM in order to approximate the surface coverage from recorded images. The used ellipsometer is a SE 400adv null-ellipsometer from Sentech equipped with a 632.8 nm He-Ne-LASER. The angle of incidence can be selected manually in steps of 5 ° between 40 ° and 85 °. In order to determine the layer thickness the coated wafer was probed at five different distances from the center.

The AFM [19, 20, 21, 22] used to investigate the surface coverage is a DI Nanoscope IIIa mounted on a Zeiss Axiovert 135 inverted optical microscope. Microgel layers were measured in tapping mode using BudgetSensors (Innovative Solutions Bulgaria Ltd., Sofia, Bulgaria) Al-Reflex Tap300Al-G cantilevers with a tip radius of <10 nm, a resonance frequency of about 300 kHz and a spring constant of 40 N/m. The images were analyzed with the AFM analysis software Gwyddion [23]. After determining the diameter of the microgel paticles in a layer and counting the visible full particles with the image analyzing software ImageJ [24] the surface coverage was calculated assuming perfectly spherical particles in the layer. The ellipsometrically measured layer thickness and the calculated surface coverage are depicted for in the following graphs and are sorted by cross linker amount used in the synthesis ((Fig. E.2) 1 mol% (pNIPAM-Q010), (Fig. E.3) 2.5 mol% (pNIPAM-Q025), (Fig. E.4) 5 mol% (pNIPAM-Q050) and (Fig. E.5) 10 mol% (pNIPAM-Q100)). The green columns in the surface coverage graph represent coverage values equal to or above the close-packing of equal spheres (74 %). The exact values are listed in the tables following the graphic illustrations ((Fig. E.1) 1 mol% (pNIPAM-Q010), (table E.2) 2.5 mol% (pNIPAM-Q025), (table E.3) 5 mol% (pNIPAM-Q050) and (table E.4) 10 mol% (pNIPAM-Q100)).

Results and Discussion

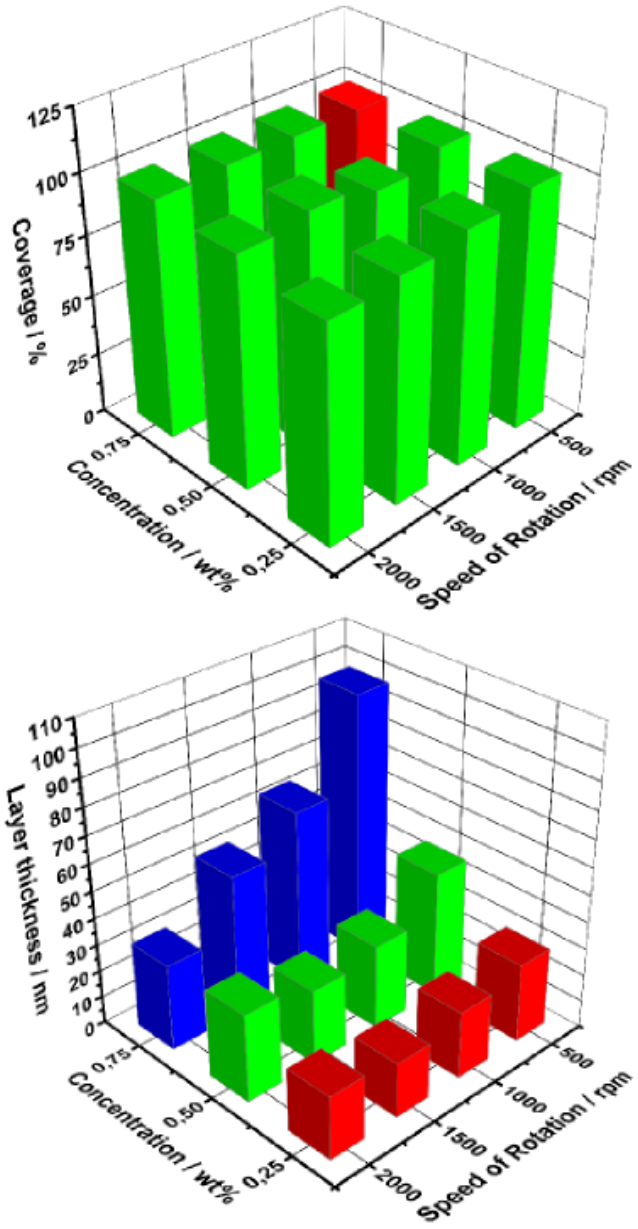

FIGURE E.2: (Top) Surface coverage for the sample pNIPAM-Q010 for all concentrations and speeds of rotation. Green columns are surface coverages between 74 % and 100 % and red columns are below 100 % or multilayers. (Bottom) Microgel layer thicknesses measured with ellipsometry.

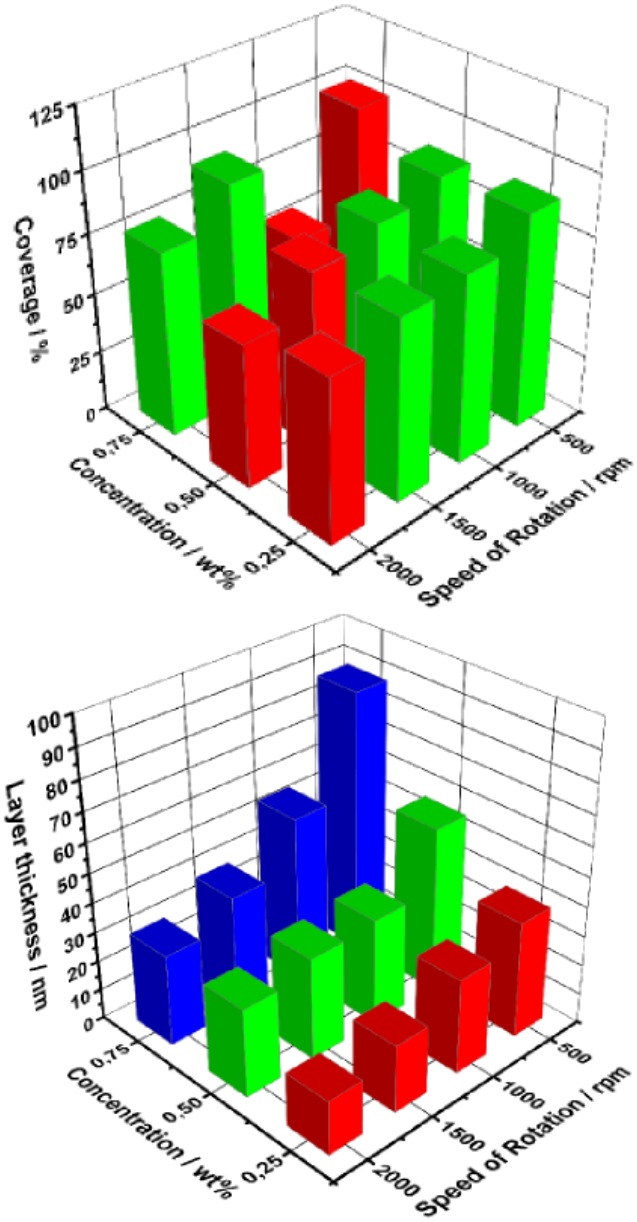

FIGURE E.3: (Top) Surface coverage for the sample pNIPAM-Q025 for all concentrations and speeds of rotation. Green columns are surface coverages between 74 % and 100 % and red columns are below 100 % or multilayers. (Bottom) Microgel layer thicknesses measured with ellipsometry.

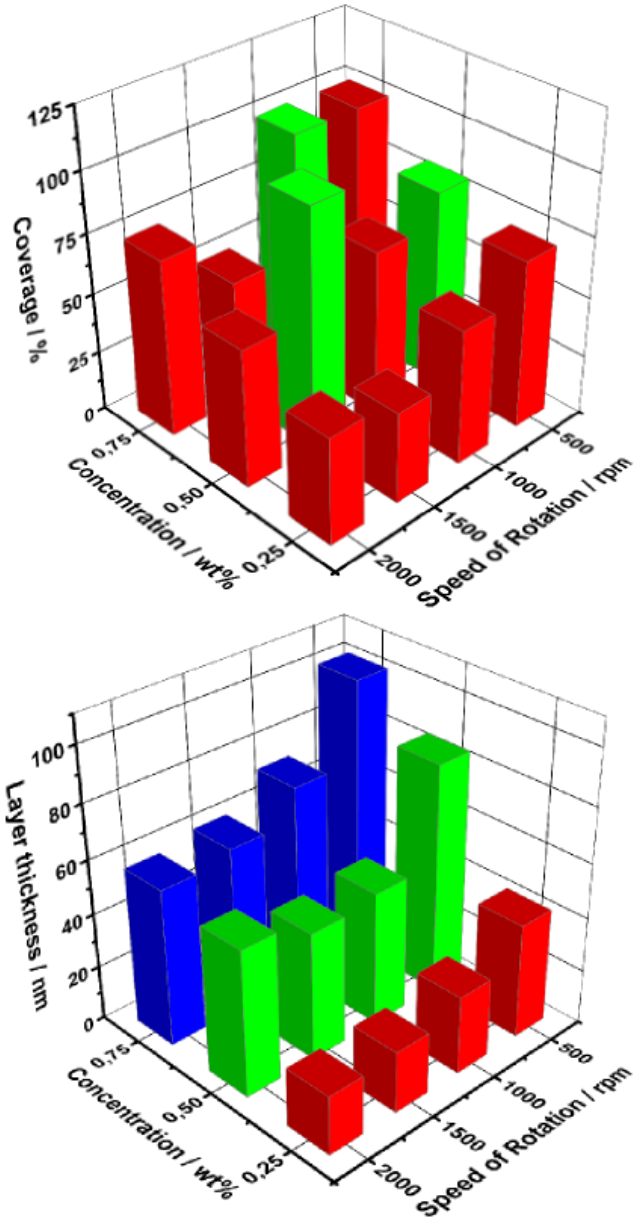

FIGURE E.4: (Top) Surface coverage for the sample pNIPAM-Q050 for all concentrations and speeds of rotation. Green columns are surface coverages between 74 % and 100 % and red columns are below 100 % or multilayers. (Bottom) Microgel layer thicknesses measured with ellipsometry.

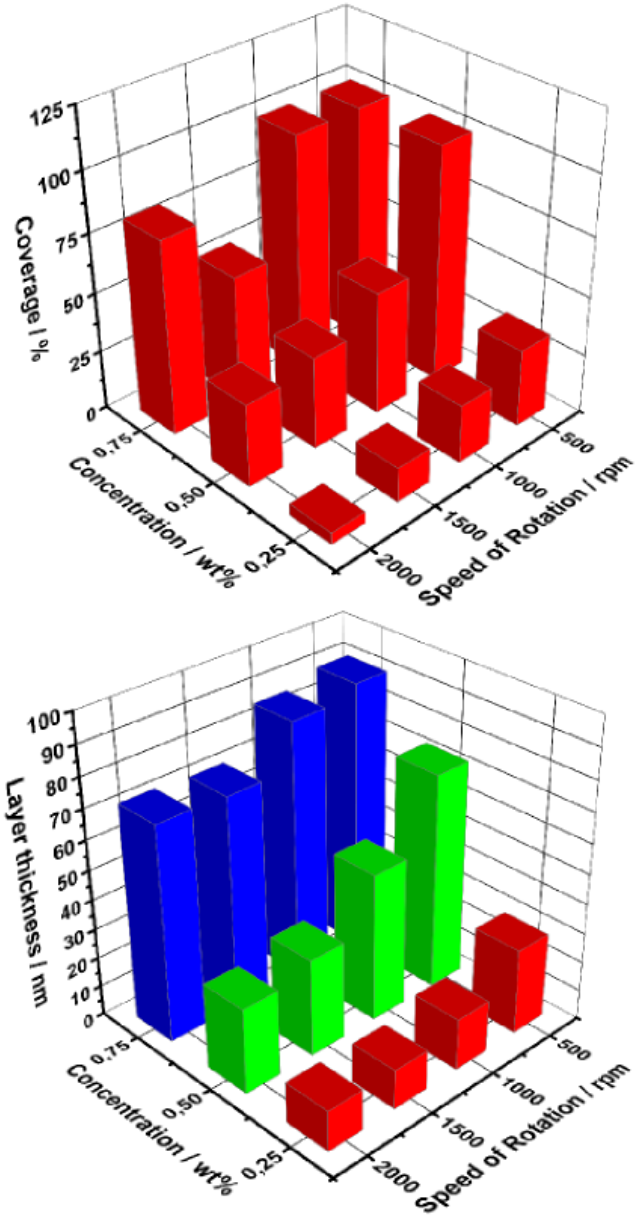

FIGURE E.5: (Top) Surface coverage for the sample pNIPAM-Q100 for all concentrations and speeds of rotation. Green columns are surface coverages between 74 % and 100 % and red columns are below 100 % or multilayers. (Bottom) Microgel layer thicknesses measured with ellipsometry.

TABLE E.1: Layer thickness th_{layer} measured with an ellipsometer, surface coverage θ calculated based on the assumption of spherical particles. Moreover, also as well as the speed of rotation v_{rot} and the microgel solution concentration c_{MGS} for the microgel sample with 1 mol% cross-linker (pNIPAM-Q010)are listed.

Sample	v_{rot} **/ rpm**	c_{MGS} **/ wt%**	th_{layer} **/ nm**	θ **/ %**
pNI-Q010-525	500	0.25	29.0 ± 0.9	100
pNI-Q010-550	500	0.50	46.2 ± 1.1	100
pNI-Q010-575	500	0.75	97.5 ± 1.6	100
pNI-Q010-1025	1000	0.25	24.7 ± 0.6	100
pNI-Q010-1050	1000	0.50	31.2 ± 0.2	100
pNI-Q010-1075	1000	0.75	65.0 ± 1.5	100
pNI-Q010-1525	1500	0.25	20.2 ± 1.4	100
pNI-Q010-1550	1500	0.50	27.6 ± 1.0	100
pNI-Q010-1575	1500	0.75	52.6 ± 0.6	100
pNI-Q010-2025	2000	0.25	23.3 ± 2.4	100
pNI-Q010-2050	2000	0.50	32.5 ± 1.3	100
pNI-Q010-2075	2000	0.75	31.9 ± 2.5	$<$100

TABLE E.2: Layer thickness th_{layer} measured with an ellipsometer, surface coverage θ calculated based on the assumption of spherical particles. Moreover, also as well as the speed of rotation v_{rot} and the microgel solution concentration c_{MGS} for the microgel sample with 2.5 mol% cross-linker (pNIPAM-Q025)are listed.

Sample	v_{rot} **/ rpm**	c_{MGS} **/ wt%**	th_{layer} **/ nm**	θ **/ %**
pNI-Q025-525	500	0.25	39.1 ± 1.3	89.3
pNI-Q025-550	500	0.50	55.8 ± 2.0	87.5
pNI-Q025-575	500	0.75	88.2 ± 3.3	$<$100
pNI-Q025-1025	1000	0.25	31.9 ± 1.5	78.6
pNI-Q025-1050	1000	0.50	35.8 ± 0.6	80.8
pNI-Q025-1075	1000	0.75	55.5 ± 3.2	56.4
pNI-Q025-1525	1500	0.25	22.8 ± 1.2	76.2
pNI-Q025-1550	1500	0.50	34.4 ± 1.9	73.6
pNI-Q025-1575	1500	0.75	39.2 ± 1.6	91.9
pNI-Q025-2025	2000	0.25	18.1 ± 0.4	68.1
pNI-Q025-2050	2000	0.50	29.9 ± 0.4	59.7
pNI-Q025-2075	2000	0.75	30.8 ± 1.8	77.1

TABLE E.3: Layer thickness th_{layer} measured with an ellipsometer, surface coverage θ calculated based on the assumption of spherical particles. Moreover, also as well as the speed of rotation v_{rot} and the microgel solution concentration c_{MGS} for the microgel sample with 5 mol% cross-linker (pNIPAM-Q050)are listed.

Sample	v_{rot} **/ rpm**	c_{MGS} **/ wt%**	th_{layer} **/ nm**	θ **/ %**
pNI-Q050-525	500	0.25	42.1 ± 1.1	70.5
pNI-Q050-550	500	0.50	84.6 ± 6.9	80.8
pNI-Q050-575	500	0.75	101.3 ± 2.8	<100
pNI-Q050-1025	1000	0.25	28.7 ± 2.0	56.0
pNI-Q050-1050	1000	0.50	49.3 ± 1.1	69.1
pNI-Q050-1075	1000	0.75	72.7 ± 1.5	100
pNI-Q050-1525	1500	0.25	22.6 ± 1.8	38.0
pNI-Q050-1550	1500	0.50	47.1 ± 5.9	100
pNI-Q050-1575	1500	0.75	61.2 ± 1.4	51.2
pNI-Q050-2025	2000	0.25	21.6 ± 2.6	44.4
pNI-Q050-2050	2000	0.50	54.1 ± 0.9	57.6
pNI-Q050-2075	2000	0.75	58.1 ± 1.3	73.8

TABLE E.4: Layer thickness th_{layer} measured with an ellipsometer, surface coverage θ calculated based on the assumption of spherical particles. Moreover, also as well as the speed of rotation v_{rot} and the microgel solution concentration c_{MGS} for the microgel sample with 10 mol% cross-linker (pNIPAM-Q100)are listed..

Sample	v_{rot} **/ rpm**	c_{MGS} **/ wt%**	th_{layer} **/ nm**	θ **/ %**
pNI-Q100-525	500	0.25	28.7 ± 1.2	32.8
pNI-Q100-550	500	0.50	72.7 ± 3.0	<100
pNI-Q100-575	500	0.75	90.2 ± 5.7	<100
pNI-Q100-1025	1000	0.25	17.4 ± 2.7	24.6
pNI-Q100-1050	1000	0.50	50.0 ± 4.3	51.9
pNI-Q100-1075	1000	0.75	86.5 ± 4.8	<100
pNI-Q100-1525	1500	0.25	13.4 ± 0.2	14.6
pNI-Q100-1550	1500	0.50	32.9 ± 1.5	39.2
pNI-Q100-1575	1500	0.75	71.8 ± 1.2	53.5
pNI-Q100-2025	2000	0.25	13.7 ± 0.8	5.0
pNI-Q100-2050	2000	0.50	28.9 ± 1.6	35.0
pNI-Q100-2075	2000	0.75	72.7 ± 2.1	67.8

The apparent information that can be extracted from the graphs and the tables is that a low cross-linker content is better suited for the production of homogeneous monolayers. Whereas almost all coatings from the microgel sample pNIPAM-Q010 form monolayers with perfect coverage of the surface the coatings from the sample pNIPAM-Q100 form patchy layers or multilayers. This can be attributed to the higher flexibility of the particles with low cross-linker content. The more flexible the microgel particles are the better they can arrange in a densely packed layer and can compensate better defects. A higher cross-linker content leads to particles that behave more like hard spheres. This seems to lead to two possible outcomes in the coating process. For one they apparently tend to act like billiard balls in the case of low concentration and/or high speeds of rotation. Due to the rotational force setting them in motion they gain a high enough impulse and adsorb so weak on the surface that in most incidents of two gels hitting each other they force each other off the substrate. In the second case, when the concentration is high and the speed of rotation is low, a layer is formed. The low impulse the particles have, the high concentration and the rough surface that is formed by the adsorbed microgels leads to a second layer being formed on top. These observations indicate a strong influence of the microgel architecture and morphology on the deposition behavior.

Further, it can be seen from the results, that the surface coverage and the layer thickness tend to increase with higher solution concentration or lower speeds of rotation. This observation is in agreement with observations and theoretical calculations for surface coatings with linear polymers [1, 2, 3, 4]. How strong these two factors influence the deposition behavior depends strongly on the morphology. The more cross-linker is used in the synthesis the stronger microgel particles tend to be influenced by these factors. Therefore, a theory of the deposition behavior can presumably only be achieved empirically for each microgel species. This means, that if the microgel particles from two samples differ in size, cross-linker content, monomer composition or anything of that kind, they cannot be described in the same way with respect to deposition behavior.

The AFM images recorded in order to calculate the surface coverage also illustrate the difference in surface coverage. The figures Fig.E.6, Fig.E.7 and Fig.E.8 depict a selection from the recorded AFM images. Figure E.6 shows four images of each microgel sample with different cross-linker respectively, deposited from 0.5 wt% solutions at a speed of rotation 1000 rpm. The only difference between the images is the amount of cross-linker used in the microgel synthesis in order to illustrate the influence of the cross-linker content. Figure E.7 illustrates the influence of the speed of rotation. The images are all from surfaces made from the sample pNIPAM-Q025 deposited from solutions with a concentration of 0.25 wt% at different speeds of rotation. The influence of the concentration of the microgel solution is depicted in Fig. E.8. The images are taken for coatings from the sample pNIPAM-Q050 deposited at a speed of rotation of 1000 rpm from solutions of different concentrations.

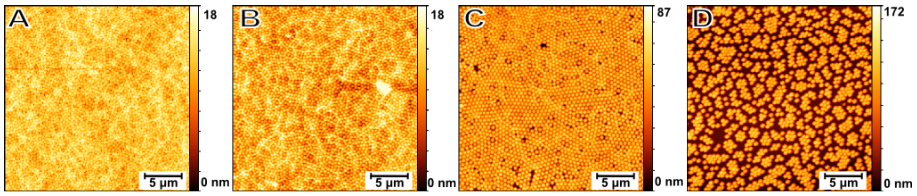

FIGURE E.6: AFM images $25 \times 25\,\mu m^2$ of layers from the samples pNIPAM-Q010 (A), pNIPAM-Q025 (B), pNIPAM-Q050 (C) and pNIPAM-Q100 (D) deposited from 0.5 wt% microgel solutions on silicon wafers with a speed of rotation 1000 rpm.

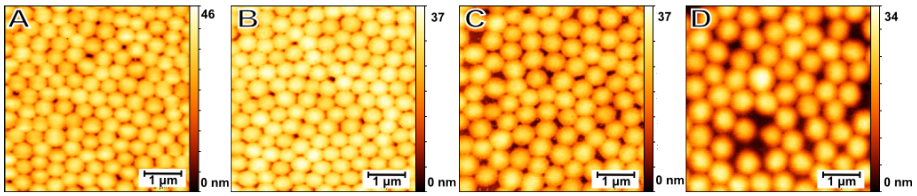

FIGURE E.7: AFM images $5 \times 5\,\mu m^2$ of layers from the samples pNIPAM-Q025 deposited from 0.25 wt% microgel solutions on silicon wafers with varying speeds of rotation 500 rpm (A), 1000 rpm (B), 1500 rpm (C) and 2000 rpm (D).

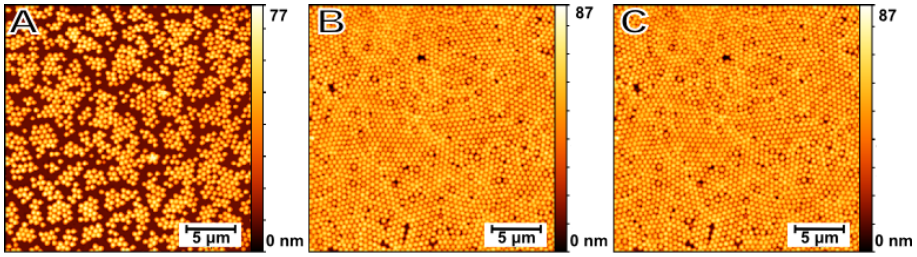

FIGURE E.8: AFM images $5 \times 5\,\mu m^2$ of layers from the samples pNIPAM-Q050 deposited with a speed of rotation of 1000 rpm on silicon wafers from microgel solutions with the concentrations 0.25 wt% (A), 0.5 wt% (B) and 0.75 wt% (C).

Conclusion

From spin-coating experiments with the aromatic microgels NcBH5, NcBH10, NcBH15, NcBH20 and NcBH30 (see Chapter 5) it has been found that these microgels synthesized with 5 mol% cross-linker BIS behave more like pNIPAM-Q100 or for that matter, like hard-spheres. This behavior can be attributed to the aromatic moieties incorporated in the microgels due to the copolymerization with NBHAM. For this case a spin-coating routine was developed which led to the best results for cross-linkable monolayers.

Dip-coating

Dip-coating procedure

The dip-coating experiments were performed with a R & K Dipping Ropbot Dr-0 (Riegler & Kirstein GmbH, Berlin, Germany) with a one dimensional moving axis (x-z) ppwered by an isel (isel Germany AG, Eichenzell, Germany) Schrittmotor-modul MS 200HT2 elctro motor. All materials and analytical devices are identical to the previously described. The general procedure to coat silicon wafers using dip-coating included a previous spin-coating of the wafers with 0.25 wt% solution of PEI followed by a dip-routine including the immersion in the microgel solution followed by a washing step with desalted water and a drying step with compressed air, this is referred to as one cycle. The silicon wafers were immersed in solutions with a concentration of 0.5 wt% or 1 wt% at three different dip-velocities, 0.027 cm/s, 0.007 cm/s and the slowest possible speed 0.0003 cm/s. This procedure was done with up to three cycles with microgel solutions from the samples pNIPAM-Q010, pNIPAM-Q025 and pNIPAM-Q050. Characterization of the layers was performed using AFM and ellipsometry. In this part the focus will be on the analysis of the AFM data gathered.

Results and Discussion

Figure E.9 depicts the difference in surface coverage between a 0.5 wt% and 1 wt% deposited with a dip-velocity of 0.027 cm/s from a solution of the microgel sample pNIPAM-Q025 with one cycle. It can be clearly seen, that both layers form a dense cover of the surface with next to no defects. The Layer from the 1 wt% solution is rougher in contrast to the much more homogeneous layer from the 0.5 wt% solution. From the ellipsometric data it can though be concluded that both layers are monolayers with a layer thickness of 66 ± 3 nm for the sample from the 0.5 wt% solution and 76 ± 4 nm for the layer from the 1 wt% solution. Therefore, except from the surface roughness and a slightly increased layer thickness of the layer from the 1 wt% solution possibly due to slightly denser packing , no real difference between layers produced from solutions of different concentration can be concluded.

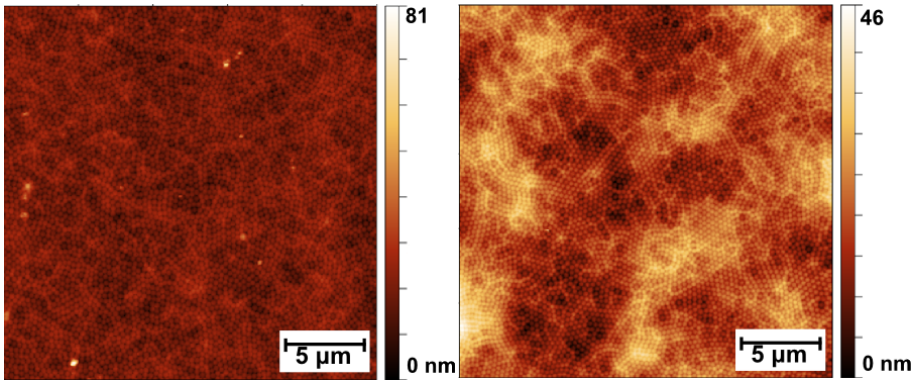

FIGURE E.9: AFM images $25 \times 25\,\mu m^2$ of layers from the samples pNIPAM-Q025 (1 cycle) deposited with dip-velocity of 0.027 cm/s from microgel solutions of 0.5 wt%(left) and 1 wt%(right).

Figure E.10 illustrates the influence of the dip-velocity on the formed layer. The images depict layers produced from a 0.5 wt% solution of pNIPAM-Q025 using one

cycle and dip-velocities of 0.027 cm/s, 0.007 cm/s and 0.0003 cm/s. The apparent most obvious difference is the surface roughness that seemingly increases with decreasing dip-velocity. From ellipsometry measurements the layer thickness was obtained and it has been been found that the thickness increases drastically with decreasing dip-velocity. The measured thickness are 41 ± 2 nm for a speed of 0.027 cm/s, 63 ± 3 nm for a speed of 0.007 cm/s and 120 ± 6 nm for a speed of 0.0003 cm/s. None of the measured thicknesses hint at the formation of a multilayer. All measured layer thicknesses can be attributed to an increased roughness and a dense packing due to the flexibility of the microgels with low cross-linker content.

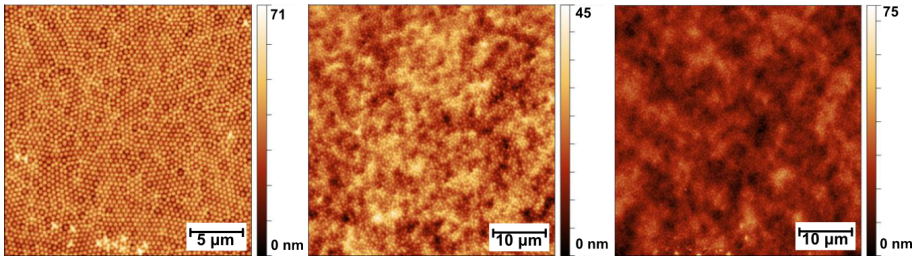

FIGURE E.10: AFM images 25 x 25 μm^2 and 50 x 50 μm^2 of layers from the samples pNIPAM-Q025 (1 cycle) deposited from 0.5 wt% microgel solution with dip-velocities of 0.027 cm/s(left), 0.007 cm/s(center) and 0.0003 cm/s(right).

Figure E.11 shows the difference in surface coverage depending on the number of applied dipping cycles. The AFM images depict microgel surface coatings produced from a 0.5 wt% solution of the sample pNIPAM-Q025 deposited with a dip-velocity of 0.007 cm/s. After each dipping cycle an AFM image was obtained and the layer thickness was probed using ellipsometry. The AFM images do not differ significantly, pointing to a similar morphology of the layers. The measured layer thickness on the other hand increased with every dipping cycle. After the first cycle a thickness of 66 ± 3 nm was measured, on the second cycle this thickness increased to 99 ± 5 nm and a measured thickness of 103 ± 5 nm after the third cycle shows no further increase in layer thickness. Again nothing hints at the formation of double multilayers, the thickness increase can be attributed to a denser packing of the microgels in the layer. Probably with each cycle the force of the receding liquid, upon pulling the wafer out of the solution pushed the microgels closer together and thereby forcing the microgel particles into a denser packing.

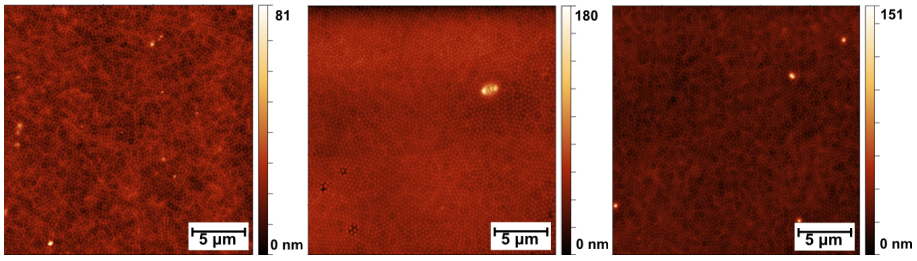

FIGURE E.11: AFM images 25 x 25 μm^2 of layers from the samples pNIPAM-Q025 deposited from 0.5 wt% with a dip-velocity 0.007 cm/s. The number of dip-cycles is increased from left to right. After 1-dip-cycle (left), after 2-dip-cycles (center) and after 3-dip-cycles (right).

Figure E.12 displays the influence the amount of cross-linker in the microgel has

on the layer formed in the dip-coating process. The AFM images show layers made from the samples pNIPAM-Q010, pNIPAM-Q025 and pNIPAM-Q050 deposited on the wafer from solutions with a concentration of 1 wt% deposited at a dip-velocity of 0.027 cm/s. All images show a rough surface but the roughest surface is displayed by the layer from the sample pNIPAM-Q050. Ellipsometrically determined layer thicknesses confirm this first impression. The measured layer thicknesses are 47 ± 2 nm for the layer from the sample pNIPAM-Q010, 76 ± 4 nm for the pNIPAM-Q025 layer and 84 ± 4 nm for the pNIPAM-Q050 layer. This result for the pNIPAM-Q050 layer is in strong contrast to the thickness of around 180 nm the AFM measurements suggest. Analyzing the AFM images it can be seen that besides large piles of microgels also defects can be observed this explains the low layer thickness measured with ellipsometry.

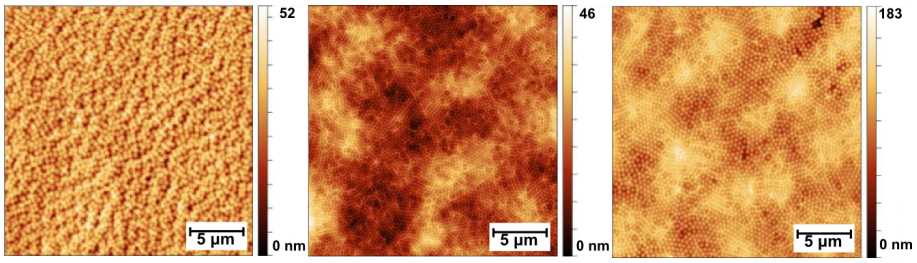

FIGURE E.12: AFM images $25 \times 25\,\mu m^2$ of layers from the samples pNIPAM-Q010 (left), pNIPAM-Q025 (center) and pNIPAM-Q050 (right) deposited from 1 wt% with a dip-velocity 0.027 cm/s.

Conclusion

In conclusion it can be said that dip-coating is a suitable method for the production of microgel monolayers but with certain limitations. First it is suitable for microgels with low cross-linker content. Experiments with pNIPAM-Q050 have all resulted in layers with blemishes even after multiple cycles. The number of cycles and the dip-velocity do not seem to influence the resulting layers strongly though it can be recommended to use just a single cycle for time reasons and a dip-velocity between 0.027 cm/s and 0.007 cm/s in order to avoid a rough surface. The concentration of the microgel solution should idealy be chosen between 0.5 wt% and 1 wt%. One of the biggest disadvantages in comparison to spin-coating is the amount of material and time needed for this procedure. It takes over 5 times longer using dip-coating compared to spin-coating and the difference in quantity of material needed is about 0.1 mL of microgel solution for the spin-coating process and about 10 mL for the dip-coating process to fully immerse a substrate with a size of 10 x 10 mm. Due to the layers not being more homogeneous and the limitation to microgels with a low cross-linker content spin-coating remains the preferred method.

Spray-coating

Spray-coating experiments have been performed using a chromatography laboratory sprayer (DESAGA GmbH, Heidelberg, Germany). The microgel solutions are filled into a small storage chamber from which the solution is nebulized using manual air compression. The nozzle is aimed at the silicon wafer and the microgel solution is sprayed onto the wafer. The substrate is spin-coated with a 0.25 wt% solution of PEI prior to the spray-coating procedure. For the spray coating microgels from the samples pNIPAM-Q010, pNIPAM-Q025 and pNIPAM-Q050 were used in

the concentrations 0.5 wt% and 1 wt%. After the microgel solution was applied to the surface with the laboratory sprayer the coated substrate was dried at ambient conditions for 12 h in order for the water to evaporate from the substrate. The coated and dried wafer was than washed with deionized water and dried with compressed air using the dip-robot. Characterization of the produced layers was done using AFM and ellipsometry before and after the washing step.

Figure E.13 depicts AFM images from the spray-coated layers of every microgel sample used (pNIPAM-Q010, pNIPAM-Q025 and pNIPAM-Q050) in both concentrations applied (0.5 wt% and 1 wt%). The most apparent observation is that most of the layers are not homogeneous. All layers produced with a 1 wt% solution form rough surface layers. The layer thicknesses measured using ellipsometry are 70 ± 3 nm for the pNIPAM-Q010 layer (E.13B), 40 ± 2 nm for pNIPAM-Q025 (E.13D) and 97 ± 5 nm for the pNIPAM-Q050 layer (E.13F). The only homogeneous surface coating is exhibited by the layer deposited from a 0.5 wt% solution of pNIPAM-Q010 (E.13A) for which the measured layer thickness is 76 ± 4 nm. The layers produced from 0.5 wt% solutions of pNIPAM-Q025 and pNIPAM-Q050 are both inhomogeneous and show numerous defects.

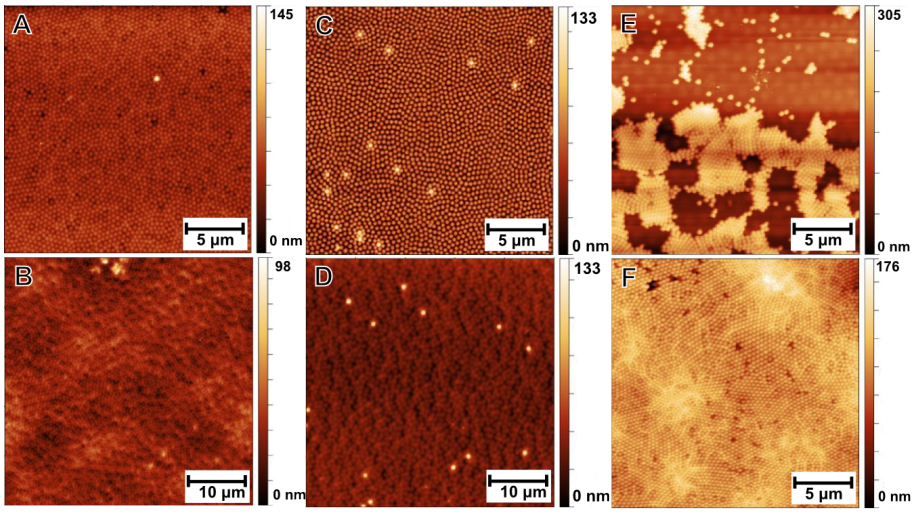

FIGURE E.13: AFM images $25 \times 25\,\mu m^2$ and $50 \times 50\,\mu m^2$ of layers from the samples pNIPAM-Q010 (A and B), pNIPAM-Q025 (C and D) and pNIPAM-Q050 (E and F) deposited on silicon wafers via spray-coating from solutions with a concentration of 0.5 wt% (A,C and E) and 1 wt% (B,D and F).

These images illustrate very clear, that direct spray-coating of microgels with a laboratory sprayer is an unfit method for the production of homogeneous surface coatings. The results are unsatisfying and above all unreproducible. Therefore simple spray-coating can not be recommended as a method of choice when aiming at homogeneouse microgel surface coatings.

References

[1] S. Schemmel, G. Rother, A. Brûlet, T. Hellweg, and G. H. Findenegg, "Phase separation of a binary liquid system in controlled-pore glass," in *Rapport d'activité 2003* (L. L. B. (CEA-CNRS), ed.), LLB, 2003.

[2] E. M. Sparrow and J. L. Gregg, "Mass transfer, flow and heat transfer about a rotating disk," *Journal of Heat Transfer*, vol. 82, pp. 294–302, 1960.

[3] A. Münch, C. P. Please, and B. Wagner, "Spin coating of an evaporating polymer solution," *Physics of Fluids*, vol. 23, no. 10, p. 102101, 2011.

[4] D. E. Bornside, R. A. Brown, P. W. Ackmann, J. R. Frank, A. A. Tryba, and F. T. Geyling, "The effects of gas phase convection on mass transfer in spin coating," *Journal of Applied Physics*, vol. 73, no. 2, pp. 585–600, 1993.

[5] C. Elosua, D. Lopez-Torres, M. Hernaez, I. R. Matias, and F. J. Arregui, "Comparative study of layer-by-layer deposition techniques for poly(sodium phosphate) and poly(allylamine hydrochloride)," *Nanoscale Research Letters*, vol. 8, p. 539, 2013.

[6] T. Radeva, K. Kamburova, and I. Petkanchin, "Formation of polyelectrolyte multilayers from polysaccharides at low ionic strength," *Journal of Colloid and Interface Science*, vol. 298, no. 1, pp. 59 – 65, 2006.

[7] D. von Saatweber and B. Vollmert, "Versuche zum abscheidungsvorgang bei der elektrotauchlackierung 2. teil," *Die Angewandte Makromolekulare Chemie*, vol. 9, pp. 61–88, 1969.

[8] S. Roland, R. E. Prud'homme, and C. G. Bazuin, "Morphology, thickness, and composition evolution in supramolecular block copolymer films over a wide range of dip-coating rates," *ACS Macro Letters*, vol. 1, no. 8, pp. 973–976, 2012.

[9] M. Bruening and D. Dotzauer, "Polymer films: Just spray it," *Nat. Mater.*, vol. 8, pp. 449–450, 2009.

[10] G. Decher and J. B. Schlenhoff, *Multilayer Thin Films: Sequential Assembly of Nanocomposite Materials*. Wiley, 2003.

[11] J. B. Schlenoff, S. T. Dubas, and T. Farhat, "Sprayed polyelectrolyte multilayers," *Langmuir*, vol. 16, no. 26, pp. 9968–9969, 2000.

[12] R. Pelton, "Temperature-sensitive aqueous microgels," *Adv. Colloid Interf. Sci.*, vol. 85, pp. 1–33, 2000. review.

[13] W. Richtering and B. R. Saunders, "Gel architectures and their complexity," *Soft Matter*, vol. 10, pp. 3695–3702, 2014. Review.

[14] A. Pich and W. Richtering, "Polymer nanogels and microgels," *Polymer Science: A Comprehensive Reference*, vol. 6, pp. 309–350, 2012.

[15] F. L. McCrackin, E. Passaglia, R. R. Stromberg, and H. L. Steinberg, "Measure-measurement of the thickness and refractive index of very thin films and the optical properties of surfaces by ellipsometry," *Journal of Research of the National Bureau of Standards*, vol. 67A, pp. 363–377, 1963.

[16] R. J. Archer, "Determination of the properties of films on silicon by the method of ellipsometry," *J. Opt. Soc. Am.*, vol. 52, no. 9, pp. 970–977, 1962.

[17] F. Partovi, "Theoretical treatment of ellipsometry," *J. Opt. Soc. Am.*, vol. 52, no. 8, pp. 918–925, 1962.

[18] J. A. Faucher, G. M. McManus, and H. J. Trurnit, "Simplified treatment of ellipsometry," *J. Opt. Soc. Am.*, vol. 48, no. 1, pp. 51–54, 1958.

[19] P. A. FitzGerald, D. Dupin, S. P. Armes, and E. J. Wanless, "In situ observations of adsorbed microgel particles," *Soft Matter*, vol. 3, pp. 580–586, 2007. no copy.

[20] C. D. Sorrell and L. A. Lyon, "Bimodal swelling responses in microgel thin films," *J. Phys. Chem. B*, vol. 111, pp. 4060–4066, 2007.

[21] S. Höfl, L. Zitzler, T. Hellweg, S. Herminghaus, and F. Mugele, "Volume phase transition of smart microgels in bulk solution and adsorbed at an interface: A combined afm, dynamic light, and small angle neutron scattering study," *Polymer*, vol. 48, pp. 245–254, 2007.

[22] A. Burmistrova, M. Richter, C. Uzum, and R. von Klitzing, "Effect of cross-linker density of p(nipam-*co*-aac) microgels at solid surfaces on the swelling/shrinking behaviour and the youngs modulus," *Colloid Poly. Sci.*, vol. 289, pp. 613–624, 2011.

[23] D. Necas and P. Klapetek, "Gwyddion: an open-source software for (spm) data analysis," *Central European Journal of Physics*, vol. 10, pp. 181–188, 2012.

[24] W. Rasband, "Imagej 1.50b," *National Institute of Health, USA*, http://imagej.nih.gov/ij/.